



DREAMERS

Design REsearch, implementation And Monitoring of Emerging technologies for a new generation of Resilient Steel buildings

Results of FE studies

Deliverable D2.3-WP2-T2.3

WP 2: Executive architectural and structural design of the building

Task 2.3: FE studies to support the design of the building

Authors:

Arash Poursadrollah, Roberto Carlevaris, Mario D'Aniello, Roberto Tartaglia, Raffaele Landolfo

University of Napoli - Federico II, Italy

















____Mfreldam___

Date: 08/09/2023 (Revised)

Contents

| Task description | 4 |
|--|----|
| A. Refined FE analyses of beam-to-column joint with FREEDAM devices using ABAQUS | 5 |
| A.1 Generality of the investigated Freedam joints | 5 |
| A.2 DREAMERS building | 8 |
| B. Refined FE analyses of beam-to-column joint with FREEDAM devices using ABAQUS | 9 |
| B.1 Modelling assumptions | 9 |
| B.2 FE analyses | 10 |
| B.3 Loading Scenarios | 11 |
| B.5 Detailed analysis of the X-II-XJ joint | 14 |
| B.5.1 Monotonic Loading | 14 |
| B.5.2 Cyclic Loading | 17 |
| B.5.3 Column Loss "Hogging" | 18 |
| B.5.4 Column Loss "Sagging" | 20 |
| B.6 FE analyses of the other MRF joints | 22 |
| B.6.1 X-III-TJ | 22 |
| B.6.2 X-III-XJ | 24 |
| B.6.3 X-II-TJ | 26 |
| B.6.4 Y-III-TJ | 28 |
| B.6.5 Y-III-XJ | 30 |
| B.6.6 Y-II-TJ | 32 |
| B.6.7 Y-II-XJ | 34 |
| B.7 Strengthening of upper T-stub | 36 |
| B.7.1 T-stub as-it-is | 36 |
| B.7.2 Strengthening design | 38 |
| B.7.3 Strengthening solution for <i>Device 1</i> | 39 |
| B.7.4 Strengthening solution for <i>Device 2A</i> | 47 |
| B.8. Conclusive remarks about the activities of sub-task 2.3.a | 49 |
| B.9 References | 50 |
| C.Pushover and time-history analyses of the DREAMERS building through OpenSees | 51 |
| C.1. Numerical model | 51 |
| C.1. Nonlinear static analysis | 51 |
| C.1.1 Seismic assessment of the building based on Nonlinear static analysis | 53 |

| C.2 Nonlinear dynamic analysis | 54 |
|---|----|
| C.2.1 Mean annual frequency of collapse | 55 |
| C.2.2 Incremental dynamic analysis | 56 |
| C.2.3 Performance assessment at specific hazard level | 57 |
| C.2.4 Performance assessment based on MAF | 59 |
| C.2.5 Assessment of residual drift | 61 |
| C.2.6 Assessment of damage in the columns | 62 |
| C.3 Conclusive remarks on the seismic assement of DREAMERS building | 62 |
| C.4 References | 63 |

Task description

UNINA is the partner that was most heavily involved during the FREEDAM project in the development of numerical methods for the analysis of structures with free-from-damage joints: because of this acquired experience **UNINA** has been put in charge of developing FE studies of the DREAMERS building.

In the previous *Task 2.2: "Executive structural design of the demonstration building" UNISA* has defined the executive structural design of the DREAMERS building. Afterwards, with the present *Task 2.3: "FE studies to support the design of the building", UNINA* has developed several FE studies of the demonstration building. These studies have concerned the local behaviour of the FREEDAM joint assembly and the global analysis of the structure. In particular:

- a. Beam-to-column joint assemblies of the moment resisting frames of the building have been studied with a commercial FE software (**ABAQUS**), in order to characterize the local behaviour of all the MRFs joints under monotonic, cyclic, column loss scenarios.
- b. Pushover and Time-History analyses have been carried out to assess the seismic performance of the demonstration building, considering a set of real accelerograms selected from the European database of earthquakes through **OpenSees**.

This deliverable summarizes the work carried out in task 2.3. Since the two sub-tasks address different activities, the present document is organized in three main sections, namely:

i) section A which summarizes the generalities of the investigated joints as well as the features of the DREAMERS building; ii) section B which activities carried out in sub-task 2.3.a, and section C which reports the work carried out in sub-task 2.3.b.

A.Refined FE analyses of beam-to-column joint with FREEDAM devices using ABAQUS

A.1 Generality of the investigated Freedam joints

There are 5 different FREEDAM devices, that can be equipped on a moment resisting frame, for a certain range of beam and column profiles. These devices differ between them based on geometrical measures of their basic components and based on the number of damper bolts used.

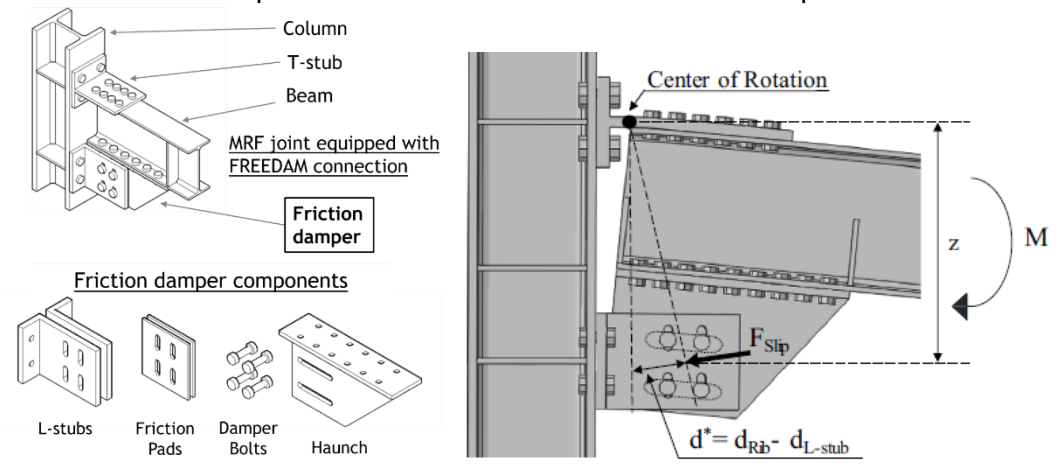


Fig 1: Elements of a FREEDAM connection (left) and its functioning (right)

An important parameter for the design of a FREEDAM connection is the desired *bending capacity level:*

$$m = \frac{M_{j,Rd}}{M_{pl,Rd,beam}}$$

which is the ratio between the bending moment resistance of the joint over the plastic bending moment resistance of the connected beam. As design procedure, this ratio is comprised between 0.3 and 0.6.

| Beam | m (Bending Capacity Level) | | | | | |
|----------------|----------------------------|-----|-----|-----|--|--|
| Size | 0.3 | 0.4 | 0.5 | 0.6 | | |
| IPE 270 | | | D1 | D1 | | |
| IPE 300 | | D1 | D1 | D1 | | |
| IPE 360 | D1 | D1 | D2 | D2 | | |
| IPE 400 | D1 | D2 | D2 | 02 | | |
| IPE 450 | D1 | D2 | D2 | D3 | | |
| IPE 500 | D2 | D2 | D3 | D3 | | |
| IPE SSO | D2 | D3 | D3 | D4 | | |
| IPE 600 | D2 | D3 | D4 | D4 | | |
| IPE 750 x 147 | D3 | D4 | DS | D5 | | |
| IPE 750 x 161 | D3 | D4 | D5 | D5 | | |
| IPE 750 x 173+ | 03 | 04 | DS | 05 | | |
| IPE 750 x 185 | D4 | D5 | DS | D5 | | |

Tab 1: Pre-qualification table from the FREEDAM Design Manual

The bending moment resistance of the joint is given by:

$$M_{i,Rd} = \mu_{dyn} F_{p,C,d} n_b n_s h_s$$

Where:

μ_{dyn}: dynamic friction coefficient of the friction pads

F_{p,C,d}: damper bolts preload force

n_b: number of bolts

- n_s: number of friction surfaces
- h_s: lever arm of the connection, that is to say the distance between the center of the damping bolts and the upper flange of the beam

The preload force of the damper bolts is designed accordingly to obtain a certain bending moment capacity. As design procedure, this preload force should be between 40% and 100% of the preload force prescribed by EN1993-1-8:

$$F_{p,C,d} = [0.4 \div 1]F_{p,C}^{EC3} = [0.4 \div 1]0.7A_{res}f_{ub}$$

The behaviour of FREEDAM MRF connections was investigated previously by Latour et alia. This study takes in consideration the two possible configurations of a FREEDAM device, with horizontal sliding surfaces and with vertical sliding surfaces. The second configuration is the one that will be used in the DREAMERS building. The specimens were tested with an experimental campaign supported by FE simulations, under monotonic and cyclic loading. Parametric FE analysis investigated the influence of the pre-loading force of the damper bolts and the dynamic friction coefficient of the friction pads on the overall behaviour of the connection.

The two assembly with vertical sliding surfaces were:

Assembly 1: Beam IPE270–Column HE220M

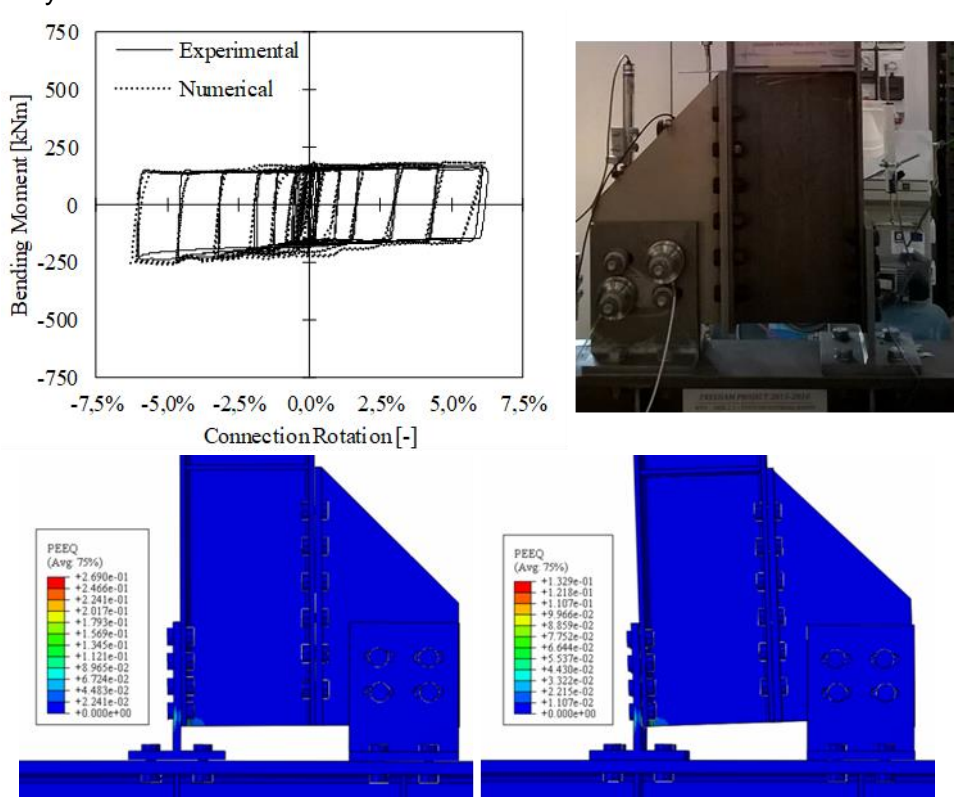


Fig 2: Assembly 1, thanks to Latour et al.

Assembly 2: Beam IPE450–Column HE500B

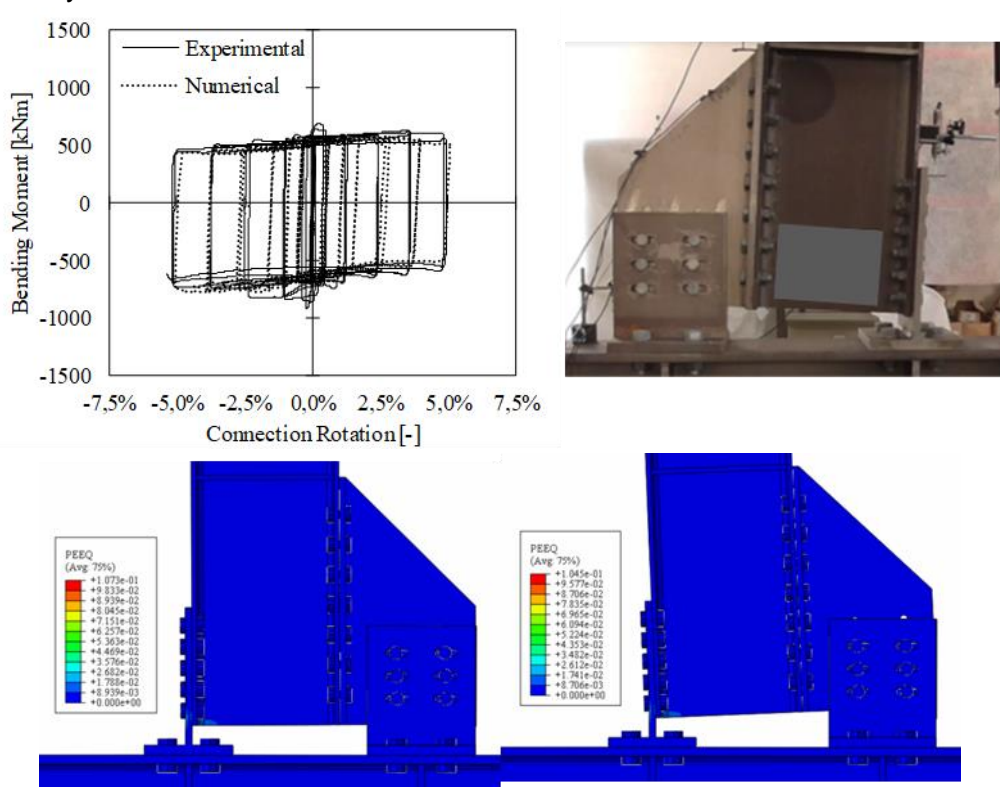


Fig 3: Assembly 2, thanks to Latour et al.

All performed tests showed an overall satisfactory response with stable hysteretic behaviour and similar features. Connections performed as rigid up to the static friction resistance of the devices. Following the activation of the sliding, a loss of strength was observed but negligible stick-slip phenomena were observed under load reversal. The different flexural resistance experienced under sagging and hogging can be explained by analysing the local deformation demand in the upper T-Stub (which connects the top flange of the beam to the column) and the lower L-Stubs (which connect the device to the column).

The experimental tests showed negligible plastic deformation in the beam or the T and L-stubs up to 0.04 rad of chord rotation. Increasing the imposed rotation up to 0.05 rad (which was set as the limit of the allowable displacement capacity of the friction device) the overall response of the joints was still satisfactory. After the tests, it was observed that the friction pads underwent significant erosion of the superficial friction coatings and signs of plastic deformation in the bolts were also spotted.

These connections are very similar to that used in the demonstrative building, so this study by Latour was also used to calibrate the FE models of the DREAMERS joint assemblies of the present report. Calibration was done also by confronting the hysteretic behaviour of the joints.

A.2 DREAMERS building

The building is characterized by a 15 m x 25 m plan and 3 storeys with a total height of about 12 m. It has wide internal spaces that allow flexible use of the areas as lecture rooms or open space offices. The **structure** have fifteen columns made with HEB 400 profiles and COFRADAL slim composite floors with HEB240-HEB300 cut-off beam, belonging to the system commercialized by Arcelor Mittal (CoSFB). This type of floors provides several technical advantages, and they are particularly suitable for medium-long spans such as those adopted in the building, that will be around 7 m. In addition, the CoSFB are very thin (about 40 cm), allowing to maximize the internal spaces of the building. The **seismic-resistant part** of the structure will be constructed, adopting four MRFs bays in the -X direction and four MRFs bays in the -Y direction. The beams of the seismic-resistant MRFs will be made of IPE 400 and IPE 450 profiles, and S355JR steel will be used for all structural components.

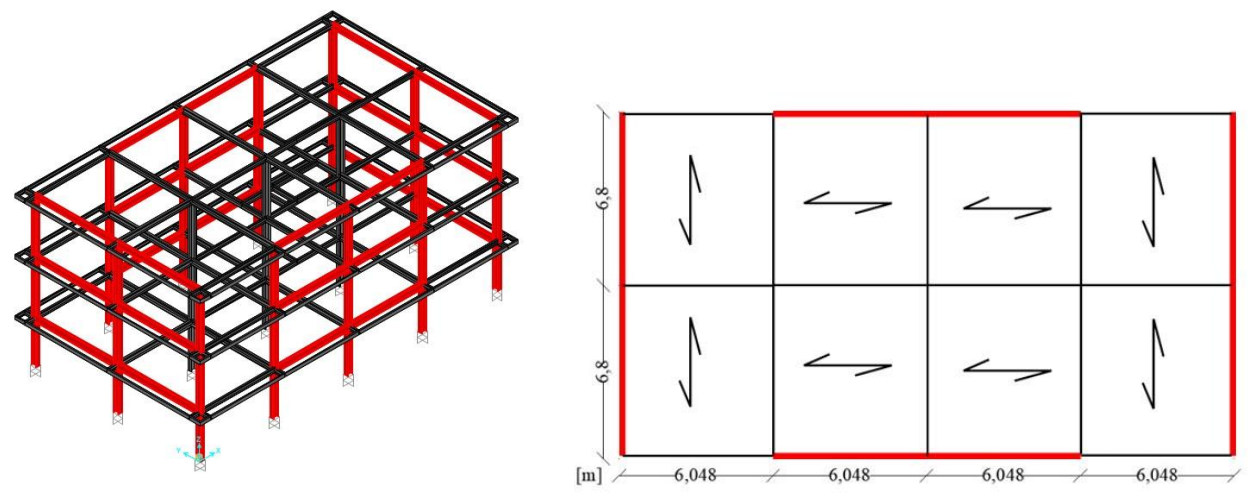


Fig 4: 3D view of the structural elements (left); plan view, with MRF bays highlighted in red (right)

The **beam-to-column joints** of the seismic-resistant MRFs will be realized adopting the devices standardized during the FREEDAM project; in particular, Device 1 and Device 2A will be used. Device 1 is used on all the MRF-X joints and on the third storey of the MRF-Y, while Device 2A is used only on the storey I and II of the MRF-Y. With this overall configuration, at I and II floor, it's possible to study the behaviour of two different devices, 1 and 2A, with the same beam-column set.

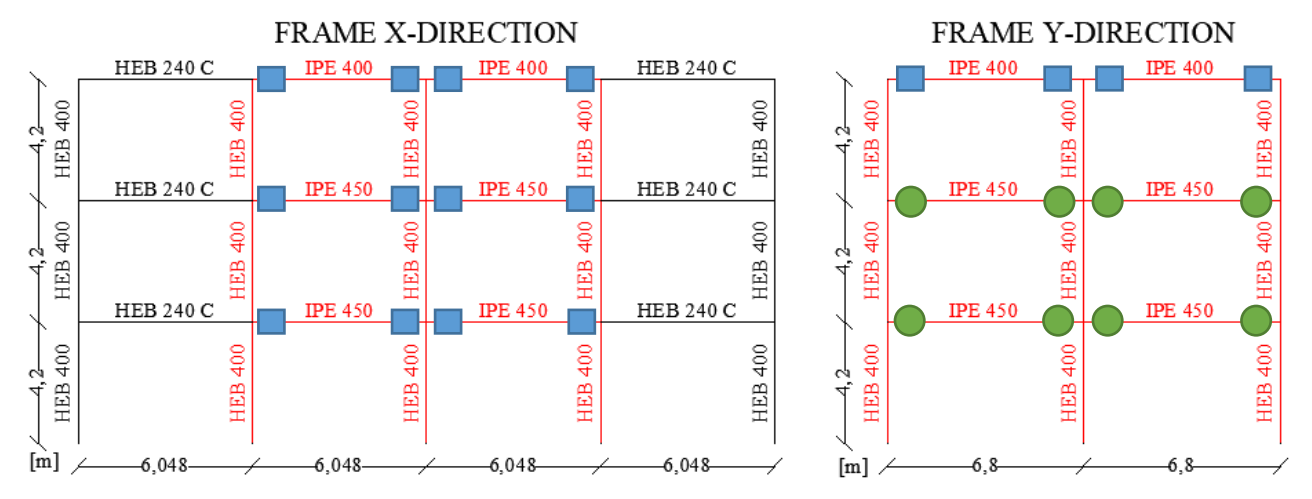


Fig 5: X-MRF (left) and Y-MRF (right), with the equipped FREEDAM devices; DEVICE 1 indicated by the blue square, DEVICE 2A indicated by the green circle

B.Refined FE analyses of beam-to-column joint with FREEDAM devices using ABAQUS

B.1 Modelling assumptions

FE Modelling was used to characterize the actual behaviour of the joint. The finite element (FE) model is developed using the commercial software **Abaqus 2017**. Dynamic implicit solver is used to reproduce the quasi-static behaviour of the investigated beam-to-column joint.

Abaqus has two analysis methods—Abaqus/Standard and Abaqus/Explicit—that it may use to solve structural problems. The implicit analysis approach, which employs numerical methods to solve ordinary and partial differential equations, discretizes the equation of motion by using *reverse Euler time integration*. The solution at a given time step depends on the state of the system at the previous step. Therefore, the state of a system calculated with implicit technique at a particular time step differs from the one calculated by using explicit techniques. Since the static response ignores any transitory behaviour that happens while the loads are being applied to the structure, static analysis can be thought of as implicit. However, solving a non-linear problem may require several iterations. The *constitutive laws* of the materials are represented by means of the engineered curves (true stress-true strain curves) derived by coupon tensile tests. The Elastic Modulus is 210 GPa for generic steel and 130 GPa for bolts. Poisson ratio is 0.3 for generic steel and for bolts. The nonlinear branch of the constitutive law was implemented using a half cycle input method and assuming both nonlinear kinematic and isotropic plastic hardening.

Based on the presented assumptions, analysis is performed in two steps, namely in the first one the preload is applied to the bolts and in the second one a vertical displacement is imposed to the chosen *reference point*. Both steps have a "dynamic implicit" procedure, with "quasi-static" application. The *geometric imperfections* are considered in the Step Module, by switching on the "NIgeom" option.

All the interactions are modelled using surface-tosurface contact formulation. Normal "hard contact" and tangential behaviour are defined for all the interactions, for steel-to-steel interaction a friction coefficient of 0.3 is considered, while the friction dynamic coefficient of the damper device is equal to 0.53, as given by experimental tests. Loads and boundary conditions are applied to reference points, which are representative of the specific crosssection. All the nodes of a certain cross-section are bounded to the corresponding reference point by using a rigid body constrain. Since no plastic deformations are expected in the welded components, full penetration welds are simulated by using Tie constraint that links together surfaces in contact.

The bolt preload is applied to the cross-section of the bolt shank, using the option "Bolt Force" available in

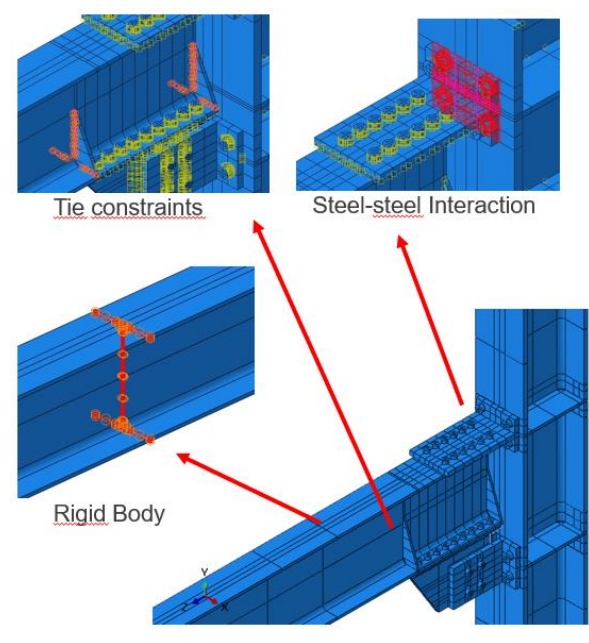


Fig 6: Modelling details

Abaqus/CAE and the magnitude is calculated following the prescription given by Eurocode 3 Part 1-8 (in case of the damper bolts this magnitude is lower, for design reason).

All elements are modelled by using *C3D8I* 8-node linear brick (incompatible modes, first-order integration) an improved version of the C3D8-element. In particular, shear locking is avoided, and volumetric locking is much reduced. This is obtained by supplementing the standard shape functions with so-called bubble functions, which have a zero value at all nodes and nonzero values in between.

The C3D8I element should be used in all instances, in which linear elements are subject to bending. Although the quality of the C3D8I element is far better than the C3D8 element, the best results are usually obtained with quadratic elements (C3D20 and C3D20R), but to lower the computational burden, the choice fell on the C3D8I element.

B.2 FE analyses

This study has concerned a total of eight beam-to-column joints belonging to the moment resisting frames along both global directions of the building. FE Analyses have been carried out on substructure level, on 2D joint assemblies. All the models were calibrated by means of Latour et al. As stated before, the horizontal forces are resisted by two identical MRFs along -X direction and by

As stated before, the horizontal forces are resisted by two identical MRFs along -X direction and by two identical MRFs along -Y direction. In addition, MRF joints of the first floor have the same characteristics (in terms of beam and column profiles, FREEDAM devices, inter-storey height) of the MRF joints of the second floor.

Given these reasons, the analyses have involved:

- Four X-MRF joints, belonging to the III and the II floor
- Four Y-MRF joints, belonging to the III and the II floor

The following table gives an overview of the modelled joints:

| Name | Device | Column | Beam | $F^d_{p,\mathcal{C}}$ [kN] | $f = F_{p,C}^d / F_{p,C}^{EC3}$ [-] | $h_{\scriptscriptstyle S}$ [mm] |
|----------|---------|--------|--------|----------------------------|-------------------------------------|---------------------------------|
| X-III-TJ | D1-0.3 | HEB400 | IPE400 | 57,59 | 0,52 | 570 |
| X-III-XJ | D1-0.3 | HEB400 | IPE400 | 57,59 | 0,52 | 570 |
| X-II-TJ | D1-0.3 | HEB400 | IPE450 | 68,96 | 0,63 | 620 |
| X-II-XJ | D1-0.3 | HEB400 | IPE450 | 68,96 | 0,63 | 620 |
| Y-III-TJ | D1-0.3 | HEB400 | IPE400 | 57,59 | 0,52 | 570 |
| Y-III-XJ | D1-0.3 | HEB400 | IPE400 | 57,59 | 0,52 | 570 |
| Y-II-TJ | D2A-0.4 | HEB400 | IPE450 | 81,43 | 0,47 | 700 |
| Y-II-XJ | D2A-0.4 | HEB400 | IPE450 | 81,43 | 0,47 | 700 |

Tab 2: Overview of the investigated joint assemblies

The joint nomenclature (*joint ID*) is composed by three field *A-NN-JJ* with the following meaning:

- First field (A) indicates the plan direction of the MRF in which the joint is located. This field can be equal to X (-X direction) or Y (-Y direction)
- Second field (NN) indicates the number of the floor where the joint is located. This field can be equal to III (third floor or roof) or II (second floor)
- Third field (JJ) indicates the type of the joint. This field can be equal to TJ (external T-joint) or XJ (internal X-joint).

Joints are equipped with FREEDAM Devices D1 or D2A, in two combinations of steel profiles: HEB400-IPE400 and HEB400-IPE450.

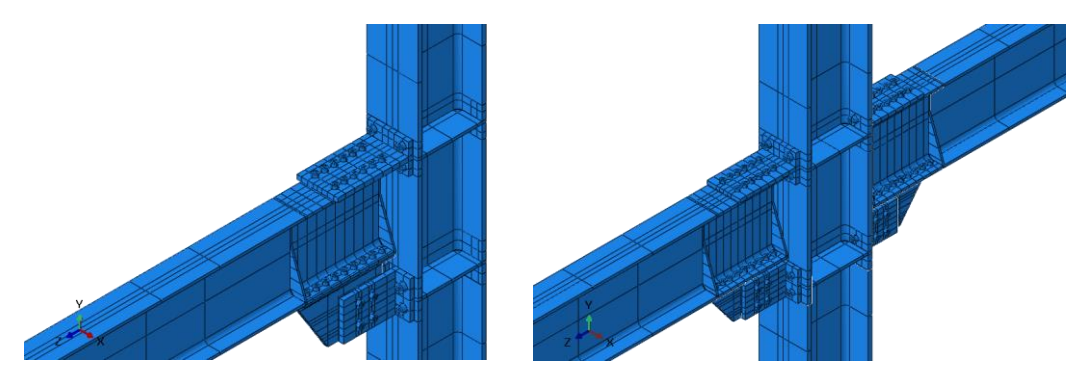


Fig 7: T-joint (left) and X-joint (right) as shown in ABAQUS

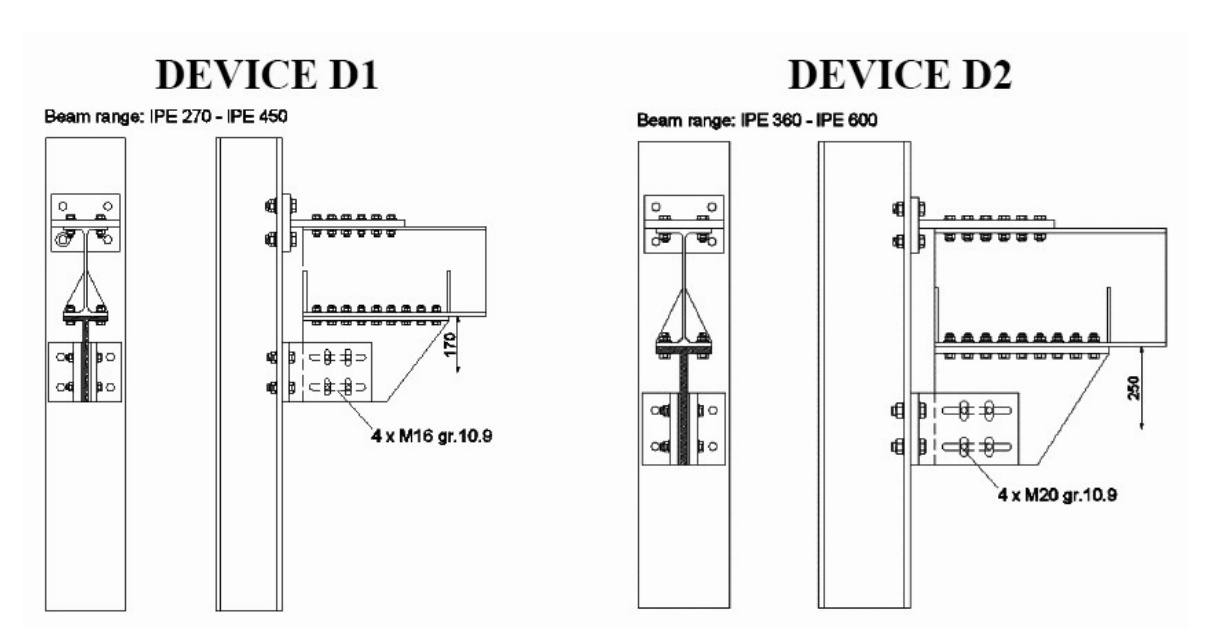


Fig 8: FREEDAM devices used in the DREAMERS building: D1 (left), D2A (right)

Damper bolts are named based on their position on the haunch:

- Bolt 1-1: top row, midspan side
- Bolt 1-2: bottom row, midspan side
- Bolt 2-1: top row, column side
- Bolt 2-2: bottom row, column side



Fig 9: Damper bolts ID

B.3 Loading Scenarios

MRFs 2D joint assemblies have been modelled and tested under monotonic, seismic and column loss scenario.

For each joint assembly, five different types of analyses have been carried out:

- Monotonic Loading "Hogging" (M-HOG): downward imposed displacement of the beam free end, resulting in a Hogging bending moment on the beam, resulting in a negative bending moment on the connection;
- Monotonic Loading "Sagging" (M-SAG): upward imposed displacement of the beam free end, resulting in a Sagging bending moment on the beam, resulting in a positive bending moment on the connection;
- Cyclic Loading (CYC): imposed displacement of the beam free end according to AISC-341 protocol;
- Column Loss "Hogging" (CL-HOG): imposed displacement of the beam free end due to the loss of a nearby column, resulting in a negative bending moment on the connection;

• Column Loss "Sagging" (**CL-SAG**): imposed displacement of the column base due to the loss of the column itself, resulting in a positive bending moment on the connection.

Boundary conditions differ based on the type of Loading Scenario. Beams and columns are taken not in their full length, but based on the zero-value of the bending moment diagram

- For the monotonic, seismic scenarios (M-HOG, M-SAG, CYC):
 - Column length is equal to the sum of the half of the upper inter-storey height and the half of the lower inter-storey height. The column has a pinned base and an horizontal axis rolley on top.
 - Beam length is equal to the half span, where the bending moment is expected to be zero. This point is not restrained in any way. In case on X-joints, displacements on the beam are hemisymmetrical.
- For the Column Loss "Hogging" (CL-HOG):
 - Column length is equal to the sum of the half of the upper inter-storey height and the half of the lower inter-storey height. The column has a pinned base and a rolley on top.
 - Beam length is equal to the half span, where the bending moment is expected to be zero. The beam which is connected to the column that fails is restrained with a horizontal axis roller in order to compute the axial action on the beam. In case of X-joints, the other beam is restrained by an horizontal axis double-rolley.
- For the Column Loss "Sagging" (CL-SAG):
 - Column length is equal to the sum of the half of the upper inter-storey height and the half of the lower inter-storey height. The column has no a free end at the base and a rolley on top.
 - Each beam has a length equal to the entire span, with a fixed end in order to simulate the constraint of the joints.

The first three analyses represent the <u>Seismic Scenario</u>, while the last two analyses represent the <u>Robustness Scenario</u>.

In case of the Cyclic Loading Scenario, AISC-341 loading protocol "Loading Sequence for Beam-to-Column Moment Connections" is used.

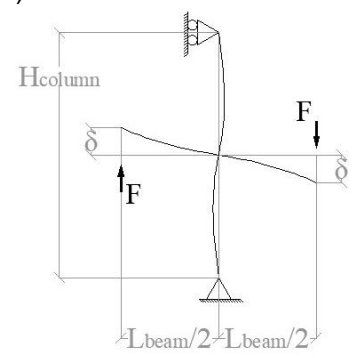


Fig 10: boundary conditions for M-HOG, M-SAG, CYC scenarios

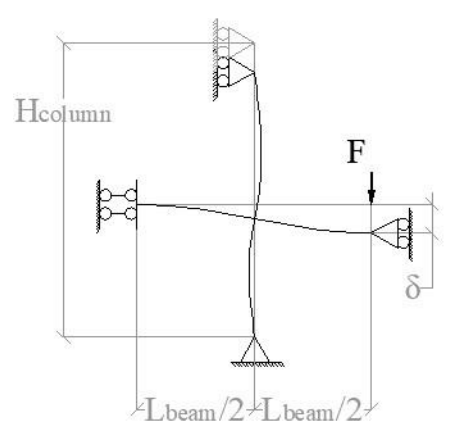


Fig 11: boundary condition for CL-HOG

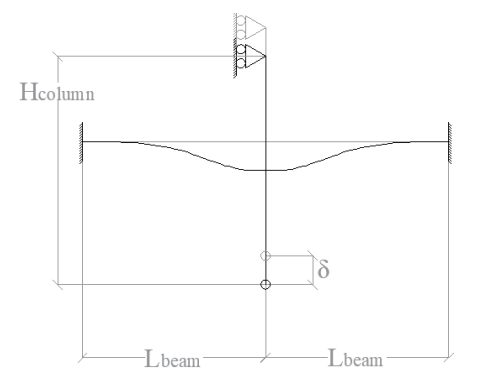


Fig 12: boundary condition for CL-SAG

- (1) 6 cycles at $\theta = 0,00375$ rad;
- (2) 6 cycles at $\theta = 0,005 \text{ rad}$;
- (3) 6 cycles at $\theta = 0,0075 \text{ rad};$
- (4) 4 cycles at $\theta = 0.01$ rad;
- (5) 2 cycles at $\theta = 0.015$ rad;
- (6) 2 cycles at $\theta = 0.02$ rad;
- (7) 2 cycles at $\theta = 0.03$ rad;
- (8) 2 cycles at $\theta = 0.04$ rad;

Continue loading at increments of $\theta = 0.01$ rad, with two cycles of loading at each step.

Fig 13: AISC-341 cyclic protocol

B.5 Detailed analysis of the X-II-XJ joint

In this chapter a detailed analysis of a MRF joint of the DREAMERS building is shown. The selected joint is the X-II-XJ, it is located on the X-MRF, II floor (II), X-joint configuration (XJ). The joint is equipped with a FREEDAM DEVICE 1, with a bending capacity level equal to 0.3, HEB400 as column profile, IPE450 as beam profile.

The design bending moment resistance of the joint is 181 kNm.

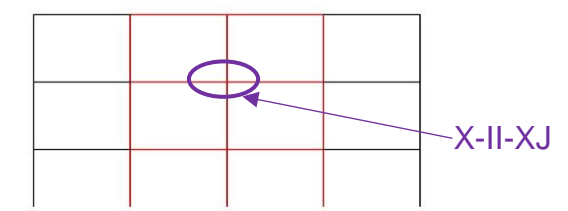


Fig 14: Selected joint with its location on the X-MRF

B.5.1 Monotonic Loading

Bending moment-chord rotation diagrams show a stable response curve both in Hogging and Sagging, with a plateau very close to the bending moment design resistance of the connection up to 0.06 rad of rotation. The lower resistance of the Sagging scenario is given by the high deformability of the L-stubs in tension, which causes a loss of clamping in the bolts.

Under hogging bending moment, after 0.06 rad the bolts of the device go in contact with the slotted holes surfaces of the haunch, while the haunch itself is pushing on the column flange. As a result, the device doesn't work properly anymore, and the *bending moment-rotation* curve shows an increase of stiffness: the damage extends also to structural parts.

Under sagging bending moment, the issue is similar since the damper bolts go in contact with the slotted holes of the haunch.

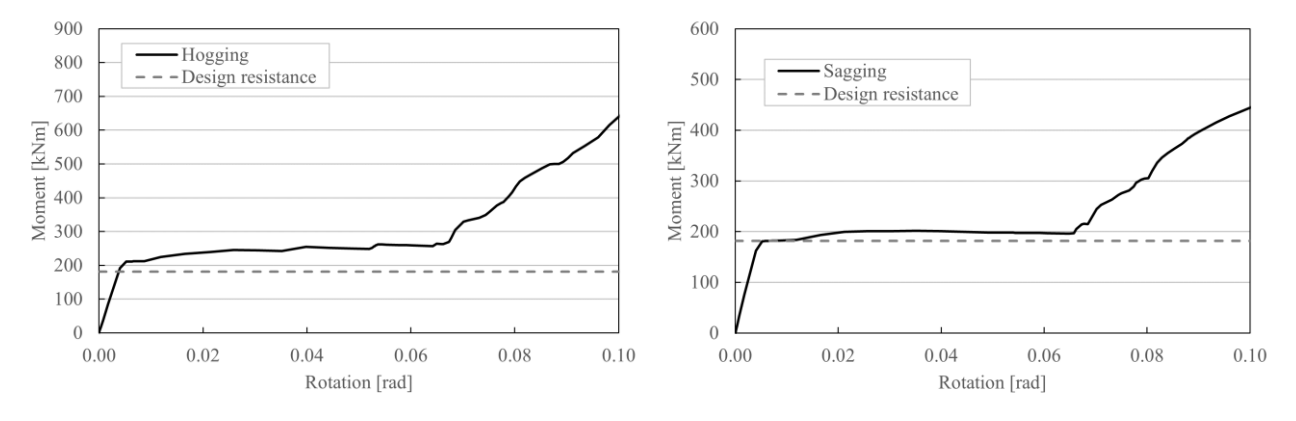


Fig 15: Bending moment-rotation diagrams; in hogging (left) and in sagging (right)

Regarding the friction device, *preload force-rotation* diagram shows that damper bolts are able to maintain the preload up to 0.06 of rotation under both the monotonic Loading Conditions. The first bolt that start losing its preload differs between the two scenarios: in case of hogging bending moment *Bolt 1-2* (bottom bolt row, midspan side) fails first, while in case of sagging bending moment *Bolt 2-2* (bottom bolt, column side) fails first.

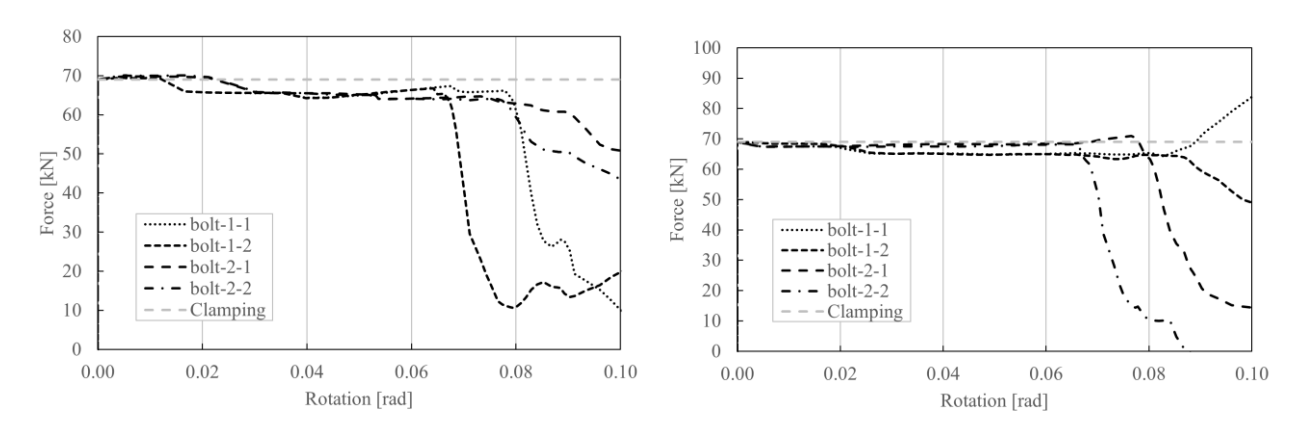


Fig 16: Evolution of the Preload Force in the damper bolts; in hogging (left) and in sagging (right)

Von Mises stress distribution and the equivalent plastic strain distributions can be useful to visualize what it's happening to the joint. The point of rotation on the T-stub web is clearly visible, as well as the sliding mechanism offered by the device. The lever arm of the connection is, as said before, the distance between the centre of damper bolts and the upper flange of the column.

Von Mises stress distribution shows:

- In Hogging, the formation of a diagonal tie at the end of the beam, which is coupled with a compressive diagonal strut on the haunch
- In Sagging, the opening of the L-stubs, with the runaway of the haunch, restrained only by damper bolts close to the column

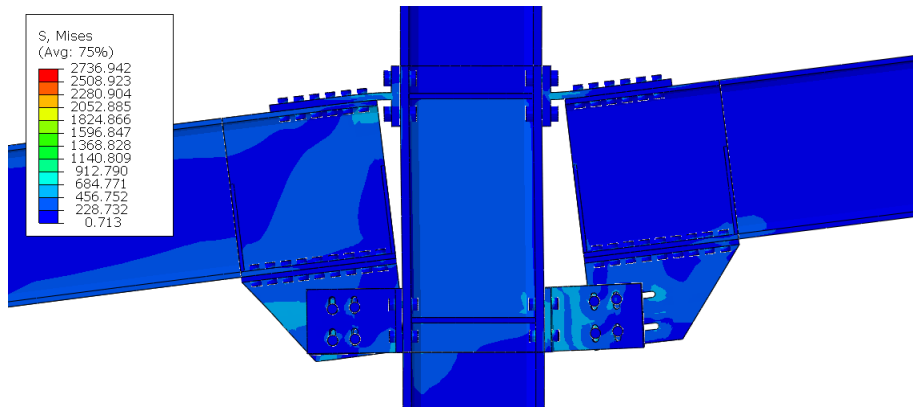


Fig 17: M-HOG Scenario (left) and M-SAG Scenario (right) Von Mises stress distributions

PEEQ (equivalent plastic deformation) distribution shows no damage in the structural part of the joint (beam and column), validating the "FREE from DAMage" behaviour of the connection. The only damage registered by the software is located on the components of the devices, which are easily replaceable.

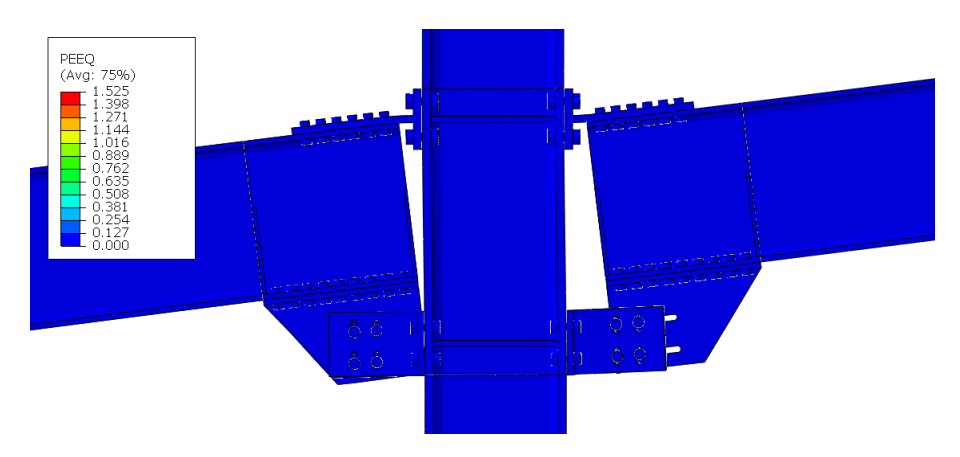


Fig 18: M-HOG Scenario (left) and M-SAG Scenario (right) PEEQ distributions

B.5.2 Cyclic Loading

Hysteretic cycles are registered thanks to the *bending moment-chord rotation* diagram. Joint exhibits a very stable cyclic behaviour with a regular and stable shape of hysteretic cycles, allowing the friction pads to dissipate energy while all the other components of the assembly remain within the elastic range. The slight asymmetry of the cycles, with the hogging side wider than the sagging side, is still due to the greater deformability of the L-stubs in tension (as stated in the previous paragraph). Joint can successful reach rotation of 0,05 rad. For the Von Mises stress and PEEQ distributions is still valid what it was said for the Monotonic Loading Scenarios.

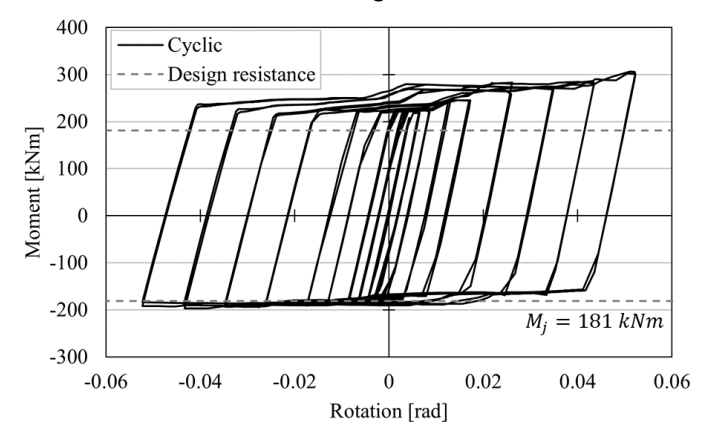


Fig 19: Cyclic response

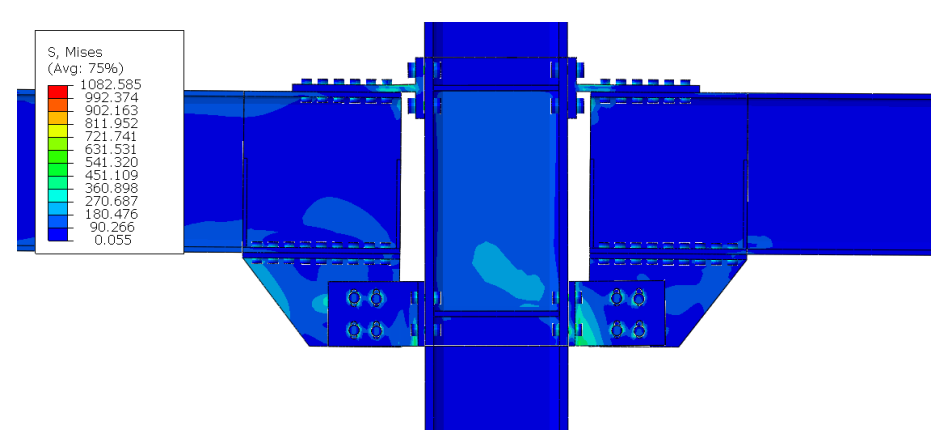


Fig 20: Von Mises stress distribution

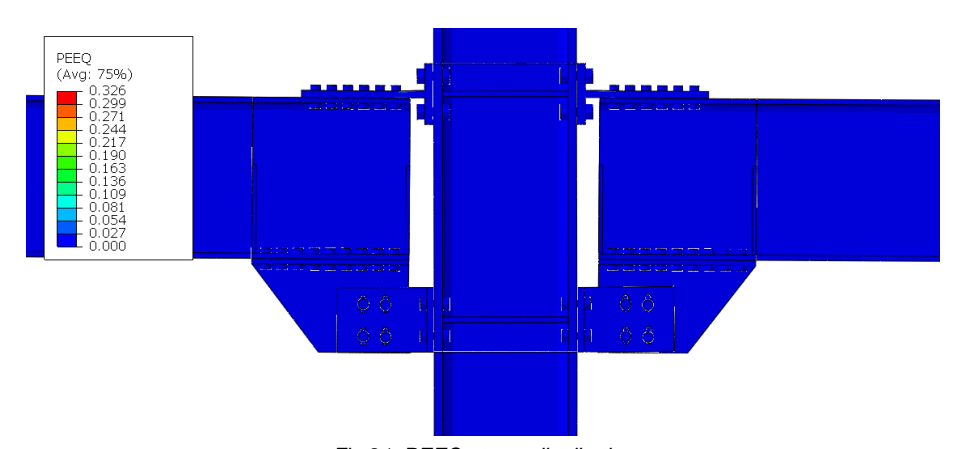


Fig 21: PEEQ stress distribution

B.5.3 Column Loss "Hogging"

In this Scenario large displacement are involved, so it's reasonable to compute the second-order bending moment, defined previously. The horizontal displacement of the beams end is restrained and then beams are now subjected to a tensile axial load, responsible of the catenary effect. In the hogging moment-rotation diagram is possible to see this catenary effect, that gives a big contribution in terms of resistance already for small rotations, when confronted with the Monotonic Hogging Loading Scenario.

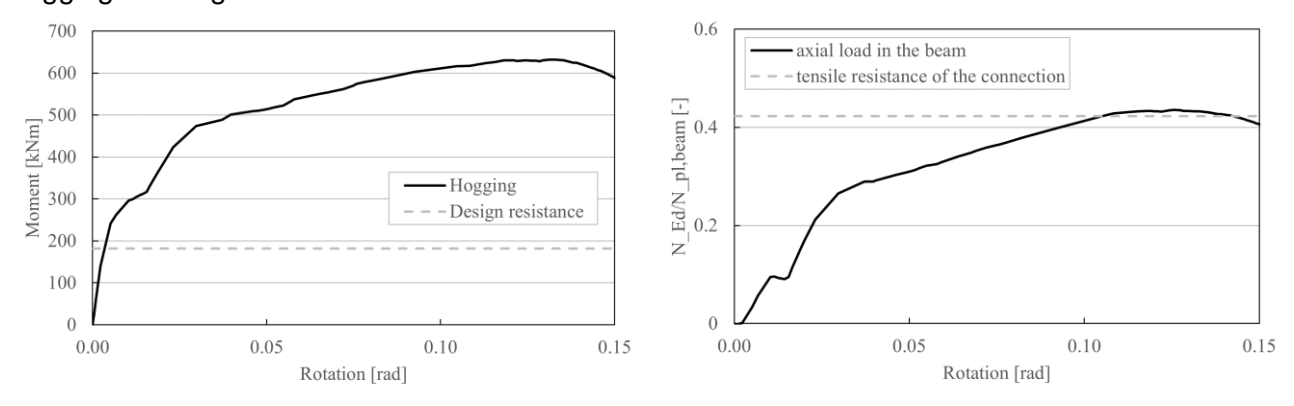


Fig 22: Bending moment-rotation curve (left); non-dimensional axial load in the beam-rotation diagram (right)

The evolution of the external axial force is here divided by the axial plastic resistance of the connected beam. It has to be noted that the maximum external axial force can be estimated as $N_{Ed} = 0.4N_{pl,Rd,beam}$. Numerical simulations have proven that this relation between acting axial force and axial resistance of the connected beam can be used as a general rule, and it can be used also for the other joints.

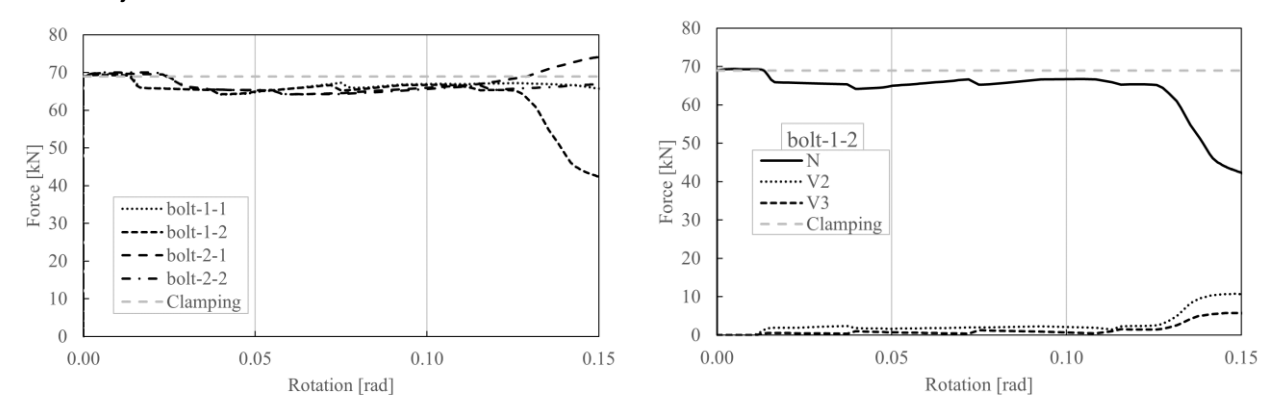


Fig 23: Evolution of the Preload Force in the damper bolts (left); evolution of the component forces in the bolt-1-2 (right)

By looking at the FE results it becomes obvious what part of the entire connection fails first. The upper T-stub is characterized by a brittle Failure Mode 2 (very close to Failure Mode 3). This aspect will be further investigated later in the document.

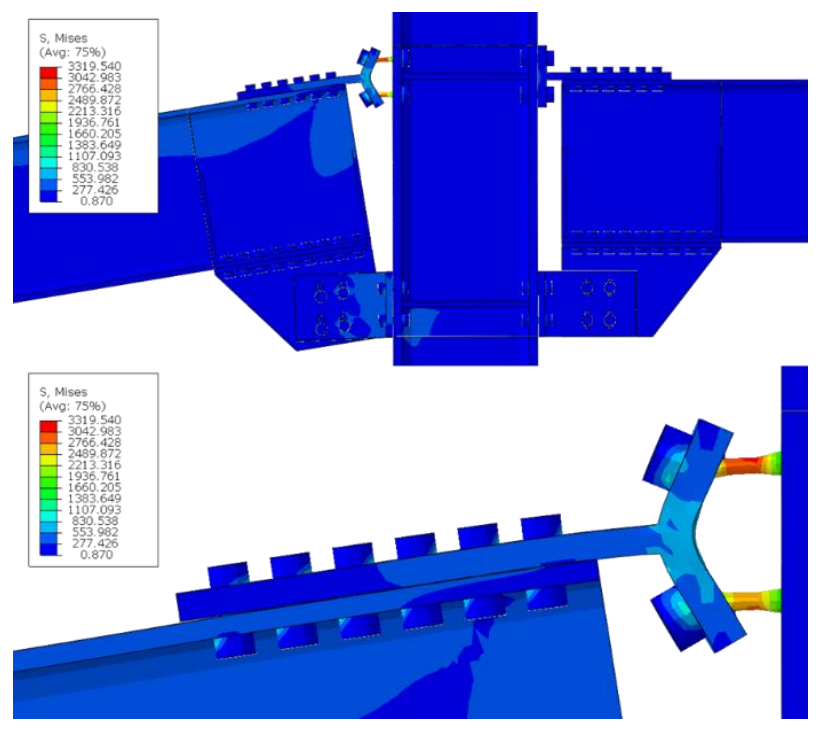


Fig 24: Von Mises stress distribution, with detail of the T-stub

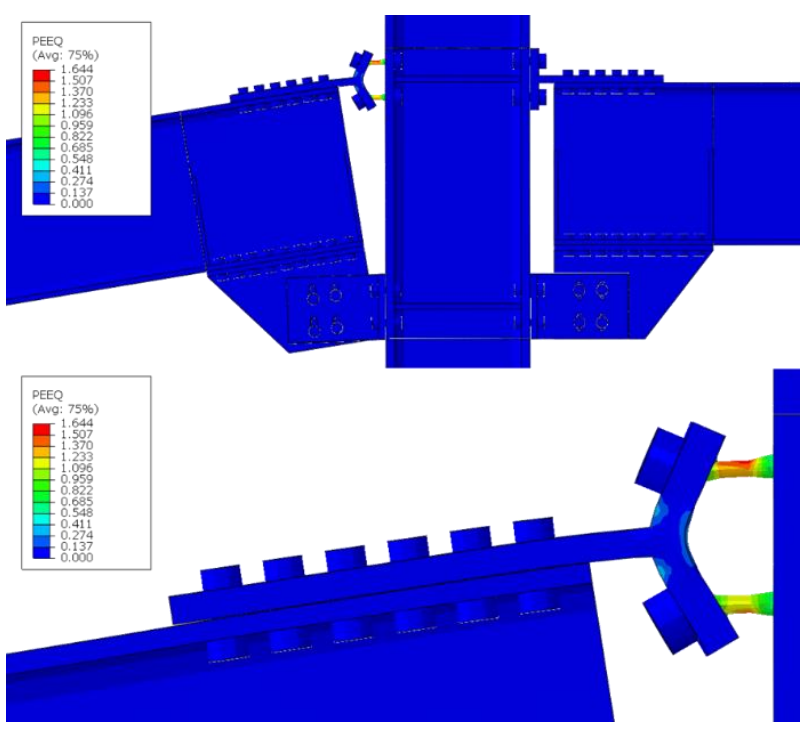


Fig 25: PEEQ distribution, with detail of the T-stub

B.5.4 Column Loss "Sagging"

Under the Sagging Column Loss Scenario, the *bending moment-rotation* diagram shows a very steep curve with a plateau of around 1000 kNm. After the 6 mrad of rotation a small increase of stiffness is registered, caused by the contact between the damper bolts and the haunch. From the *axial load in the beam-rotation* diagram it's possible to distinguish two different phases: initially the beam is compressed, as a result of a small arch effect, then after 6 mrad of rotation beam is subject to a tensile force corresponding to a catenary effect. It has to be noted that now the beam end facing the column pushed the haunch: the damper bolts are in contact with the slotted hole of the haunch and the device has extinguish its stroke.

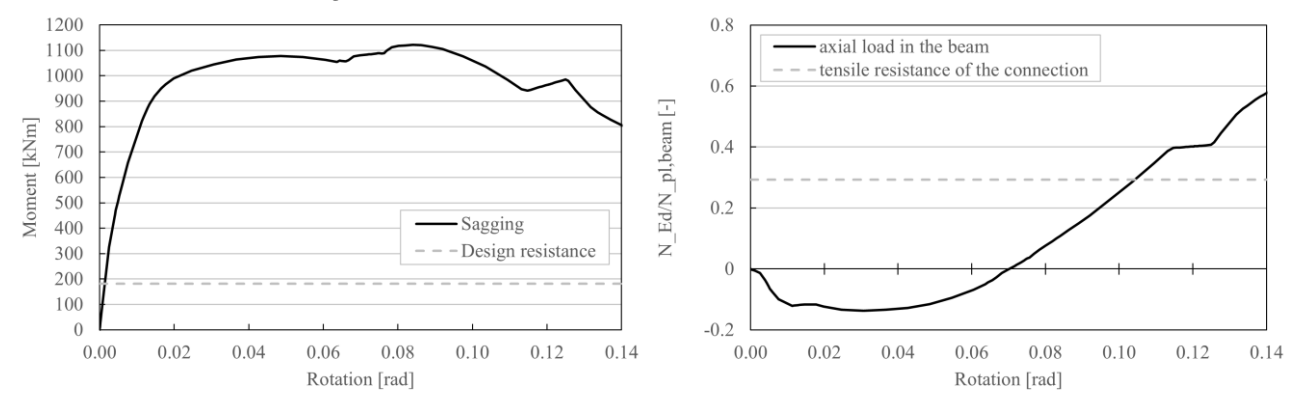


Fig 26: Bending moment-rotation curve (left); a-dimensional axial load acting on the beam-rotation curve (right)

Preload force in the damper bolts is stable up to 6% or rotation and then damper bolts *Bolt 2-1* and *Bolt 2-2* (close to the column) start to lose their clamping capacity.

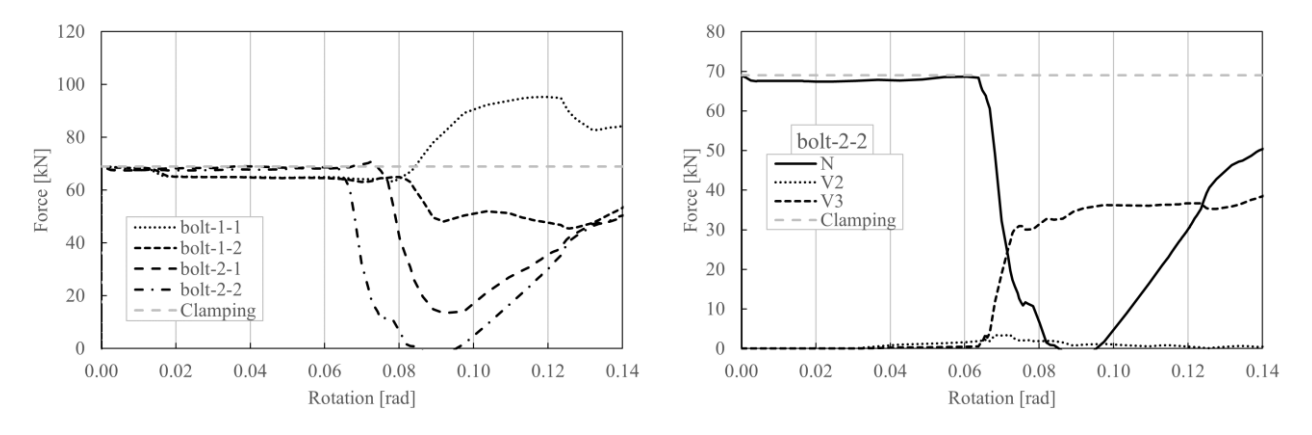


Fig 27: Evolution of the Preload Force in the damper bolts (left); evolution of the component forces in the bolt-2-2 (right)

Von Mises stress distribution shows that the slotted holes of the haunch and the damper bolts are heavily loaded since they come in contact. Haunch is characterized by bearing, while the damper bolts close to the column are subject to a combined action of shear and bending.

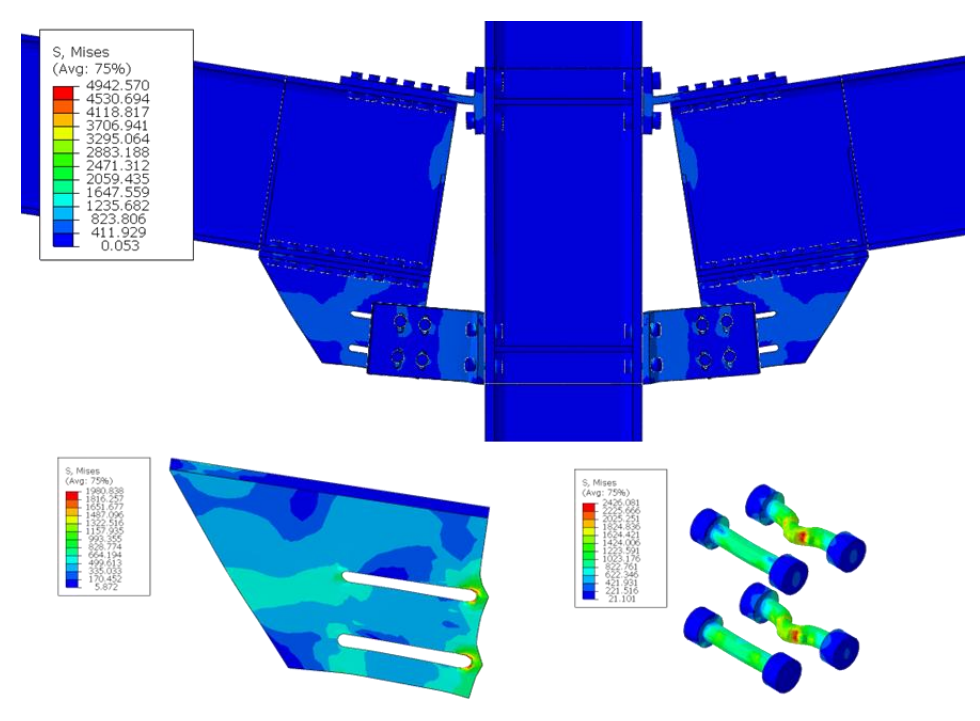


Fig 28: Von Mises stress distribution, with haunch and damper bolts in detail

PEEQ distribution shows that the aforementioned parts are subject to high plastic deformations.

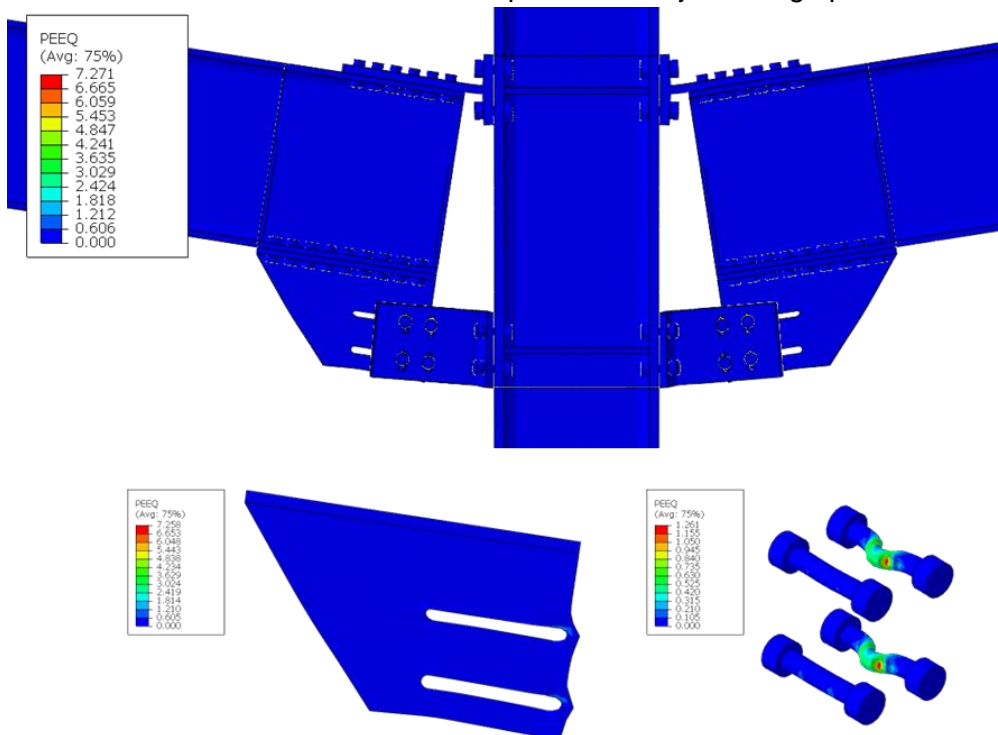


Fig 29: PEEQ distribution, with haunch and damper bolts in detail

B.6 FE analyses of the other MRF joints

FE analyses results of the remaining MRF joints of the DREAMERS building are here reported. All joints show the same behaviour of the already discussed X-II-XJ joint.

B.6.1 X-III-TJ

The joint is the X-III-TJ, located on the X-MRF, III floor, T-joint configuration. The joint is equipped with a FREEDAM DEVICE 1, with a bending capacity level equal to 0.3, HEB400 as column profile, IPE400 as beam profile.

The design bending moment resistance of the joint is 139 kNm.

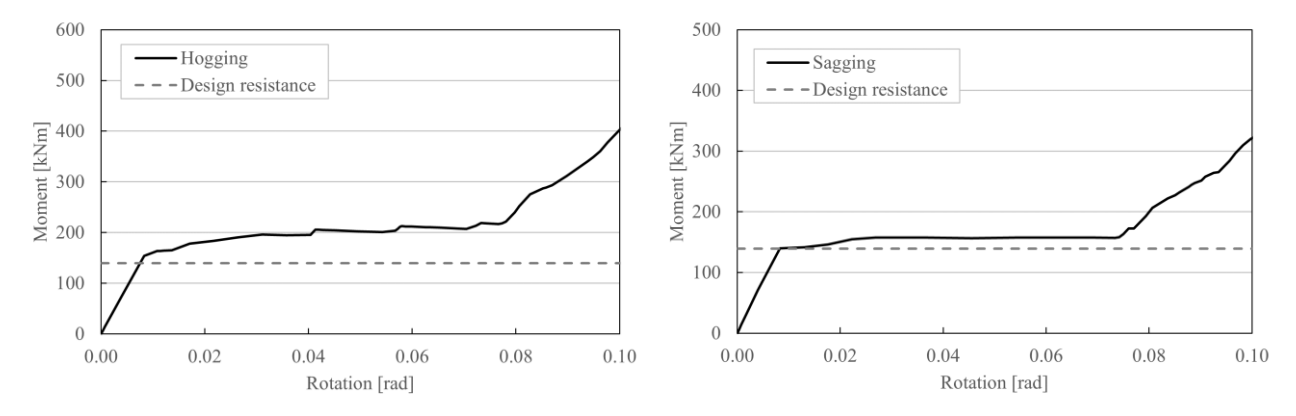


Fig 30: Monotonic Loading: bending moment-rotation diagrams in hogging (left) and in sagging (right)

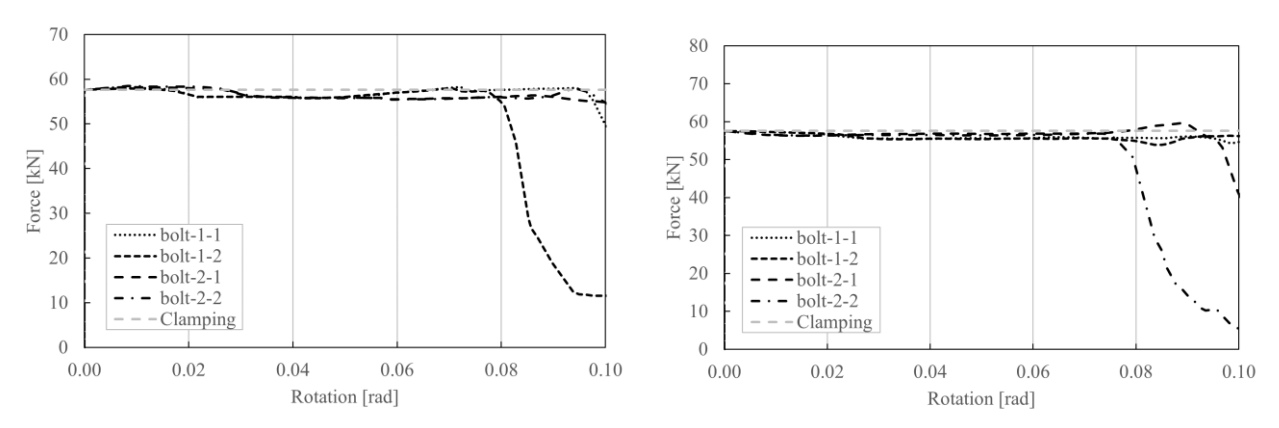


Fig 31: Monotonic Loading: evolution of the Preload Force in the damper bolts in hogging (left) and in sagging (right)

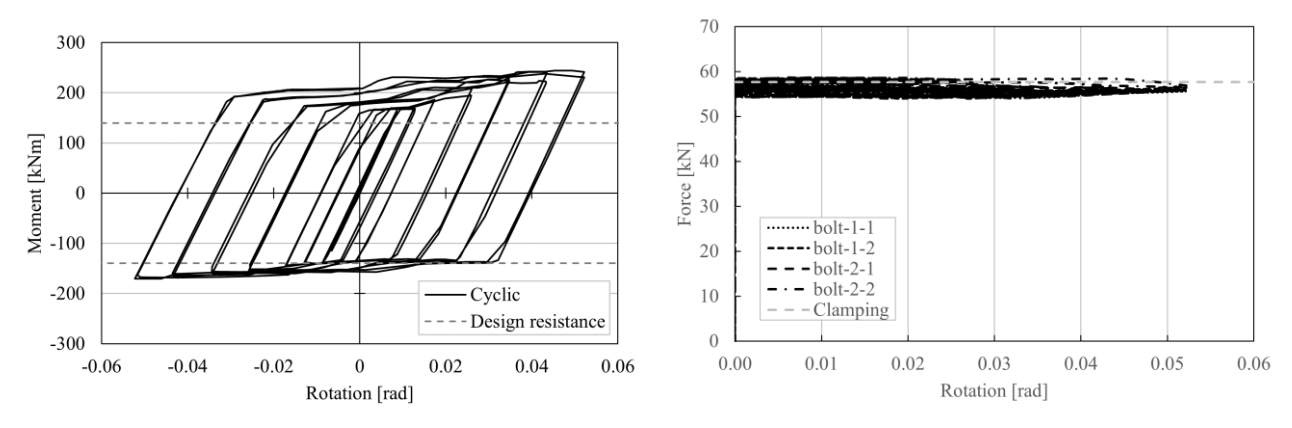


Fig 32: Cyclic Loading: cyclic response (left) and evolution of the Preload Force in the damper bolts (right)

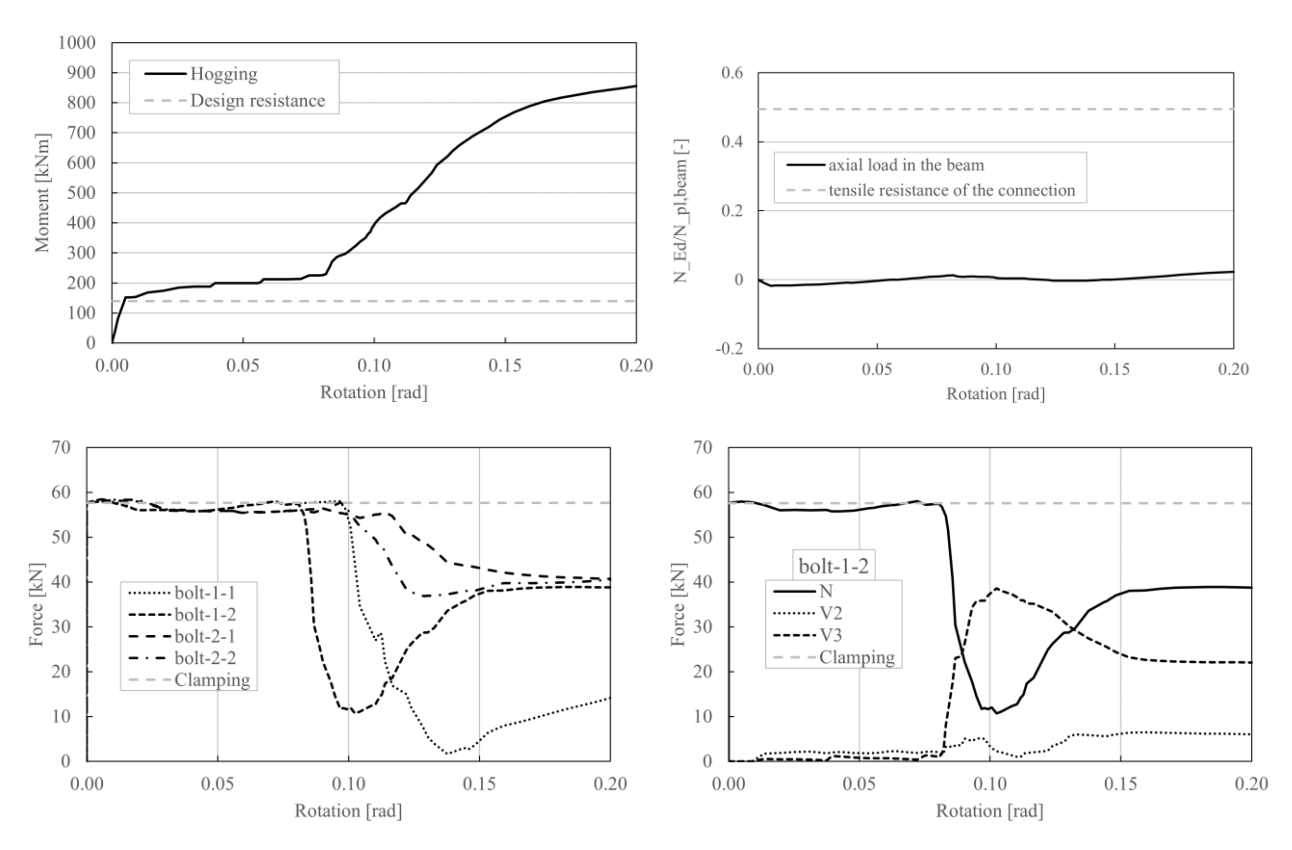


Fig 33: Column Loss "Hogging"; bending moment-rotation curve (up-left); non-dimensional axial load in the beam-rotation diagram (up-right); evolution of the Preload Force in the damper bolts (bottom-left); evolution of component forces in the bolt-1-2(bottom-right)

B.6.2 X-III-XJ

The joint is the X-III-XJ, located on the X-MRF, III floor, X-joint configuration. The joint is equipped with a FREEDAM DEVICE 1, with a bending capacity level equal to 0.3, HEB400 as column profile, IPE400 as beam profile.

The design bending moment resistance of the joint is 139 kNm.

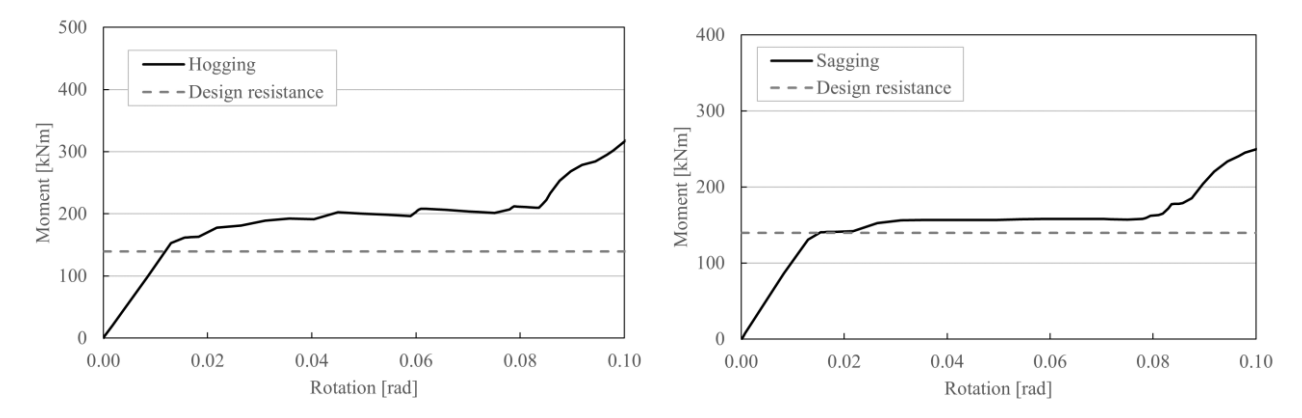


Fig 34: Monotonic Loading: bending moment-rotation diagrams in hogging (left) and in sagging (right)

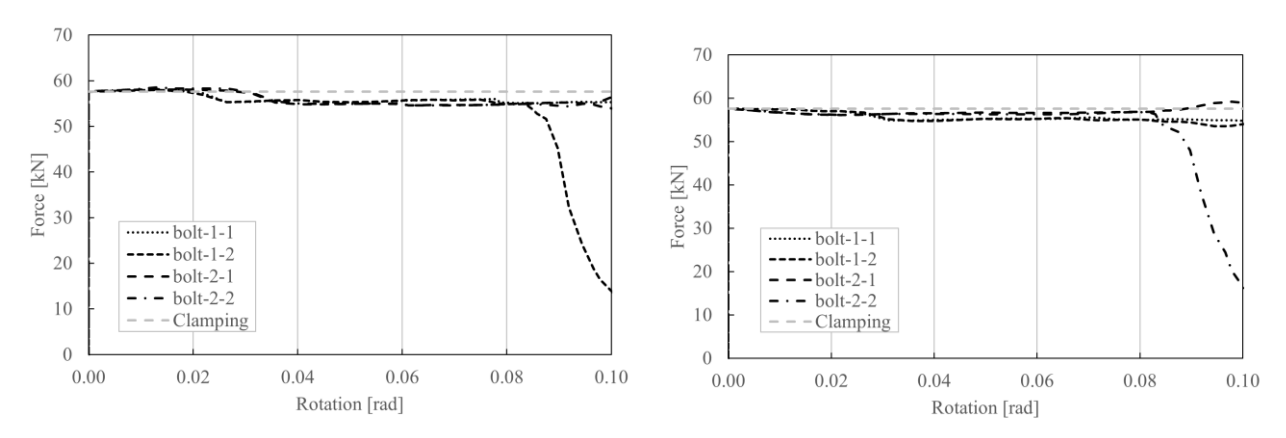


Fig 35: Monotonic Loading: evolution of the Preload Force in the damper bolts in hogging (left) and in sagging (right)

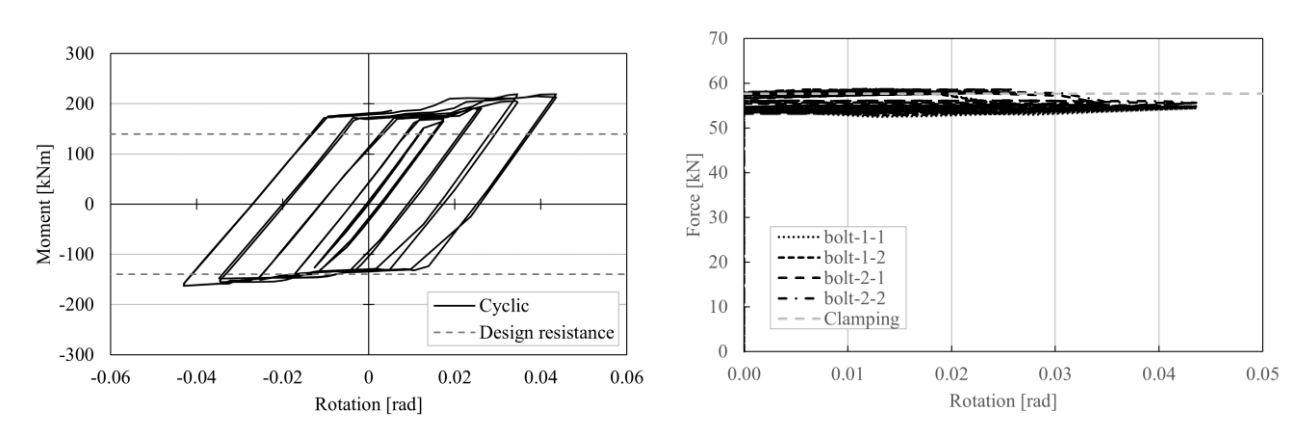


Fig 36: Cyclic Loading: cyclic response (left) and evolution of the Preload Force in the damper bolts (right)

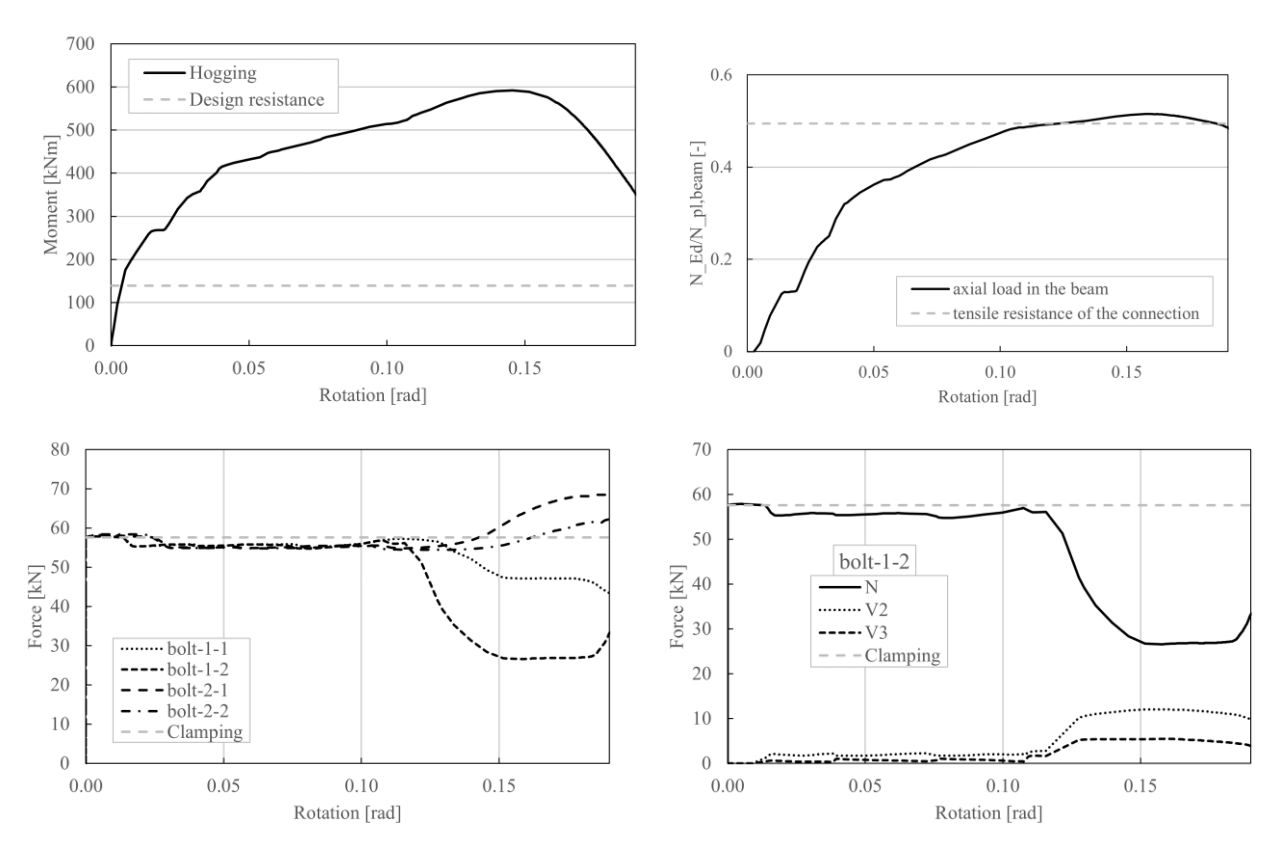


Fig 37: Column Loss "Hogging"; bending moment-rotation curve (up-left); non-dimensional axial load in the beam-rotation diagram (up-right); evolution of the Preload Force in the damper bolts (bottom-left); evolution of component forces in the bolt-1-2(bottom-right)

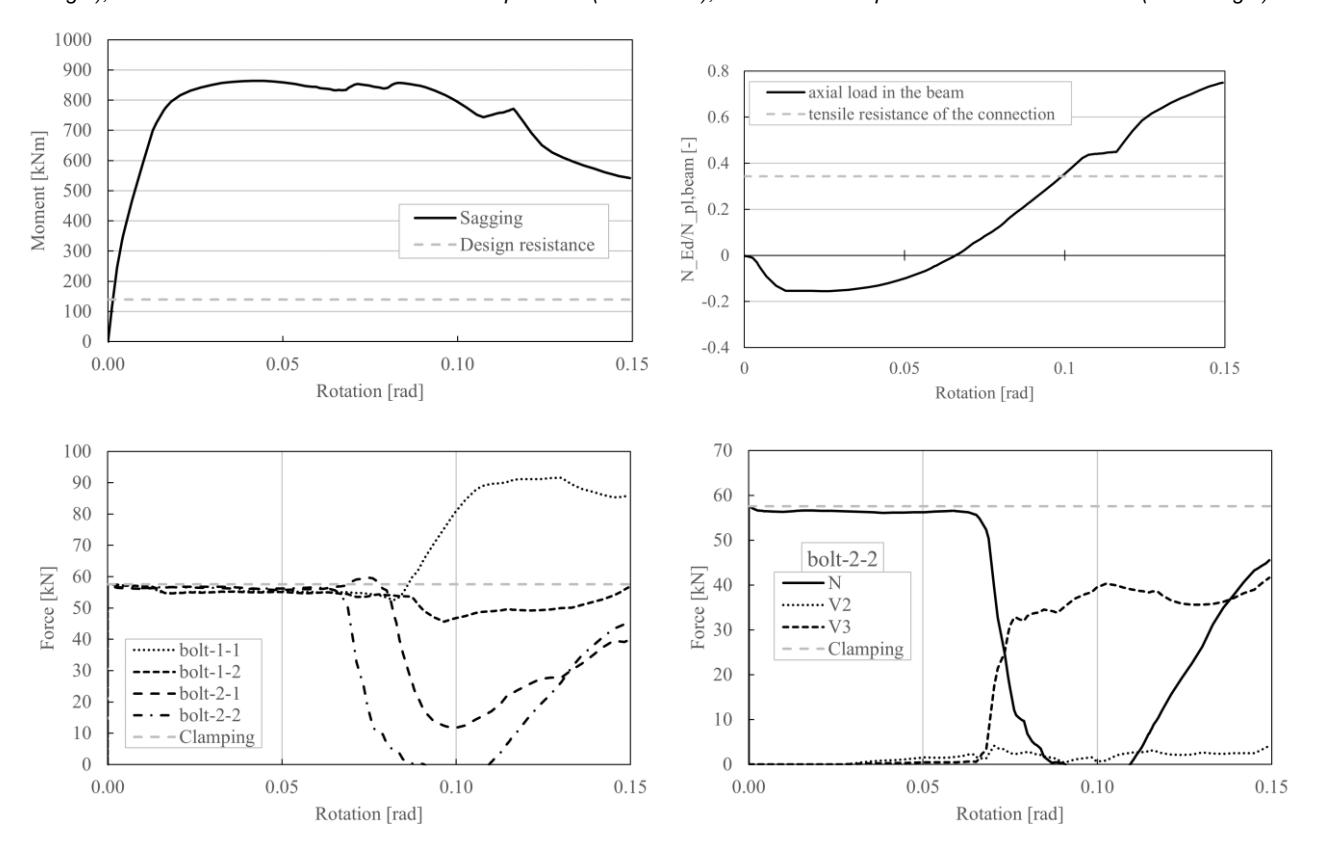


Fig 38: Column Loss "Sagging"; bending moment-rotation curve (up-left); non-dimensional axial load in the beam-rotation diagram (up-right); evolution of the Preload Force in the damper bolts (bottom-left); evolution of component forces in the bolt-2-2(bottom-right)

B.6.3 X-II-TJ

The joint is the X-II-TJ, located on the X-MRF, II floor, T-joint configuration. The joint is equipped with a FREEDAM DEVICE 1, with a bending capacity level equal to 0.3, HEB400 as column profile, IPE450 as beam profile.

The design bending moment resistance of the joint is 181 kNm.

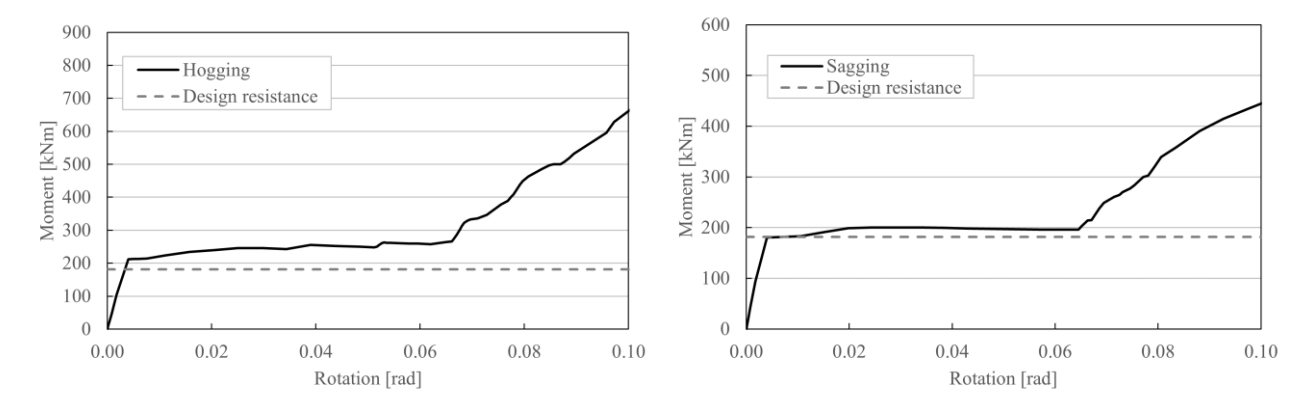


Fig 39: Monotonic Loading: bending moment-rotation diagrams in hogging (left) and in sagging (right)

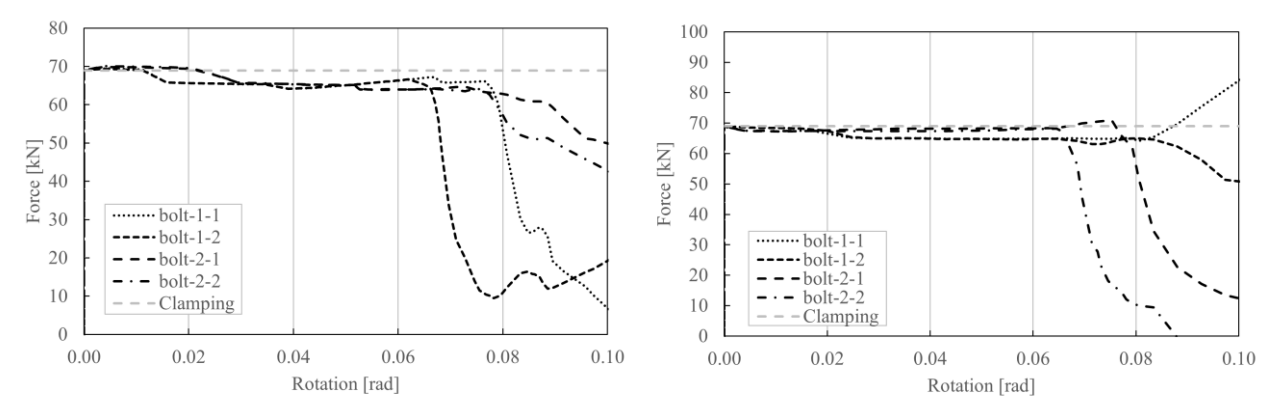


Fig 40: Monotonic Loading: evolution of the Preload Force in the damper bolts in hogging (left) and in sagging (right)

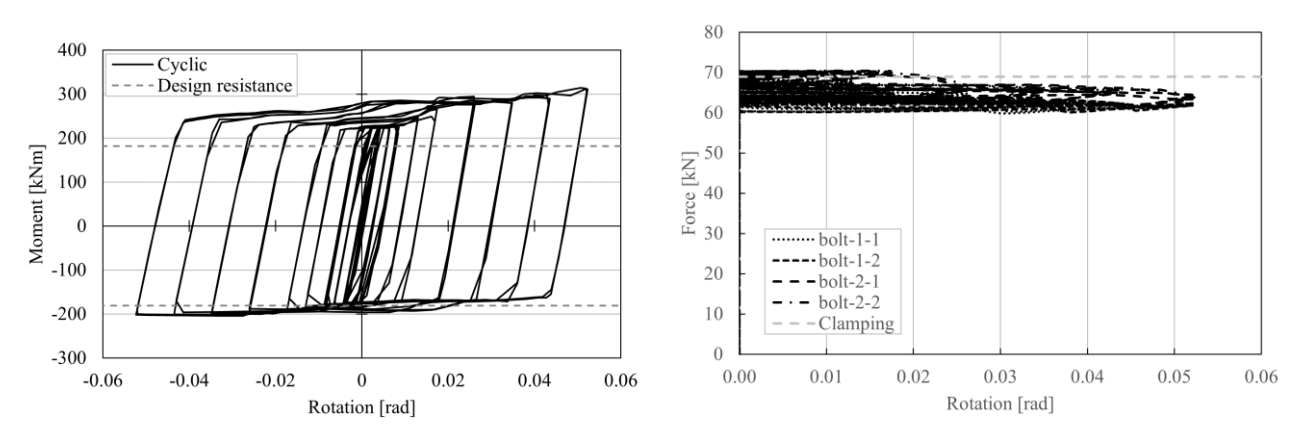


Fig 41: Cyclic Loading: cyclic response (left) and evolution of the Preload Force in the damper bolts (right)

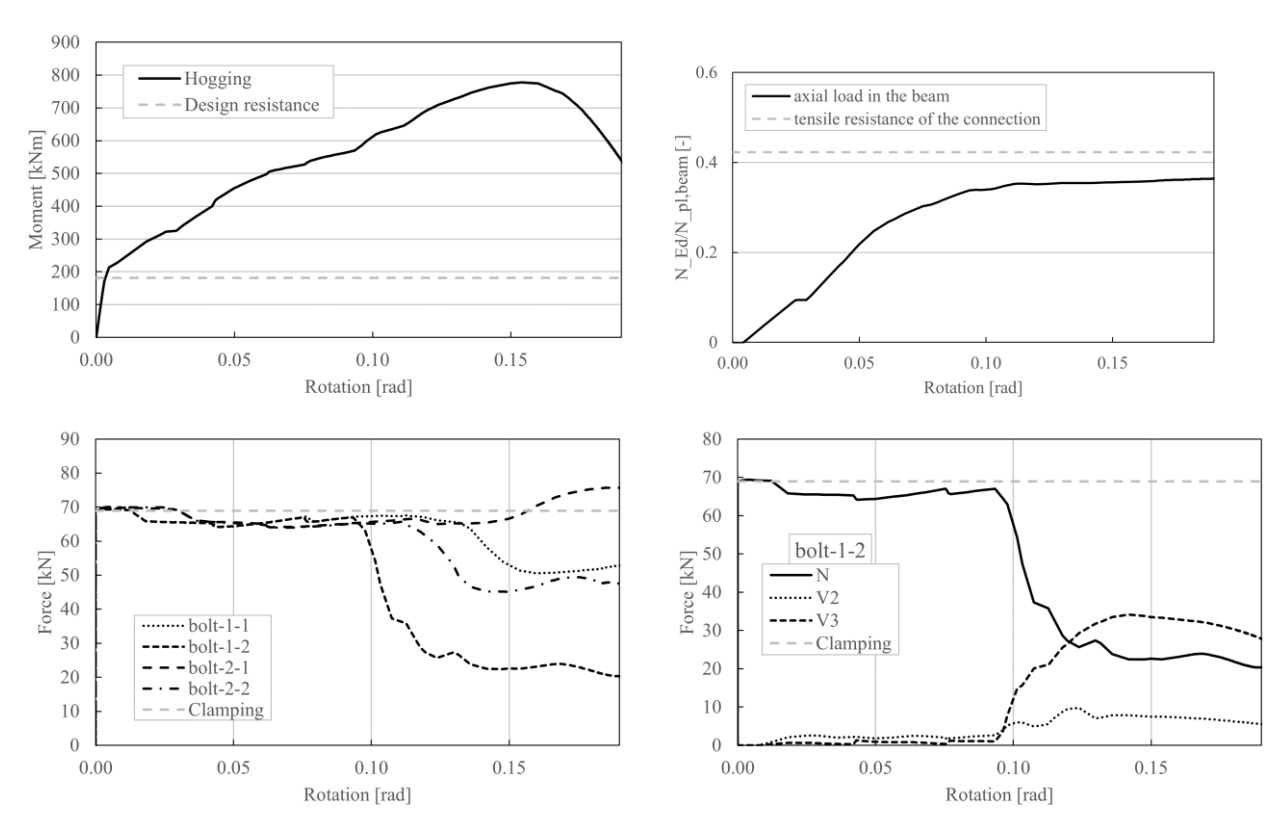


Fig 42: Column Loss "Hogging"; bending moment-rotation curve (up-left); non-dimensional axial load in the beam-rotation diagram (up-right); evolution of the Preload Force in the damper bolts (bottom-left); evolution of component forces in the bolt-1-2(bottom-right)

B.6.4 Y-III-TJ

The joint is the Y-III-TJ, located on the Y-MRF, III floor, T-joint configuration. The joint is equipped with a FREEDAM DEVICE 1, with a bending capacity level equal to 0.3, HEB400 as column profile, IPE400 as beam profile.

The design bending moment resistance of the joint is 139 kNm.

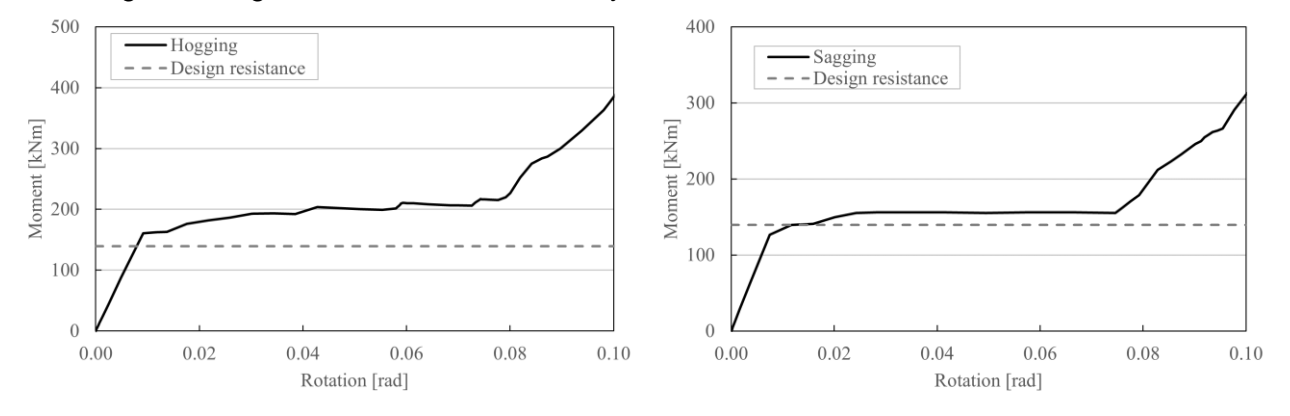


Fig 43: Monotonic Loading: bending moment-rotation diagrams in hogging (left) and in sagging (right)

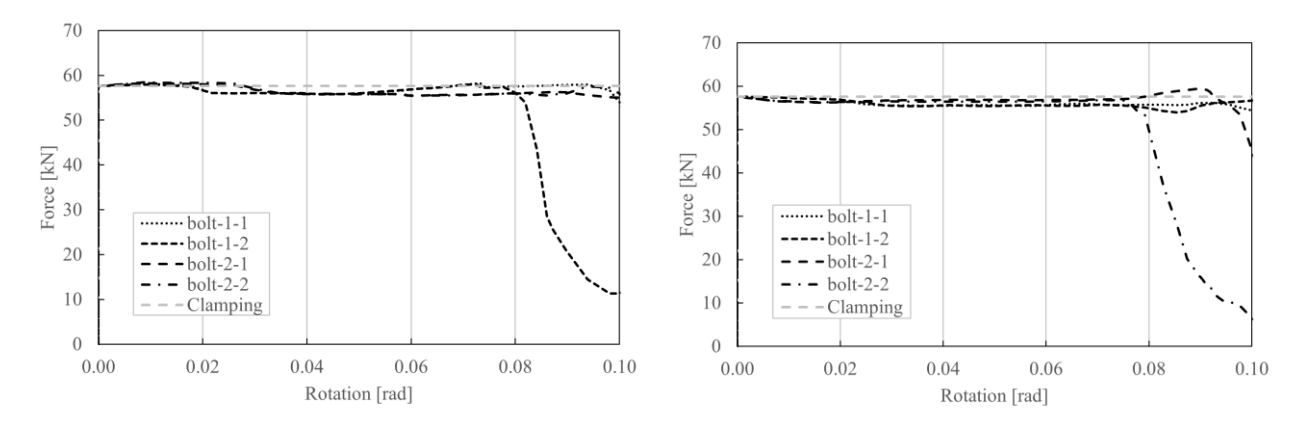


Fig 44: Monotonic Loading: evolution of the Preload Force in the damper bolts in hogging (left) and in sagging (right)

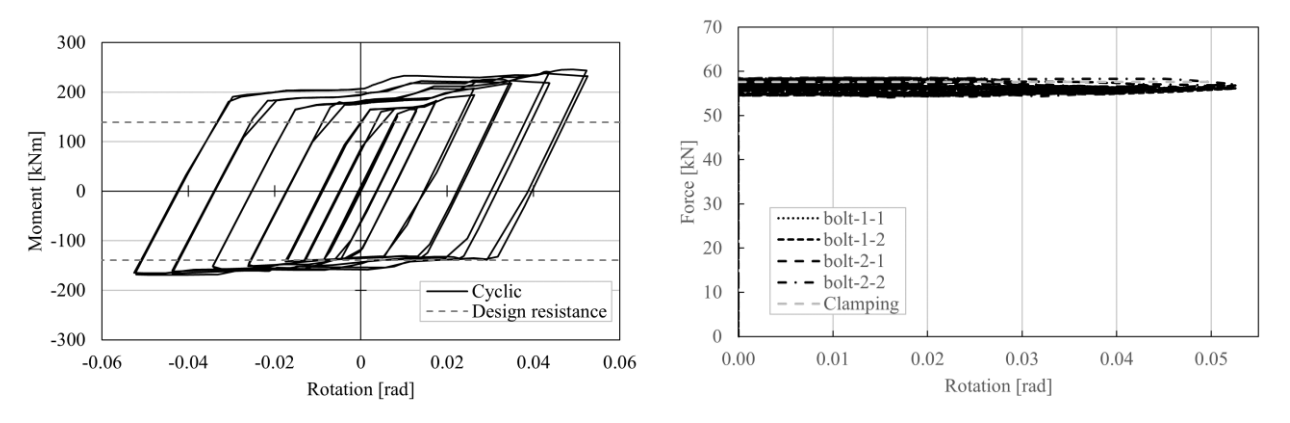


Fig 45: Cyclic Loading: cyclic response (left) and evolution of the Preload Force in the damper bolts (right)

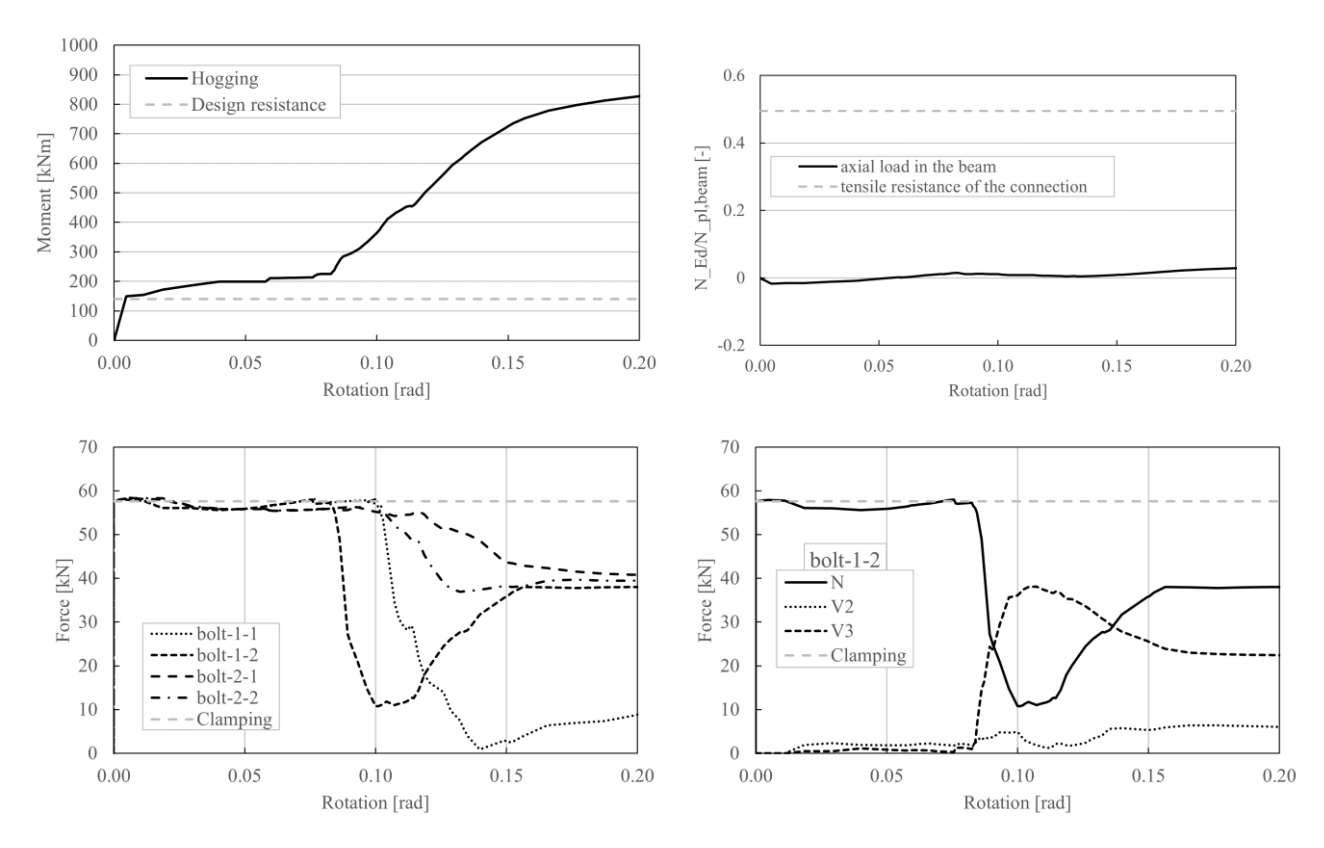


Fig 46: Column Loss "Hogging"; bending moment-rotation curve (up-left); non-dimensional axial load in the beam-rotation diagram (up-right); evolution of the Preload Force in the damper bolts (bottom-left); evolution of component forces in the bolt-1-2(bottom-right)

B.6.5 Y-III-XJ

The joint is the Y-III-XJ, located on the Y-MRF, III floor, X-joint configuration. The joint is equipped with a FREEDAM DEVICE 1, with a bending capacity level equal to 0.3, HEB400 as column profile, IPE400 as beam profile.

The design bending moment resistance of the joint is 139 kNm.

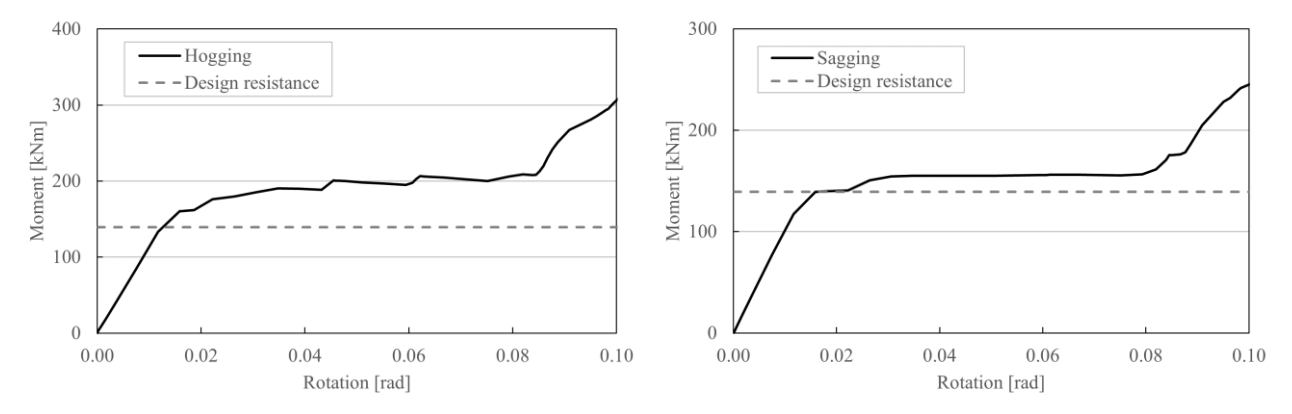


Fig 47: Monotonic Loading: bending moment-rotation diagrams in hogging (left) and in sagging (right)

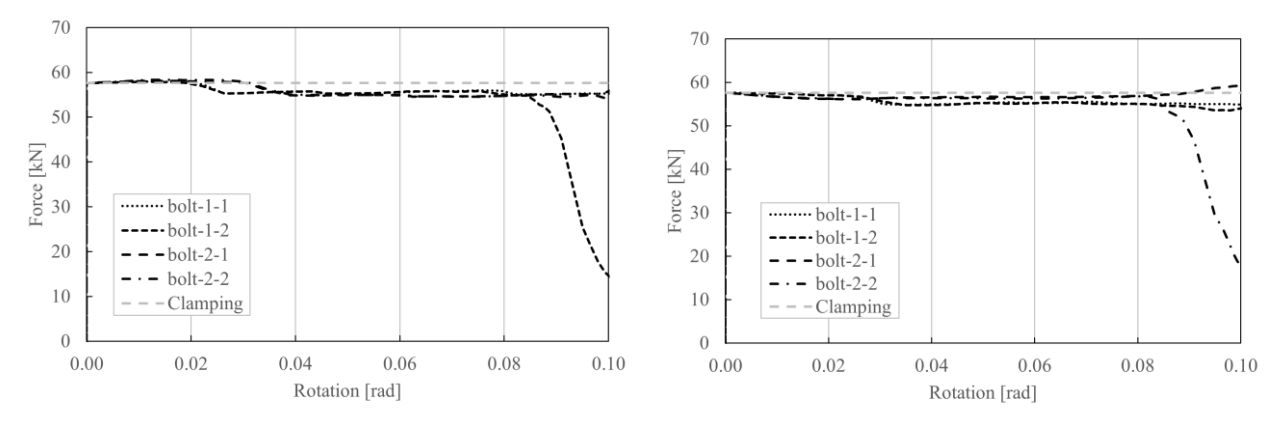


Fig 23: Monotonic Loading: evolution of the Preload Force in the damper bolts in hogging (left) and in sagging (right)

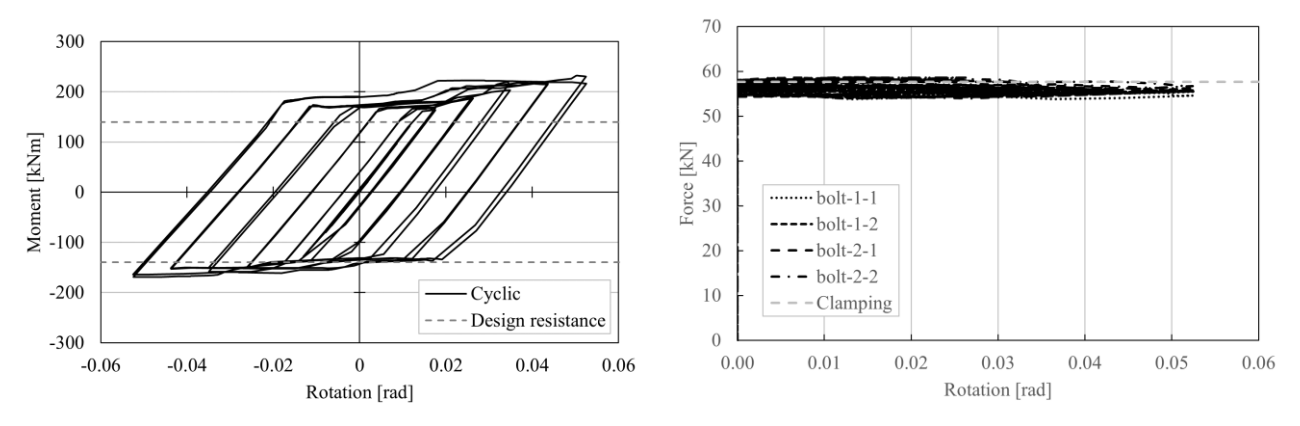


Fig 48: Cyclic Loading: cyclic response (left) and evolution of the Preload Force in the damper bolts (right)

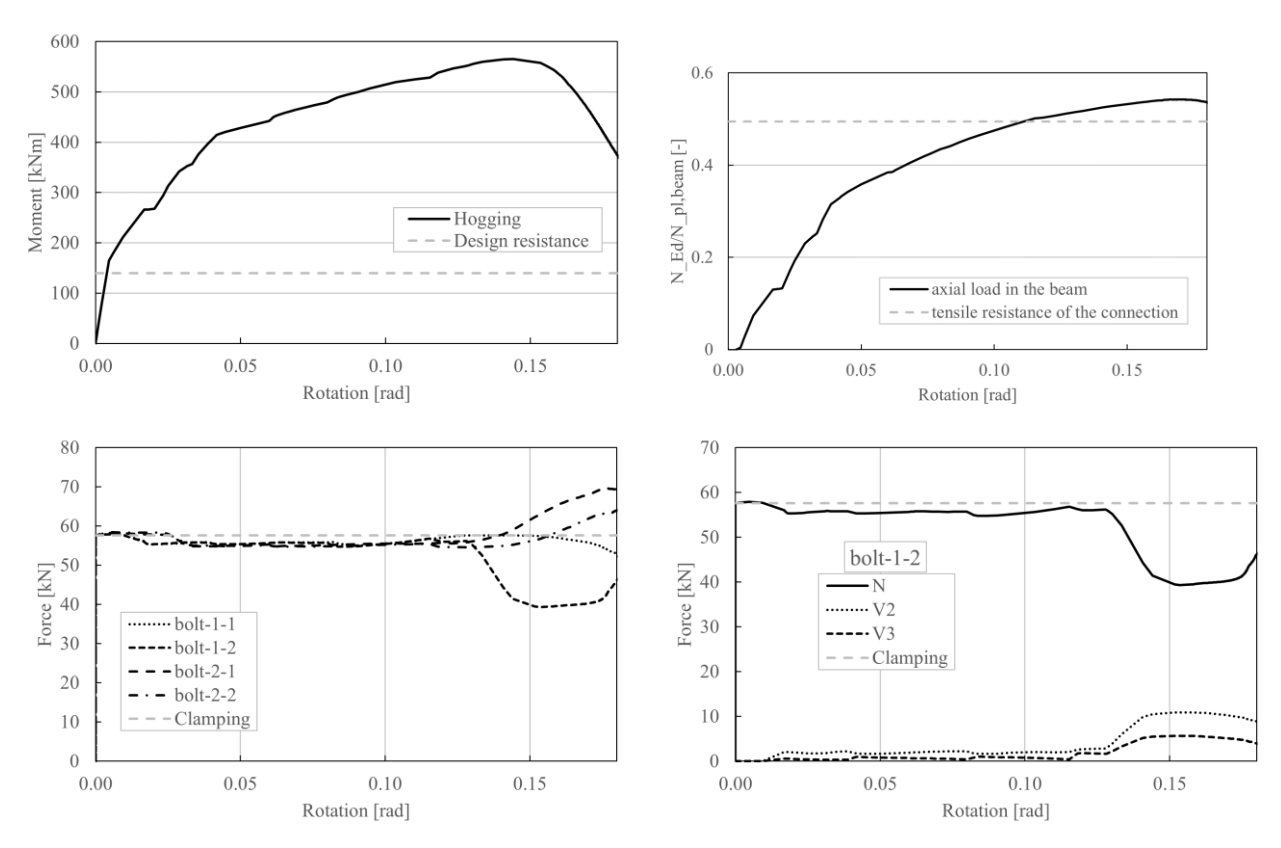


Fig 49: Column Loss "Hogging"; bending moment-rotation curve (up-left); non-dimensional axial load in the beam-rotation diagram (up-right); evolution of the Preload Force in the damper bolts (bottom-left); evolution of component forces in the bolt-1-2(bottom-right)

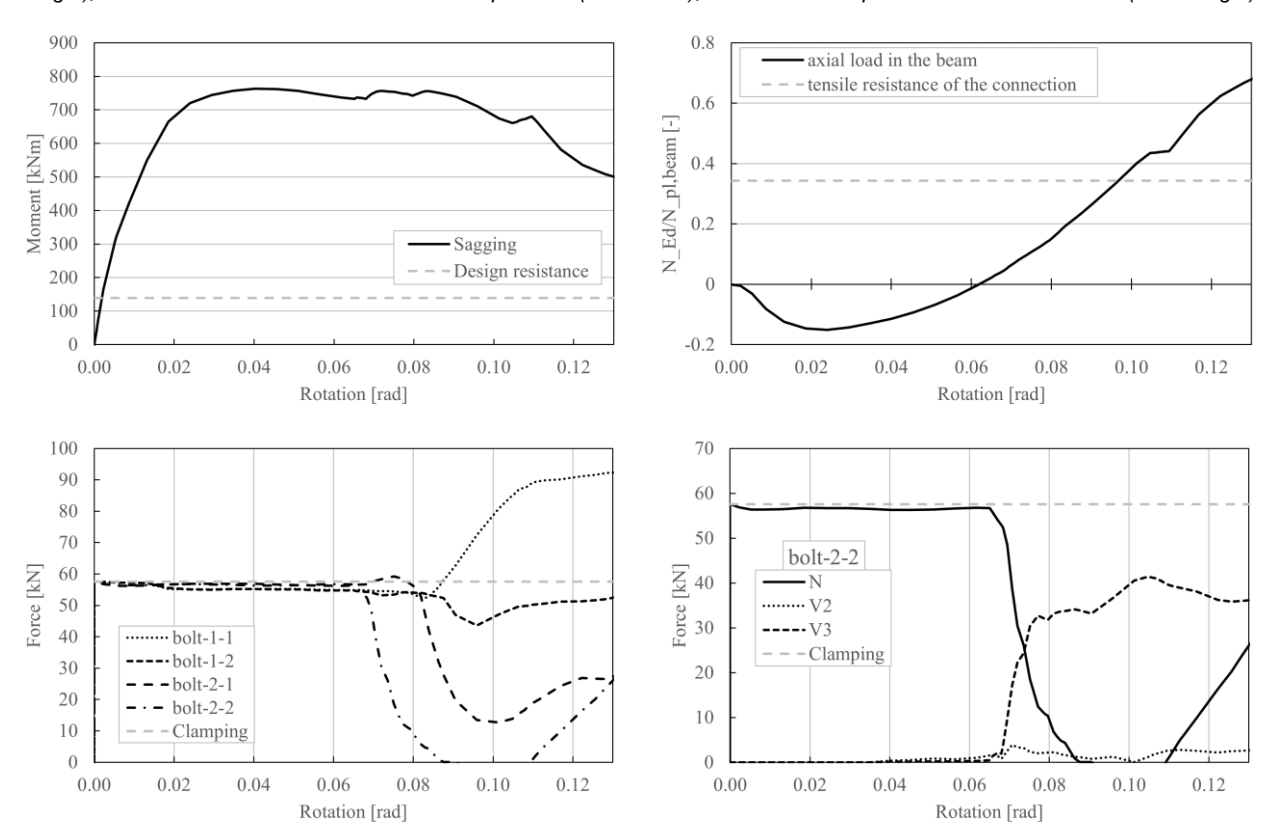


Fig 50: Column Loss "Sagging"; bending moment-rotation curve (up-left); non-dimensional axial load in the beam-rotation diagram (up-right); evolution of the Preload Force in the damper bolts (bottom-left); evolution of component forces in the bolt-2-2(bottom-right)

B.6.6 Y-II-TJ

The joint is the Y-II-TJ, located on the Y-MRF, II floor, T-joint configuration. The joint is equipped with a FREEDAM DEVICE 2A, with a bending capacity level equal to 0.4, HEB400 as column profile, IPE450 as beam profile.

The design bending moment resistance of the joint is 242 kNm.

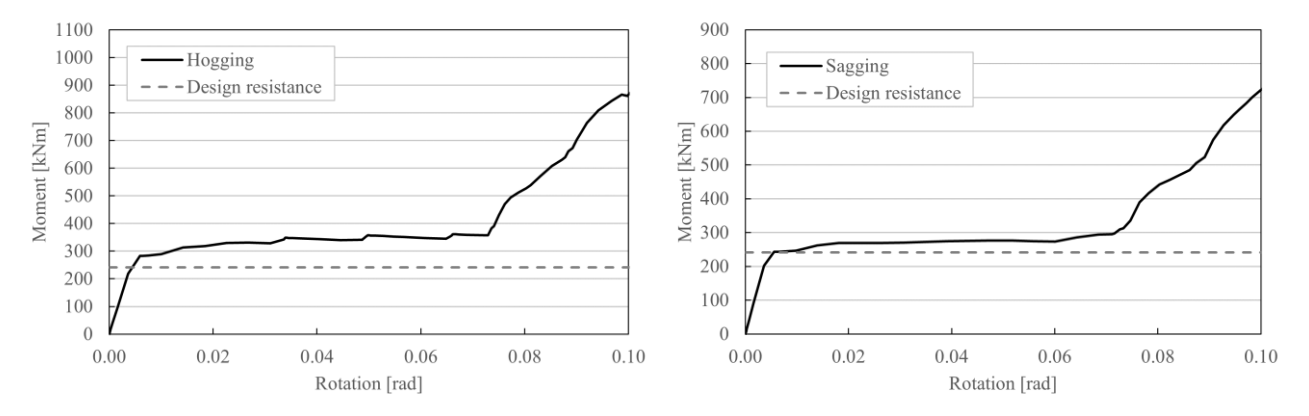


Fig 51: Monotonic Loading: bending moment-rotation diagrams in hogging (left) and in sagging (right)

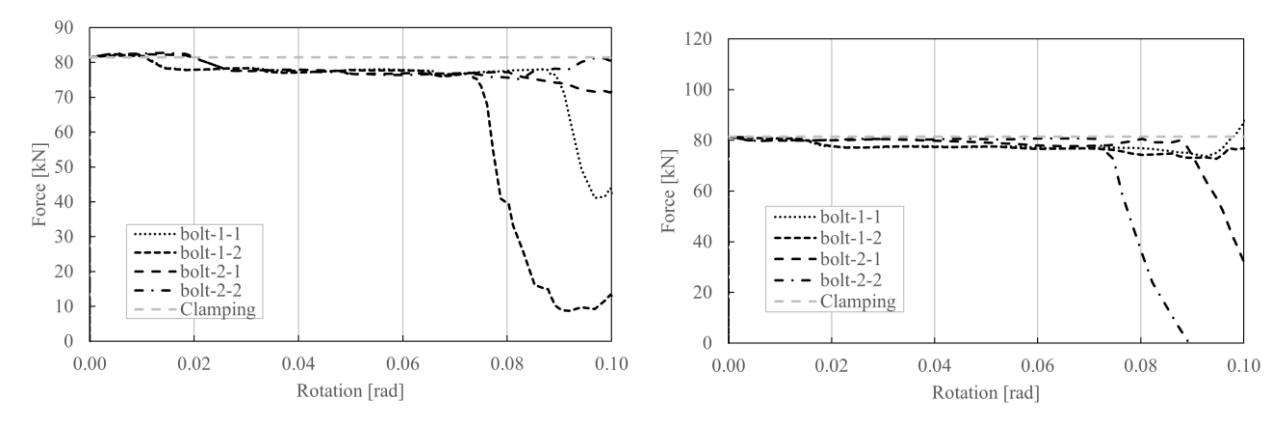


Fig 52: Monotonic Loading: evolution of the Preload Force in the damper bolts in hogging (left) and in sagging (right)

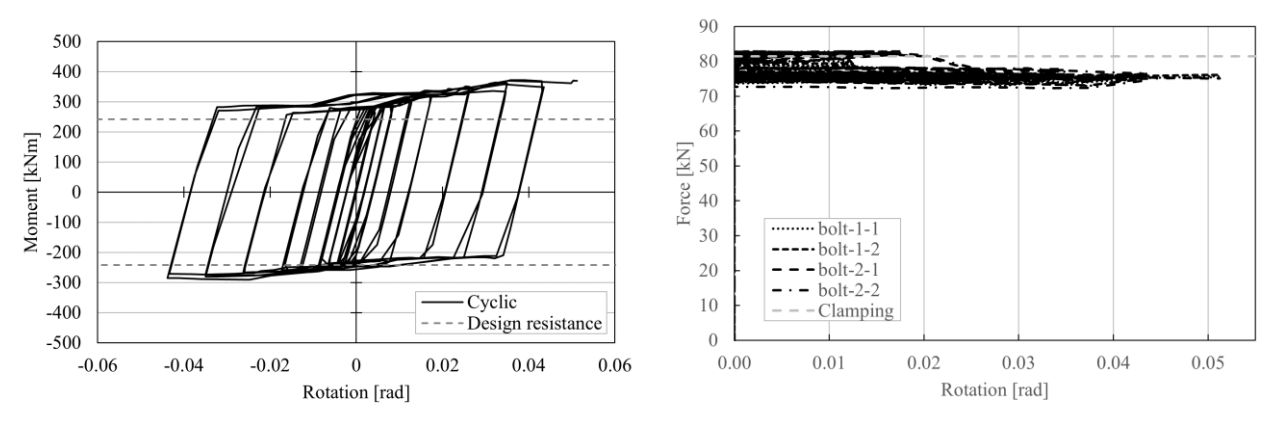


Fig 53: Cyclic Loading: cyclic response (left) and evolution of the Preload Force in the damper bolts (right)

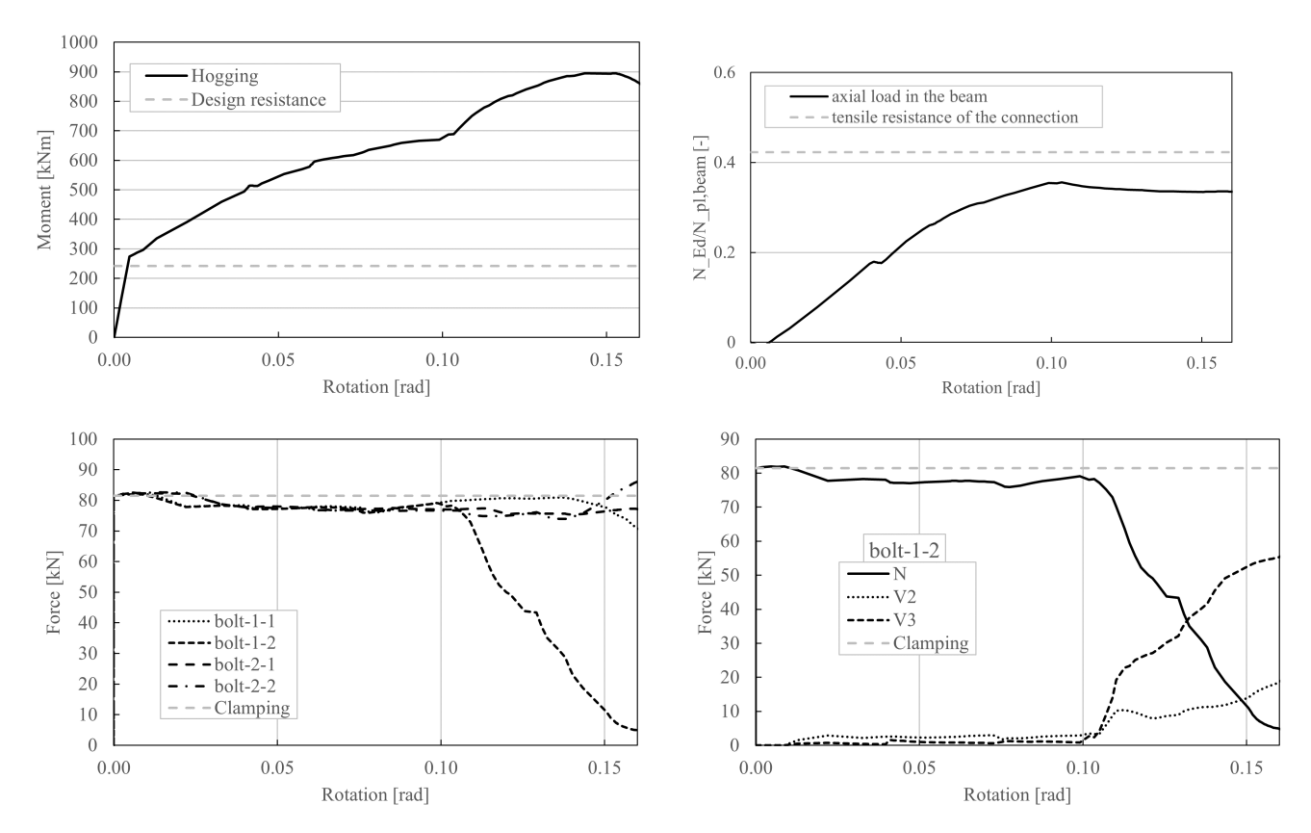


Fig 54: Column Loss "Hogging"; bending moment-rotation curve (up-left); non-dimensional axial load in the beam-rotation diagram (up-right); evolution of the Preload Force in the damper bolts (bottom-left); evolution of component forces in the bolt-1-2(bottom-right)

B.6.7 Y-II-XJ

The joint is the Y-II-XJ, located on the Y-MRF, II floor, X-joint configuration. The joint is equipped with a FREEDAM DEVICE 2A, with a bending capacity level equal to 0.4, HEB400 as column profile, IPE450 as beam profile.

The design bending moment resistance of the joint is 242 kNm.

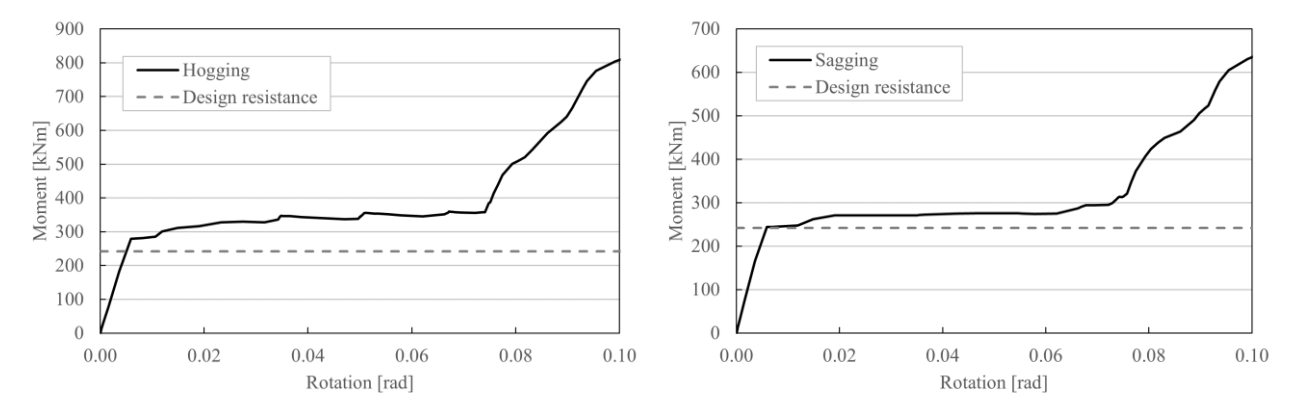


Fig 55: Monotonic Loading: bending moment-rotation diagrams in hogging (left) and in sagging (right)

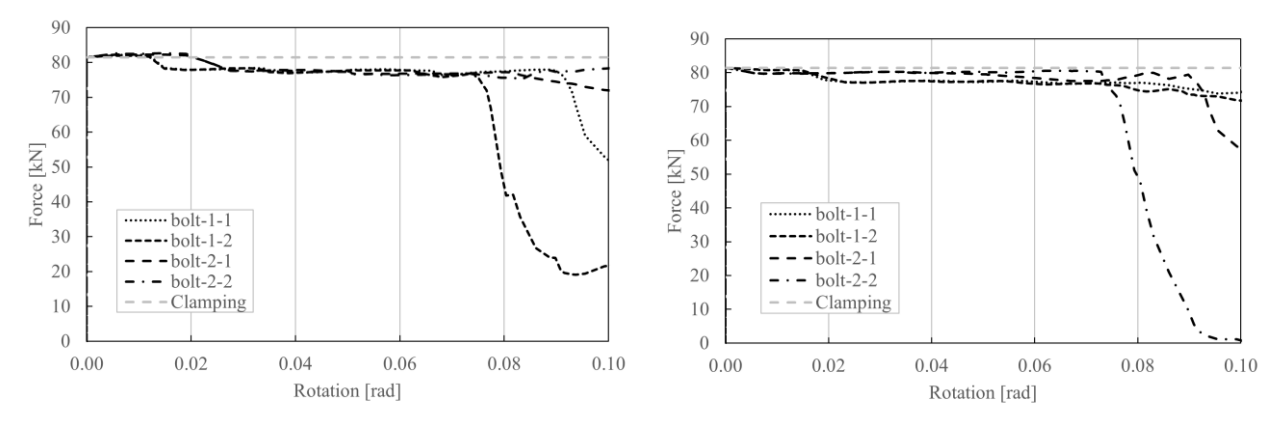


Fig 56: Monotonic Loading: evolution of the Preload Force in the damper bolts in hogging (left) and in sagging (right)

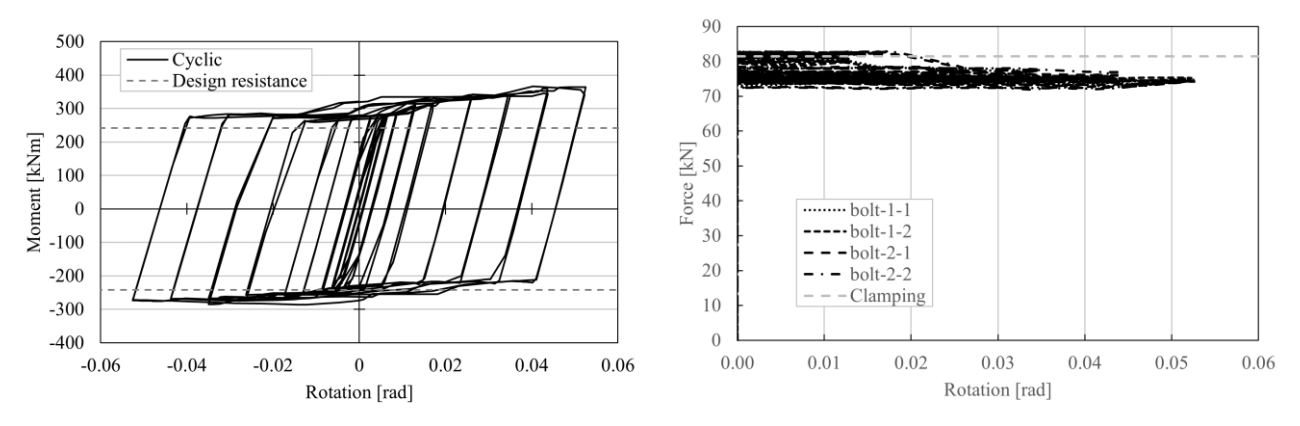


Fig 57: Cyclic Loading: cyclic response (left) and evolution of the Preload Force in the damper bolts (right)

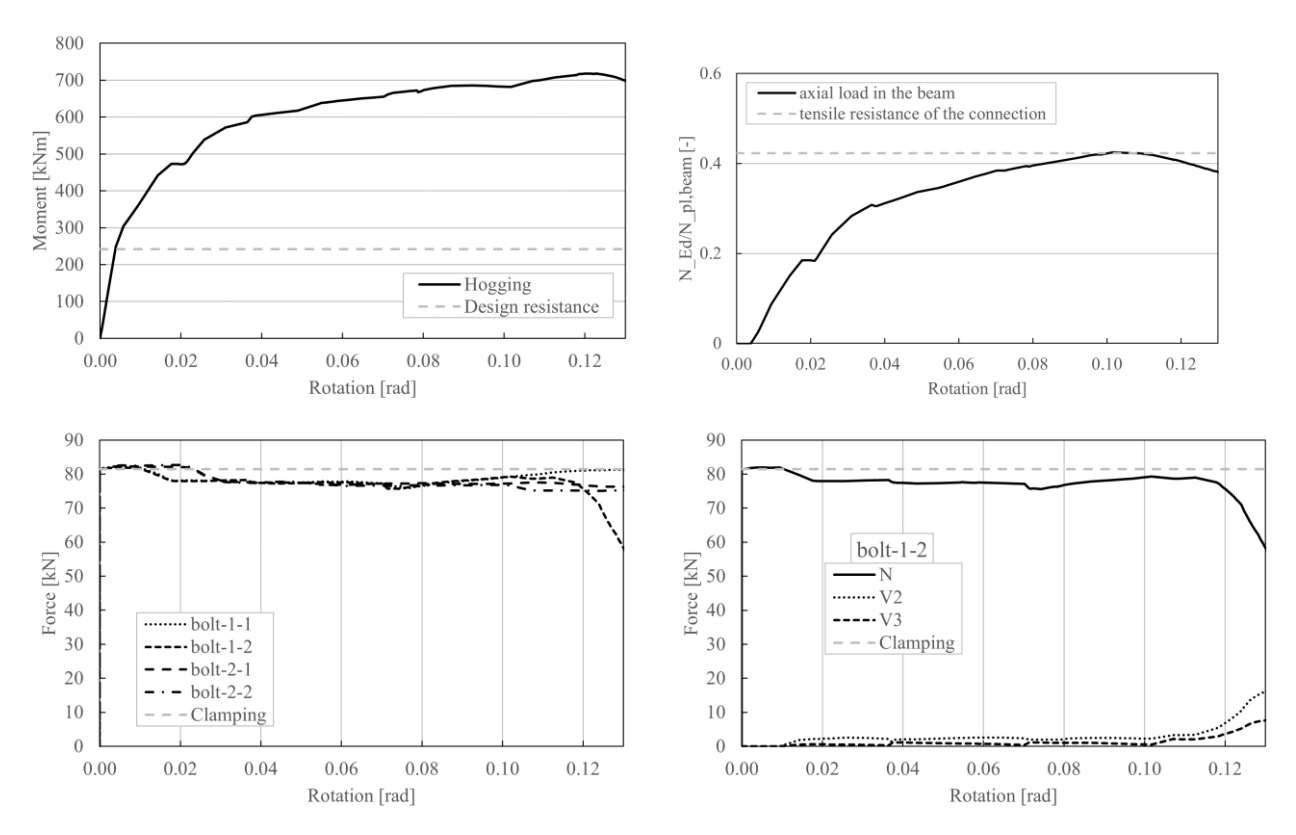


Fig 58: Column Loss "Hogging"; bending moment-rotation curve (up-left); non-dimensional axial load in the beam-rotation diagram (up-right); evolution of the Preload Force in the damper bolts (bottom-left); evolution of component forces in the bolt-1-2(bottom-right)

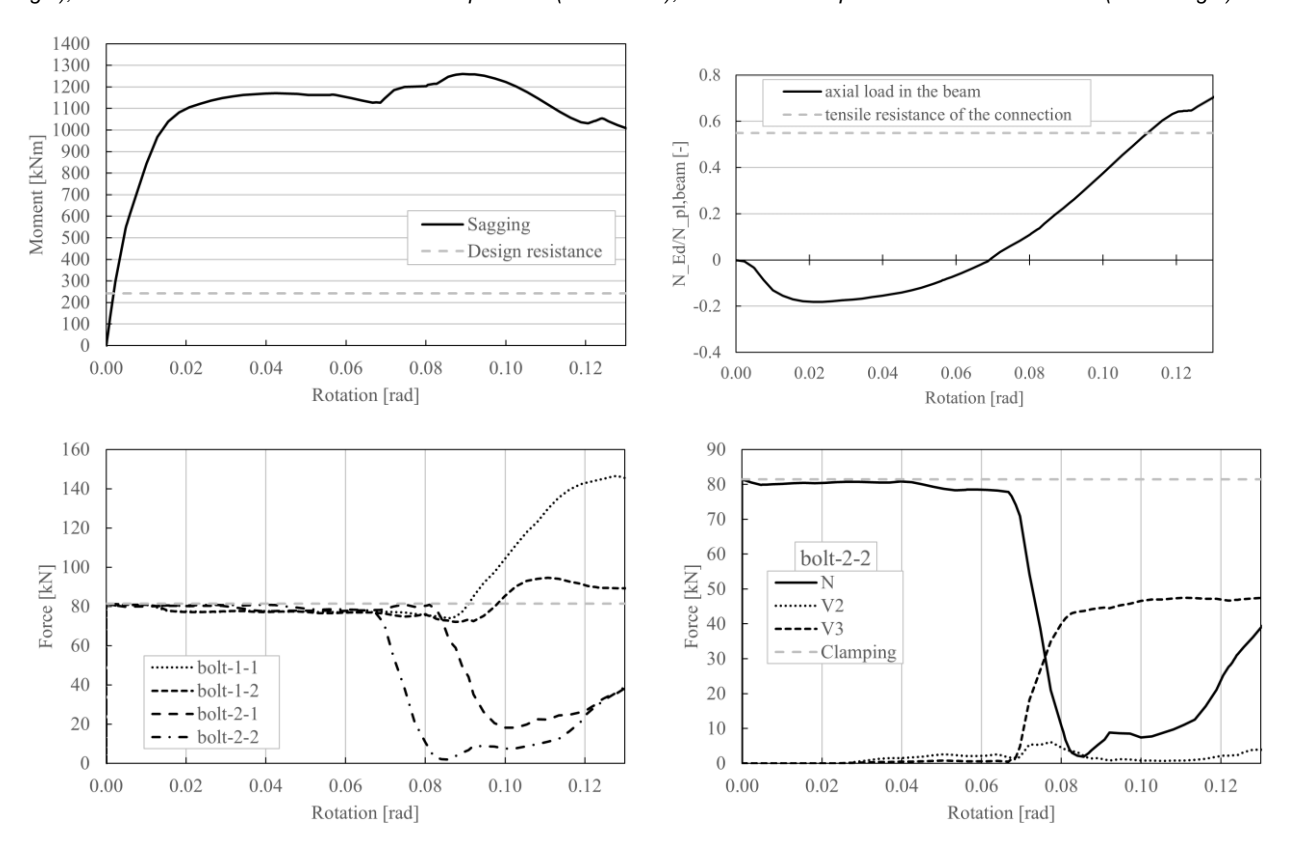


Fig 59: Column Loss "Sagging"; bending moment-rotation curve (up-left); non-dimensional axial load in the beam-rotation diagram (up-right); evolution of the Preload Force in the damper bolts (bottom-left); evolution of component forces in the bolt-2-2(bottom-right)

B.7. Strengthening of upper T-stub

B.7.1 T-stub as-it-is

Numerical simulations have highlighted an unexpected behaviour of the FREEDAM connection under Column Loss Scenario with hogging bending moment. In fact, for rotations greater than 20 mrad, the bolted connection between the upper T-stub flange and the column flange is characterized by a fragile failure, consisting in the failure of the shank of the bolts and in the partial yielding of the T-stub flange (*Failure Mode 2* according to the *Equivalent T-stub Theory*). It has been wondered if it would be possible to make the failure more ductile, which means shifting the Failure Mode from 2 to 1, without modifying too much the existing connection. The answer is affirmative and, in this chapter, a strengthening solution for the upper T-stub is proposed.

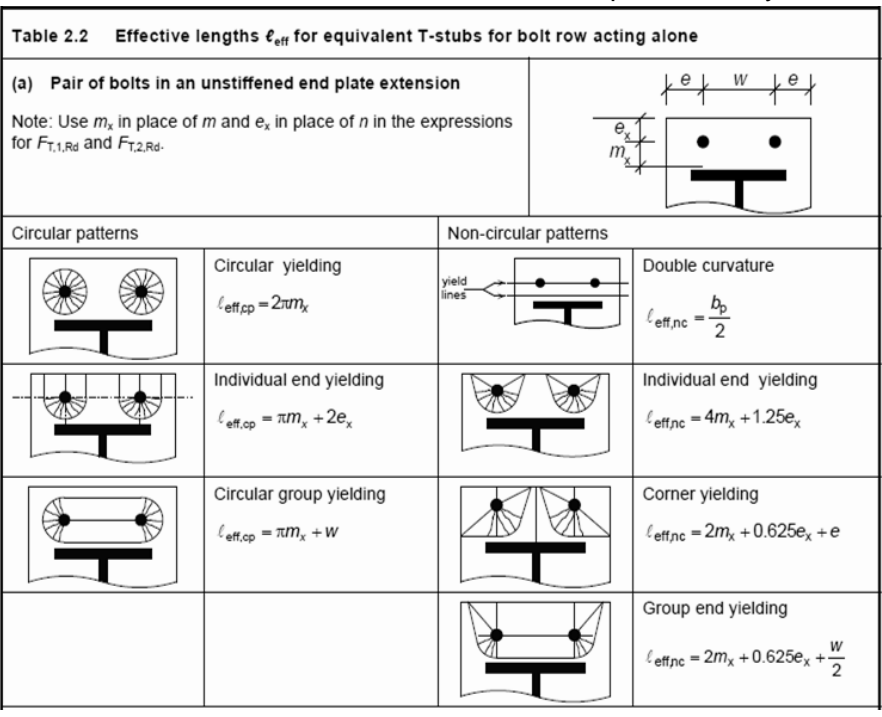
FE simulations have also shown that the design external force (pull force) acting on the T-stub web can be set equal to $N_{Ed} = 0.4 N_{pl,Rd,beam}$.

The overall assessment of the as-it-is T-stub resistance is evaluated according to the *Equivalent T-stub Method*, as given in *EN1993:1-8* and in *SCI-P398*; further details on this method are given in the *Annex* of the present report.

Resistance of bolt rows is calculated for the single bolt row and for the bolt rows acting in combination, for every component of the connection, namely in this case the T-stub flange and the column flange. For every bolt row (acting alone or acting in combination) several yielding patterns can be identified, with respect edges of the plate and stiffeners. Obviously, the presence of a stiffeners denies any group effect between the bolt rows nearby.

T-stub flange

Bolt rows on the T-stub flange can be modelled as "case (a): Pair of bolts in an unstiffened end plate extension". Here, the horizontal stiffener is represented by the T-stub web.

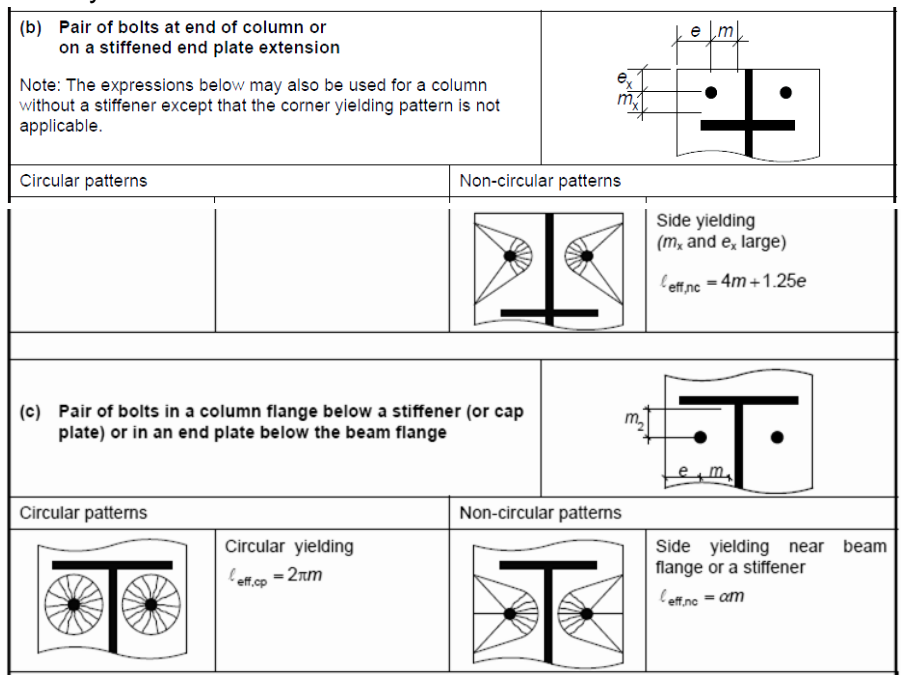


Tab 2: Effective lengths, courtesy of SCI P398

Column flange

Bolt rows on the column flange can be seen as "case (b): pair of bolts at end of column or on a stiffened end plate extension" (side yielding only) and as "case (c): pair of bolts in a column flange below a stiffener (or cap plate) or in an end plate below the beam flange". The

horizontal stiffener is represented by the continuity plates, while the vertical stiffener is represented by the column web.



Tab 3: Effective lengths, courtesy of SCI P398

It is therefore possible to evaluate the effective lengths for $Mode\ 1$ and $Mode\ 2$, then the bending moment plastic resistance for $Mode\ 1$ and $Mode\ 2$, the design resistance for $Mode\ 1$, $Mode\ 2$, the design resistance for $Mode\ 2$, the design resistance for $Mode\ 1$, $Mode\ 2$, the design resistance for $Mode\ 2$, the design resistance for $Mode\ 2$, the design resistance for $Mode\ 2$, and $Mode\ 2$, the design resistance for $Mode\ 2$, the design resistance for $Mode\ 2$, the design resistance for $Mode\ 2$, the design resistance for

| equivalent T-stub - bolt row resistance | | | | |
|---|---------------|------|---------|--|
| T-stub flange | $F_{T,tf,Rd}$ | [kN] | 518.53 | |
| Column flange | $F_{T,cf,Rd}$ | [kN] | 635.40 | |
| Failure due to: | T-STUB FLANGE | | LANGE | |
| FAILURE MODE | | | 2 | |
| ultimate resistance of the bolt row | $F_{T,Rd}$ | [kN] | 518.53 | |
| tensile resistance of the entire connection | $R_{C1,Rd}$ | [kN] | 1037.07 | |
| tensile action on the entire connection | N_{Ed} | [kN] | 1403.26 | |
| check (R/D) | | | 0.74 | |

Tab 4: Overall resistance of the T-stub

The resistance domain $\eta - \beta$ of the T-stub flange shows a *Failure Mode 2*, that is unfortunately very close to a *Failure Mode 3* (in particular, a value of $\beta < 1$ is expected for a ductile failure).

The resistance domain $\eta - \beta$ of the column flange depicts instead a different situation, with a clear Failure Mode 3. This time the type of failure is not a concern, since the column flange has a greater resistance with regards the other component of the connection, namely the T-stub flange.

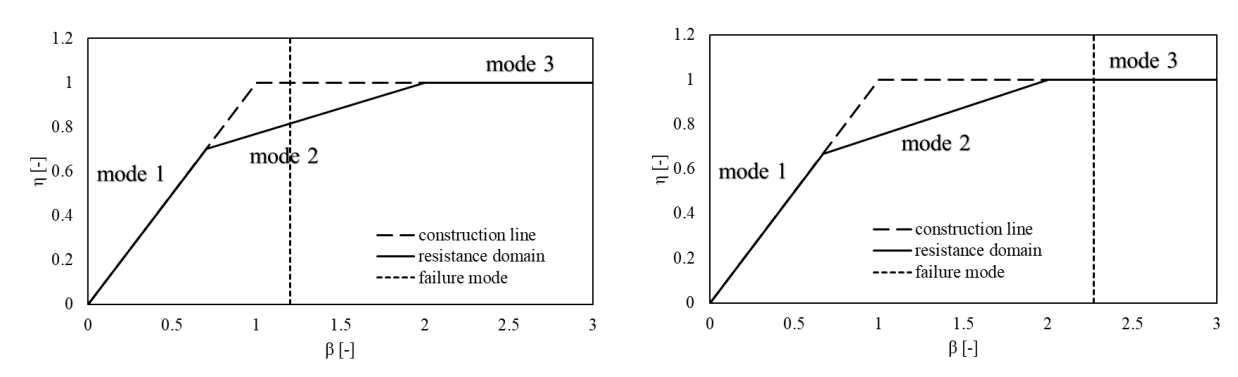


Fig 60: Resistance domains of the equivalent T-stub: T-stub flange (left), column flange (right)

Since failure is always due to the T-stub flange, strengthening strategy directly targeted this part of the connection.

B.7.2 Strengthening design

This solution must comply with several constraints, listed below:

- Bolts on the T-stub flange: not greater than M30 bolts
- Bolts on the T-stub flange: grade not higher than Grade 10.9, since stronger bolts (such as Grade 12.9) are more expensive and not so common
- Overall dimensions of the T-stub flange: base not larger than the base of the column crosssection, height not greater than 400 mm, since the connection must be included in the slab height
- Thickness of the T-stub flange and T-stub web: less than 35 mm due to manufacturing reasons
- A proper distance between column flange and beam must be guaranteed to ensure the normal functioning of the T-stub web, which is subject to bending
- General geometrical limitations for bolted connections, such as edge distances, spacing between bolts, net area check in presence of holes, etc have to be verified as usual
- For the sake of uniformity and consistency it was chosen to strengthen the joint based on the type of *Device*. This means that all the *Devices 1* will be modified in the same way as *Devices 1-S02*. This design process is done by strengthening the Device with regards the severest action and then applying these modifications to the other joints."

One of the main critical aspects of the as-it-is T-stub is the low resistance of the bolt rows on the T-stub flange side. Given the *Equivalent T-stub Method*, a possible strategy to upgrade this resistance could be that to increase the effective lengths of the bolt rows: this goal can be reached by welding stiffeners on the T-stub web. At the same time, in order to guarantee an adequate rotational capacity of the T-stub and its functioning in bending, the T-stub web needs to be disconnected by the aforementioned stiffeners by means of an access hole.

B.7.3 Strengthening solution for Device 1

In this example, the selected joint is X-II-TJ, with an IPE450 as beam profile and HEB400 as column profile.

For *Device 1*, the proposed solution *Device 1-S02* consists in the following modifications, made on the T-stub:

Flange:

- Width, 300 mm instead 205 mm
- · Height, 400 mm instead 170 mm
- Thickness: 15 mm
- · Vertical and horizontal stiffeners: max height 30 mm

Web:

- Width, 300 mm instead 205 mm
- Length, 455 mm instead 345 mm
- Thickness: 20 mm
- Access hole makes web and vertical stiffener not interfering each other

Flange bolts:

8x M27 bolts instead 4x M24 bolts

Web bolts:

12x M20 instead M16 (same quantity)

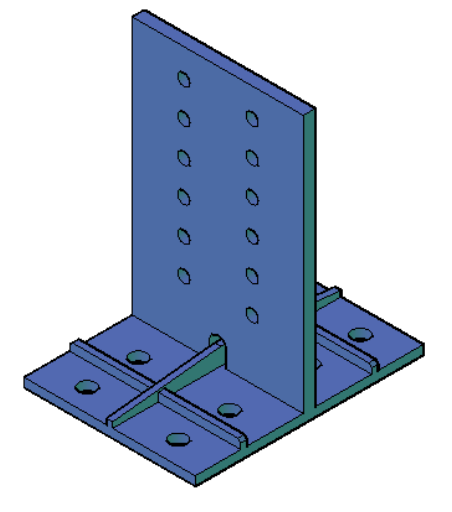
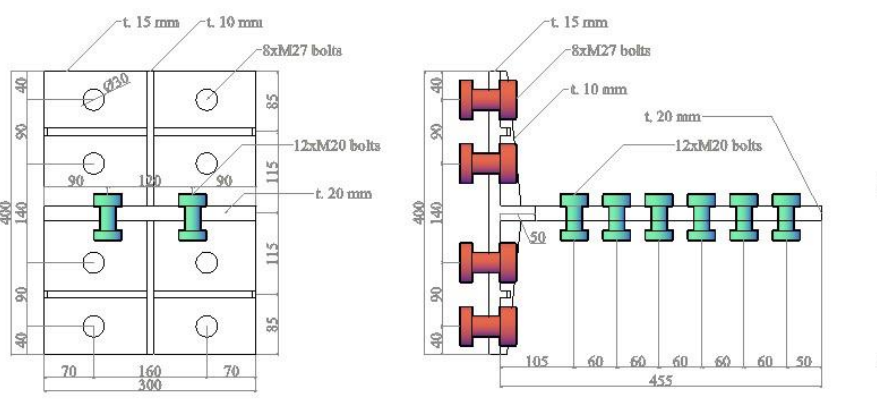


Fig 61: 3D view of the strengthened T-stub (Device 1-S02)



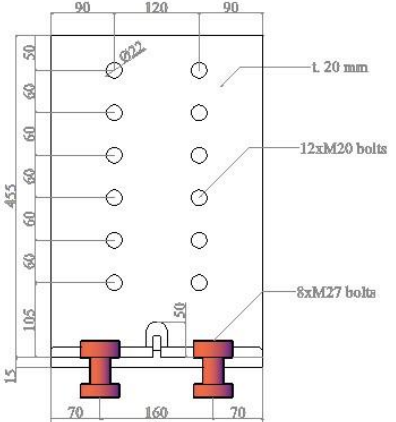
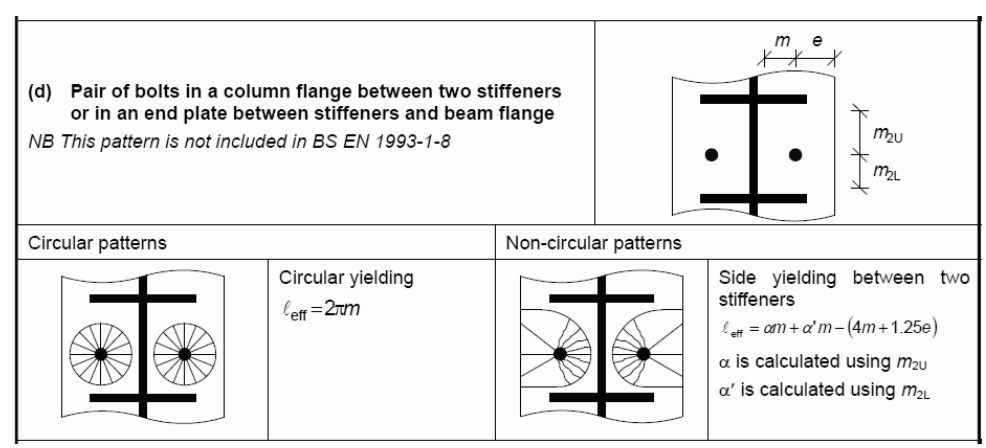


Fig 62: Strengthening Solution for the upper T-stub (Device 1-S02)

In this new configuration, the two bolt rows close to the T-stub web are loaded first by the pull force, while the two bolt rows far from the T-stub web are the ones that are loaded at last. No group effect is allowed between bolt rows due to the presence of the horizontal stiffeners and T-stub web.

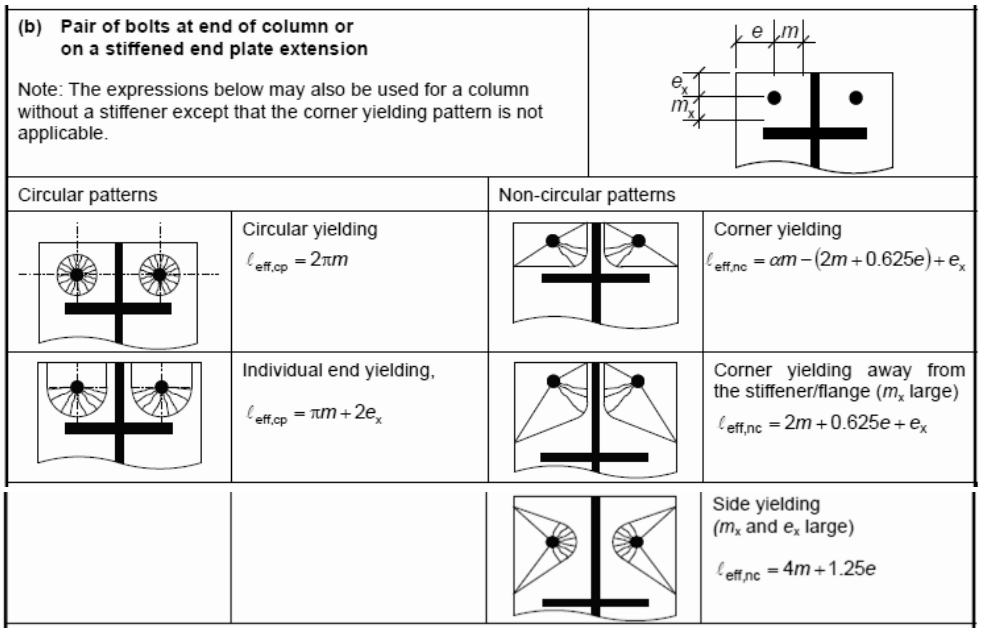
T-stub flange

Bolt Row 1 can be evaluated as "case (d): pair of bolts in a column flange between two stiffeners or in an end plate between stiffeners and beam flange"



Tab 5: Effective lengths, courtesy of SCI P398

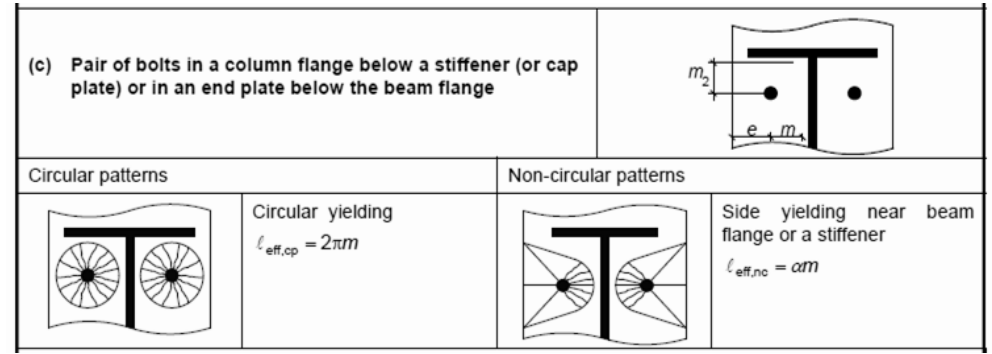
Bolt Row 2 can be evaluated as "case (b): pair of bolts at end of column or on a stiffened end plate extension"



Tab 6: Effective lengths, courtesy of SCI P398

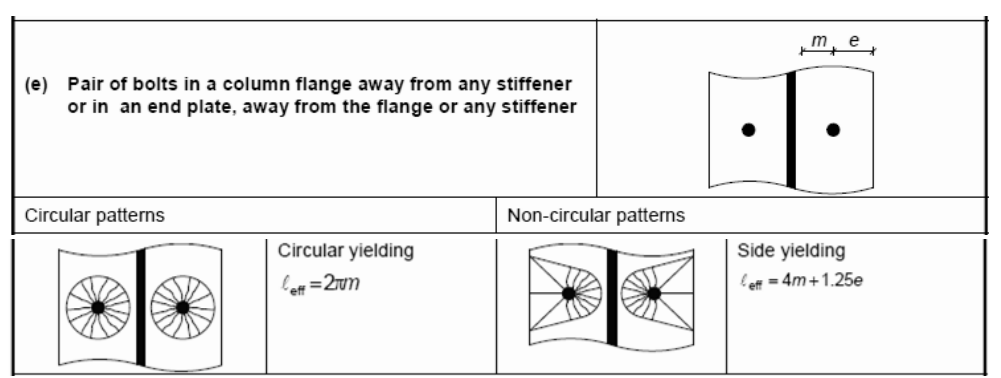
Column flange

Bolt Row 1 can be evaluated as "case (c): pair of bolts in a column flange below a stiffener (or cap plate) or in an end plate below the beam flange"



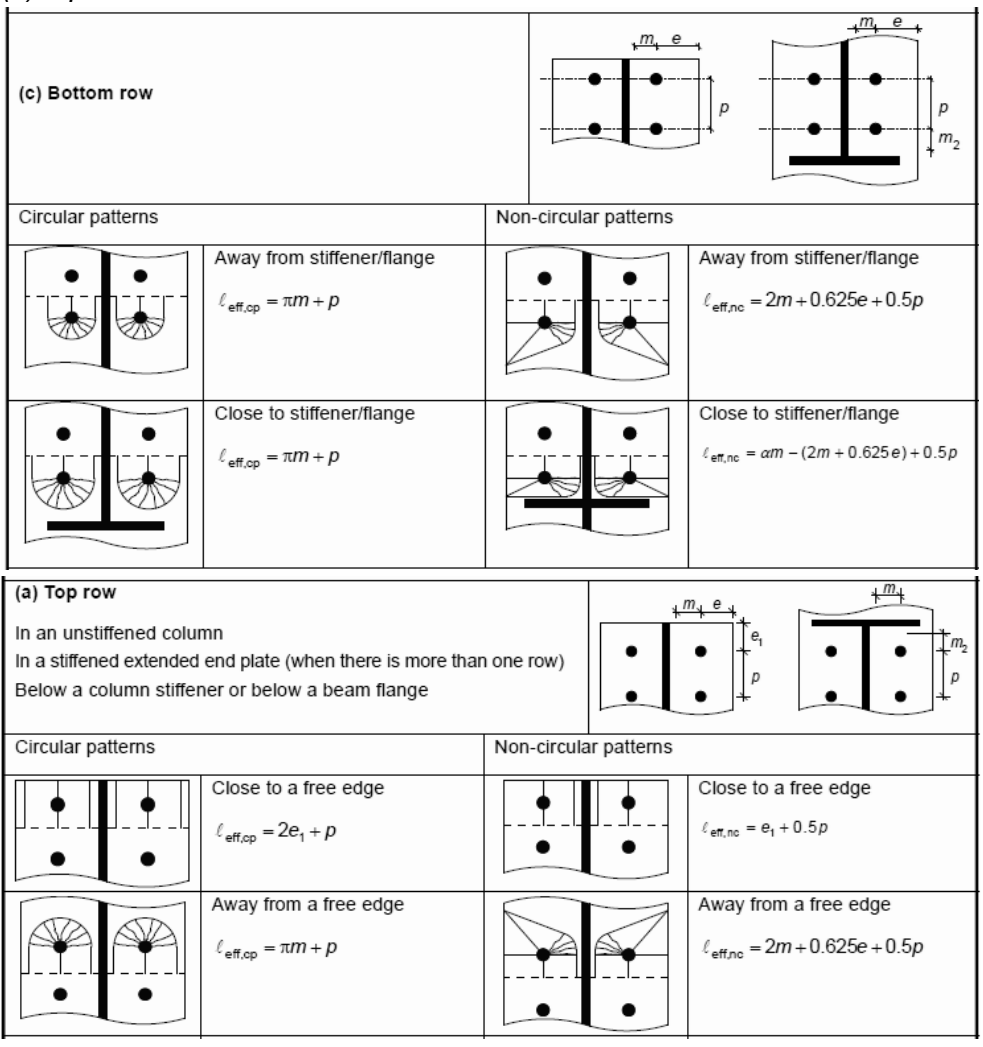
Tab 7:Effective lengths, courtesy of SCI P398

Bolt Row 2 can be evaluated as "case (e): pair of bolts in a column flange away from any stiffener or in an end plate, away from the flange or any stiffeners"



Tab 8:Effective lengths, courtesy of SCI P398

Bolt rows 1 and 2 acting in combination can be evaluated as "(c) bottom row" for Bolt Row 1 and as "(a) top row" for Bolt Row 2



Tab 9: Effective lengths, courtesy of SCI P398

In order, we proceed to calculate: the effective lengths for $Mode\ 1$ and $Mode\ 2$, their respective plastic bending moment resistance, tensile resistance of bolts $Mode\ 3$, and finally the design resistance $F_{T,Rd}$ of the equivalent T-stub. As result, the failure of the equivalent T-stub is still due to the T-stub flange, which now undergoes to $Failure\ Mode\ 1$.

| top row (away from the T-stub web) | | | |
|---|-------------------------|------|---------|
| T-stub flange - BR 2 | F _{T2,tf,Rd} | [kN] | 521.68 |
| Column flange - BR 2 | F _{T2,cf,Rd} | [kN] | 717.74 |
| Failure due to: | T-STUB FLANGE | | |
| FAILURE MODE | | | 1 |
| ultimate resistance of the bolt row | $F_{T,Rd}$ | [kN] | 521.68 |
| bottom row (close to the T-stub web) | | | |
| T-stub flange - BR 1 | F _{T1,tf,Rd} | [kN] | 501.87 |
| Column flange - BR 1 | $F_{T1,cf,Rd}$ | [kN] | 754.36 |
| Column flange - BR 1 (as group) | F _{T1+2,cf,Rd} | [kN] | 538.18 |
| Failure due to: | | | ANGE |
| FAILURE MODE | | | 1 |
| ultimate resistance of the bolt row | $F_{T,Rd}$ | [kN] | 501.87 |
| tensile resistance of the entire connection | R _{C1,Rd} | [kN] | 2047.11 |
| tensile action on the entire connection | N_{Ed} | [kN] | 1403.26 |
| check (R/D) | | | 1.46 |

Tab 10: Overall resistance of the T-stub

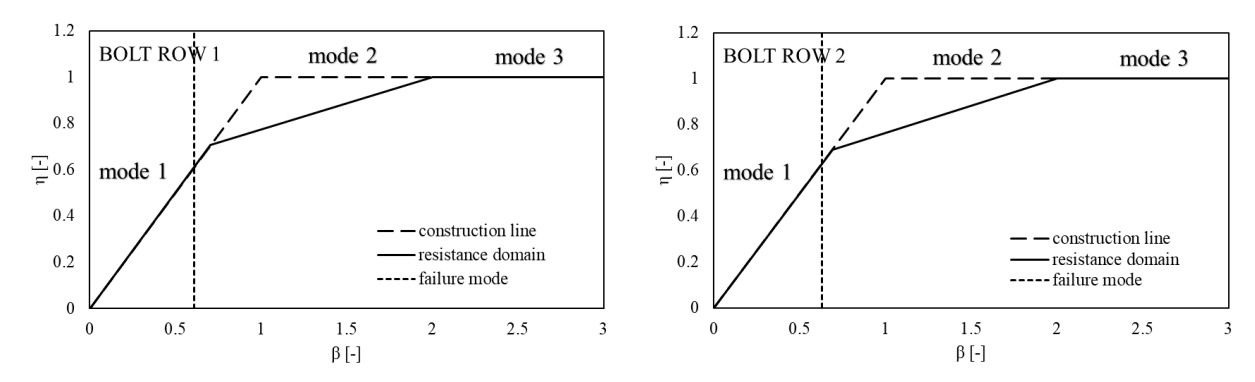


Fig 63: Resistance domains of the equivalent T-stub (T-stub flange): Bolt Row 1 (left), Bolt Row 2 (right)

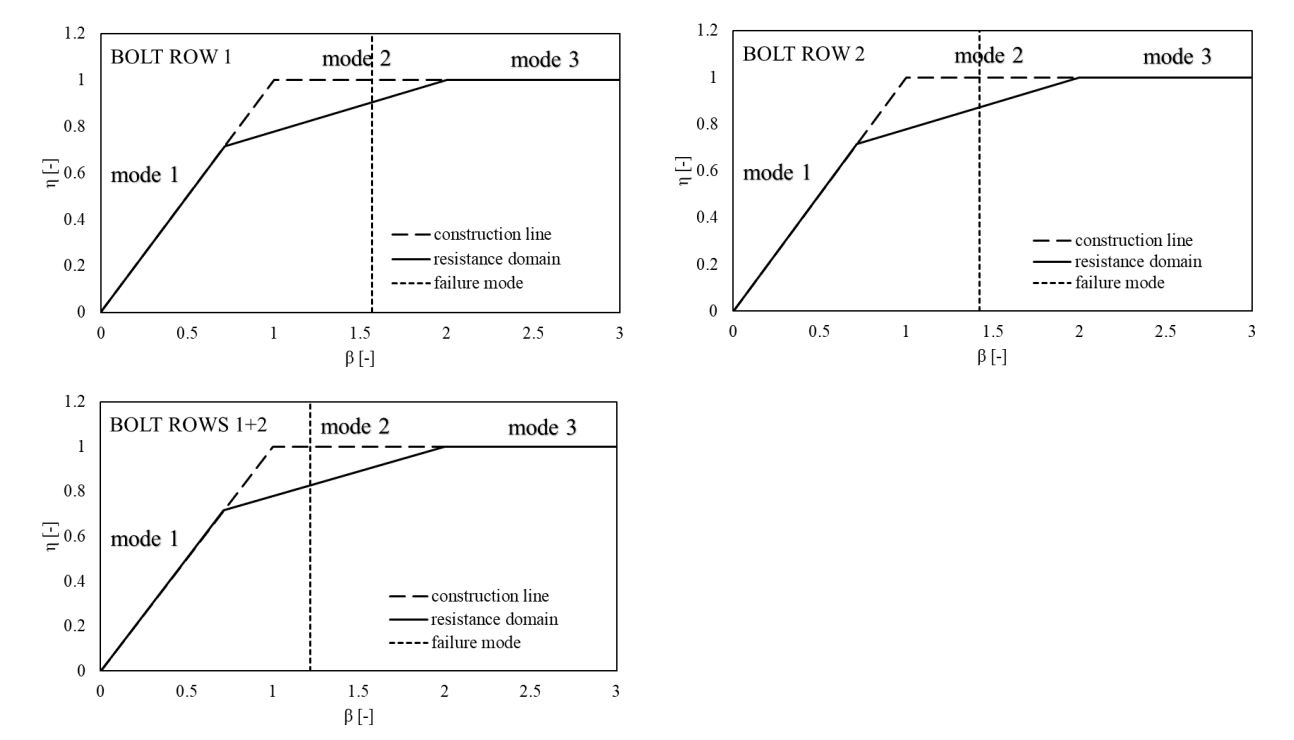


Fig 64: Resistance domains of the equivalent T-stub (column flange): Bolt Row 1 (up left), Bolt Row 2 (up right), Bolt Rows 1+2 (bottom)

The presence of the modified T-stub doesn't change the global behaviour of the joint. By plotting the response curves of the strengthened joint and of the as-it-is joint, we can see that the behaviour of the two joints is more or less the same, both in hogging scenario and sagging scenario.

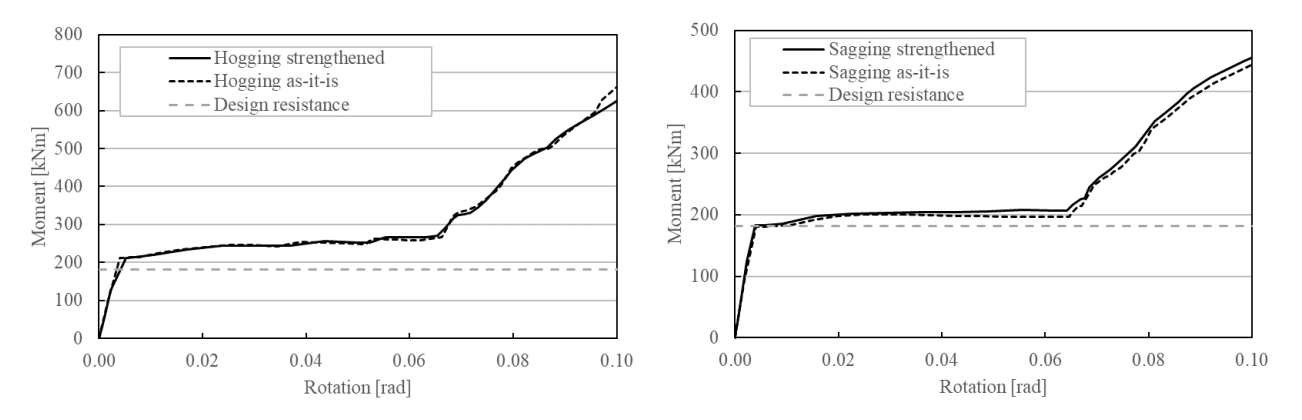


Fig 65: Comparison between the strengthened joint and the as-it-is joint: monotonic loading with hogging bending moment (left) and with sagging bending moment (right)

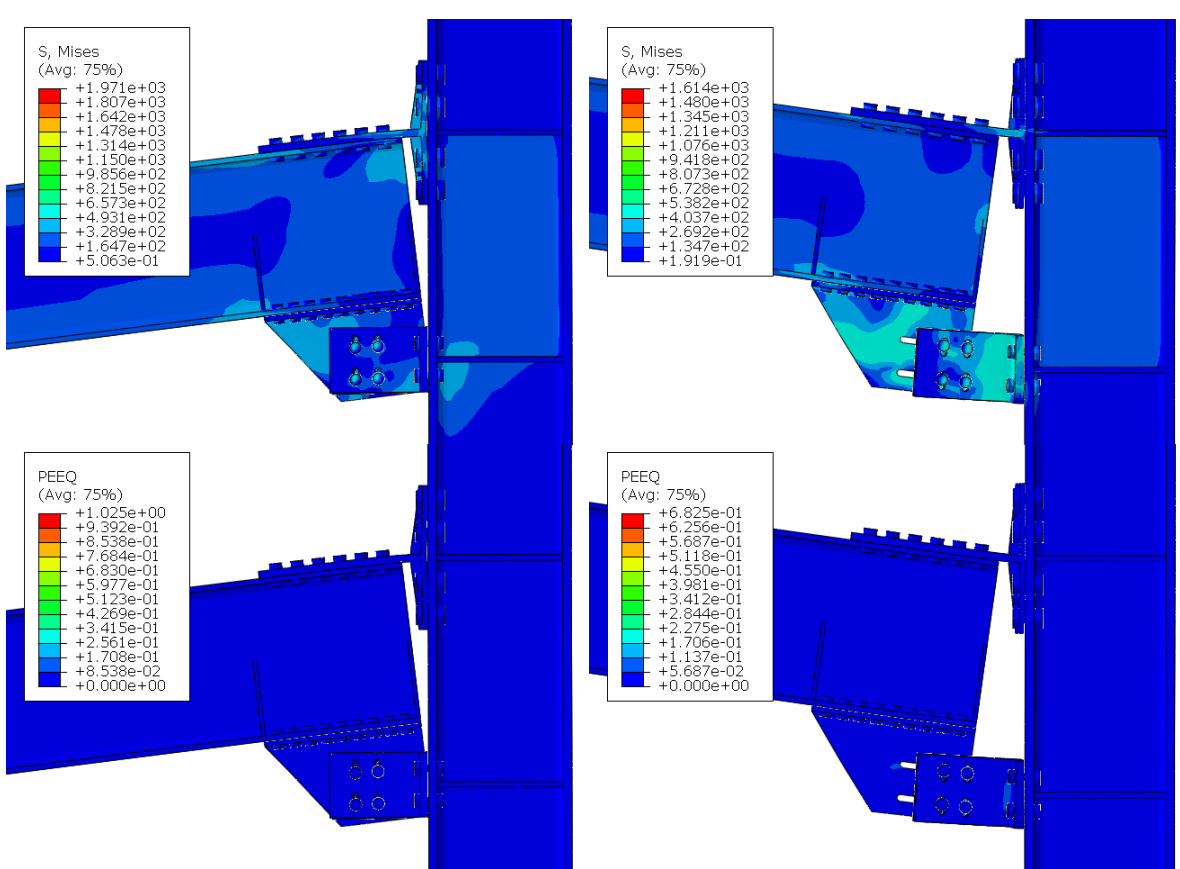


Fig 66: Von Mises stress and PEEQ distributions of the strengthened joint, in hogging (left) and sagging right)

Cyclic behaviour of the joint isn't affected neither by the changes made in the T-stub: hysteretic cycles of the strengthened joint and the as-it-is joint are pretty much superimposed.

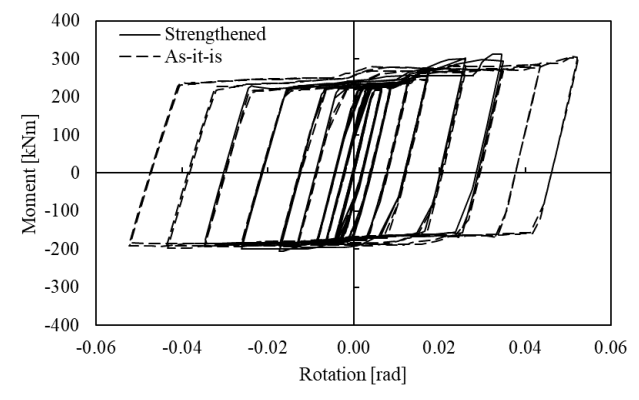


Fig 67: Cyclic response of the strengthened joint and the as-it-is joint

The big difference given by the modified T-stub is clearly visible in the Column Loss scenario with hogging bending moment. The *moment-rotation* curve of the strengthened joint overwhelms a lot the curve of the as-it-is joint, with a significant improvement in terms of resistance, stiffness, ultimate rotation. The strengthened joint curve has a crescent slope until 18 mrad, while the as-it-is joint curve present a change in slope at already 15 mrad. At 15 mrad the acting bending moment on the connection is around 750 kNm for the as-it-is joint and around 1300 kNm for the strengthened joint. On the other hand, the *axial load in the beam-rotation* curves are similar, with a slight difference between 5 mrad and 12 mrad, due to the local stiffness of the two T-stubs.

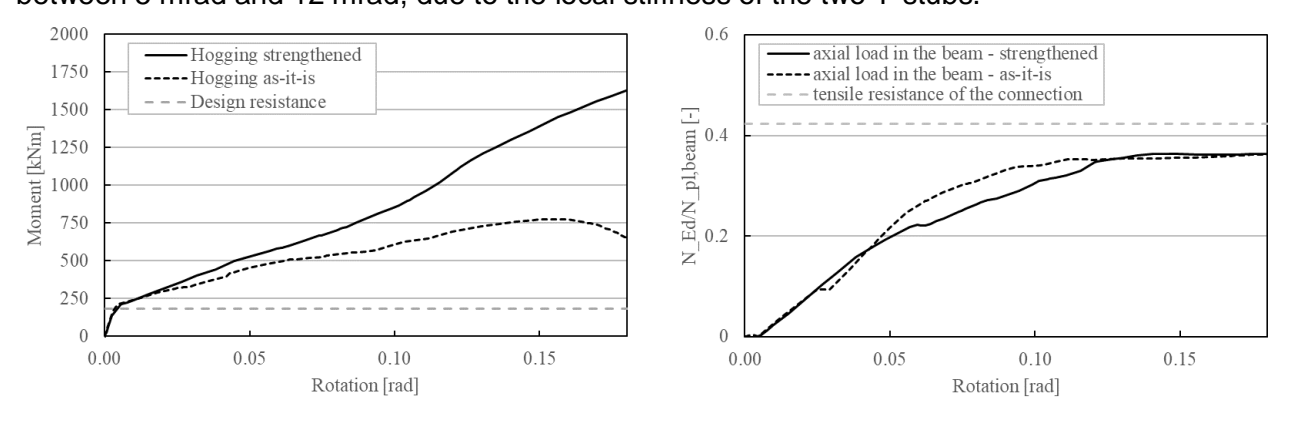


Fig 68: Comparison between the strengthened joint and the as-it-is joint for the Column Loss scenario in hogging: moment-rotation curves (left) and non-dimensional axial load-rotation (right)

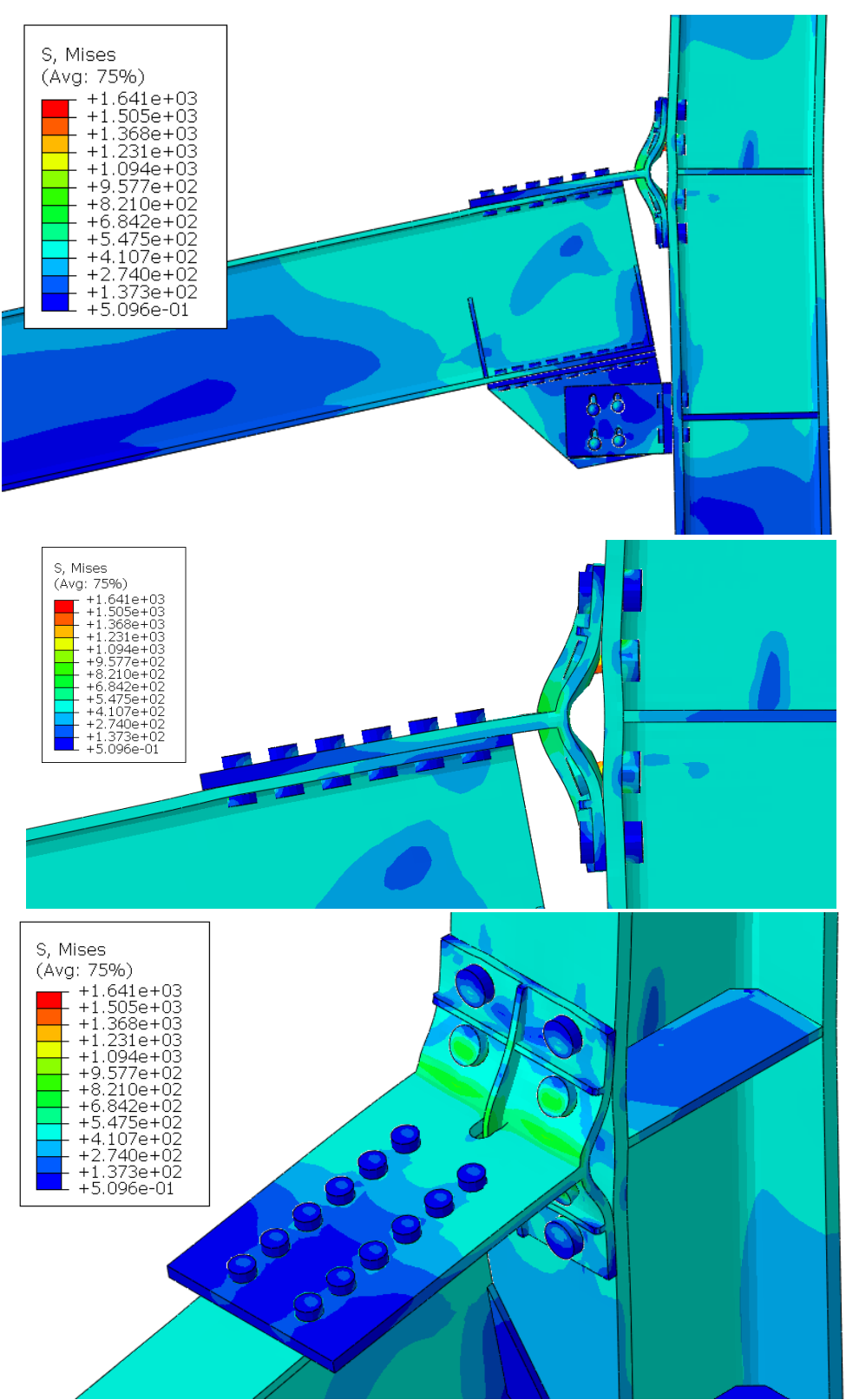


Fig 69: Von Mises stress distribution of the strengthened joint under Column Loss "Hogging"; 2D side view of the joint (top), 2D side view of the T-stub (middle), 3D view of the T-stub (bottom)

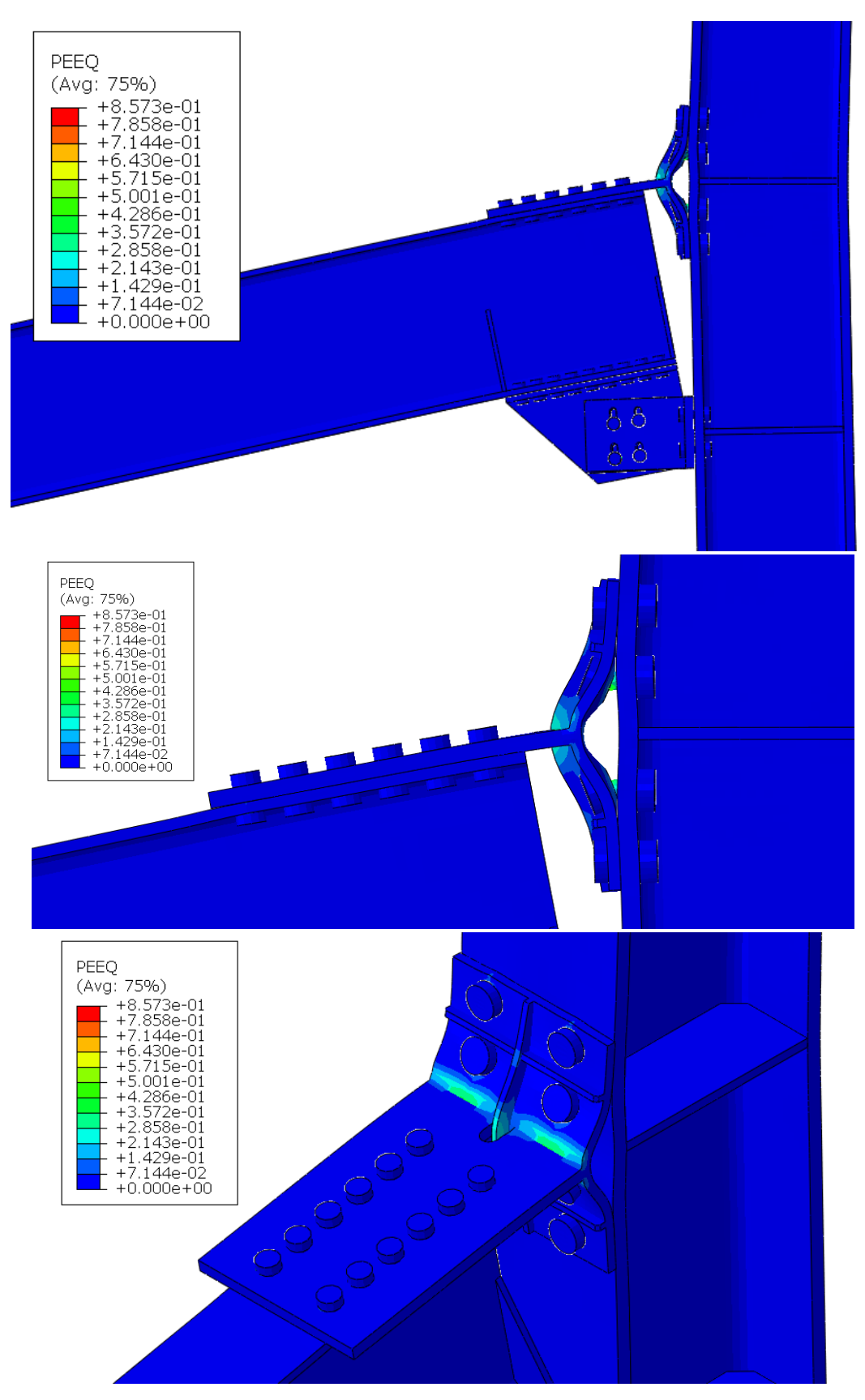


Fig 70: PEEQ distribution of the strengthened joint under Column Loss "Hogging"; 2D side view of the joint (top), 2D side view of the T-stub (middle), 3D view of the T-stub (bottom)

B.7.4 Strengthening solution for Device 2A

In this example, the selected joint is Y-II-TJ, with an IPE450 as beam profile and HEB400 as column profile.

For *Device 2A*, the proposed solution *Device 2A-S02* consists in the following modifications, made on the T-stub:

Flange:

- Width, **300** mm instead **240** mm
- Height, 400 mm instead 175 mm
- Thickness: 18 mm
- Vertical and horizontal stiffeners: max height 30 mm

Web:

- Width, 300 mm instead 240 mm
- Length, 527 mm instead 415 mm
- Thickness: 25 mm
- Access hole makes web and vertical stiffener not interfering each other

Flange bolts:

• 8x M27 bolts instead 4x M24 bolts

Web bolts:

• 14x M24 bolts instead 12x M20 bolts

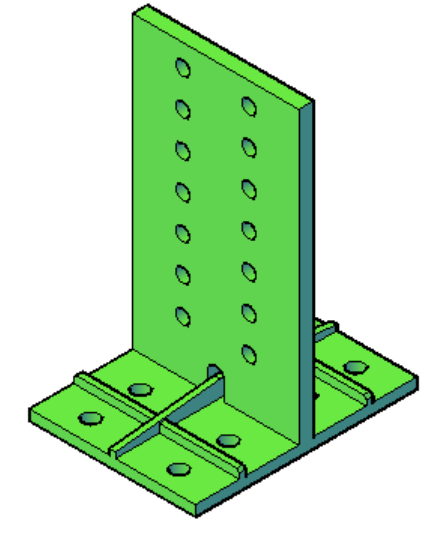


Fig 71: 3D view of the strengthened T-stub (Device 2A-S02)

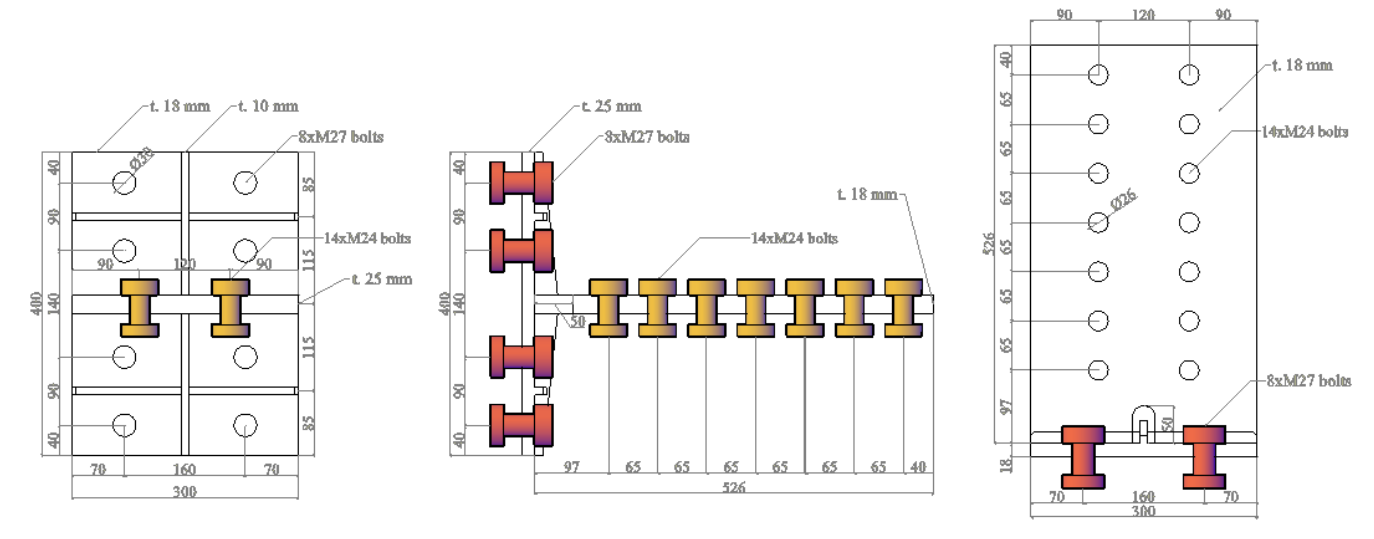
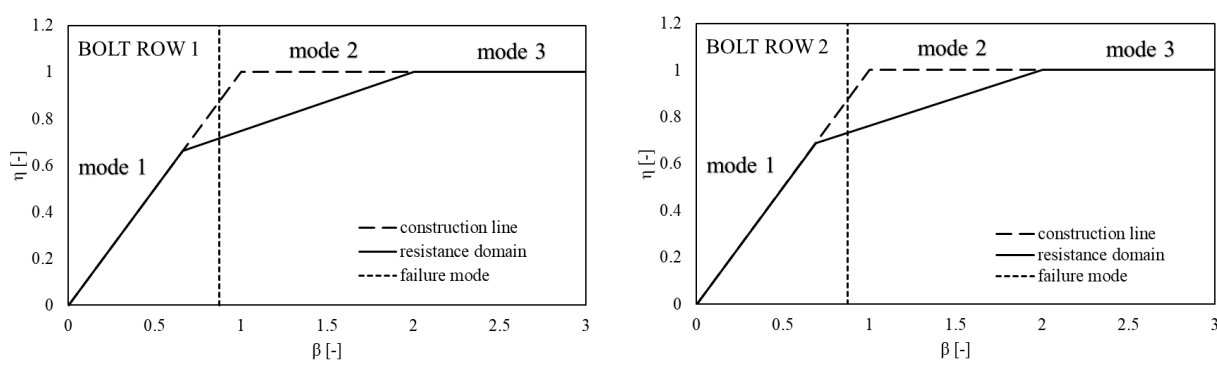


Fig 72: Strengthening Solution for the upper T-stub (Device 2A-S02)

| top row (away from the T-stub web) | | | | |
|---|-----------------------|------|---------|--|
| T-stub flange - BR 2 | F _{T2,tf,Rd} | [kN] | 605.67 | |
| Column flange - BR 2 | F _{T2,cf,Rd} | [kN] | 713.76 | |
| Failure due to: | T-STUB FLANGE | | | |
| FAILURE MODE | | | 2 | |
| ultimate resistance of the bolt row | $F_{T,Rd}$ | [kN] | 605.67 | |
| bottom row (close to the T-stub web) | | | | |
| T-stub flange - BR 1 | F _{T1,tf,Rd} | [kN] | 722.69 | |
| Column flange - BR 1 | F _{T1,cf,Rd} | [kN] | 728.17 | |
| Column flange - BR 1 (as group) | $F_{T1+2,cf,Rd}$ | [kN] | 527.61 | |
| Failure due to: | COLUMN F | | LANGE | |
| FAILURE MODE | | | 1 | |
| ultimate resistance of the bolt row | $F_{T,Rd}$ | [kN] | 527.61 | |
| tensile resistance of the entire connection | R _{C1,Rd} | [kN] | 2266.55 | |
| tensile action on the entire connection | N_{Ed} | [kN] | 1403.26 | |
| check (R/D) | | | 1.62 | |

Tab 11: Overall resistance of the T-stub



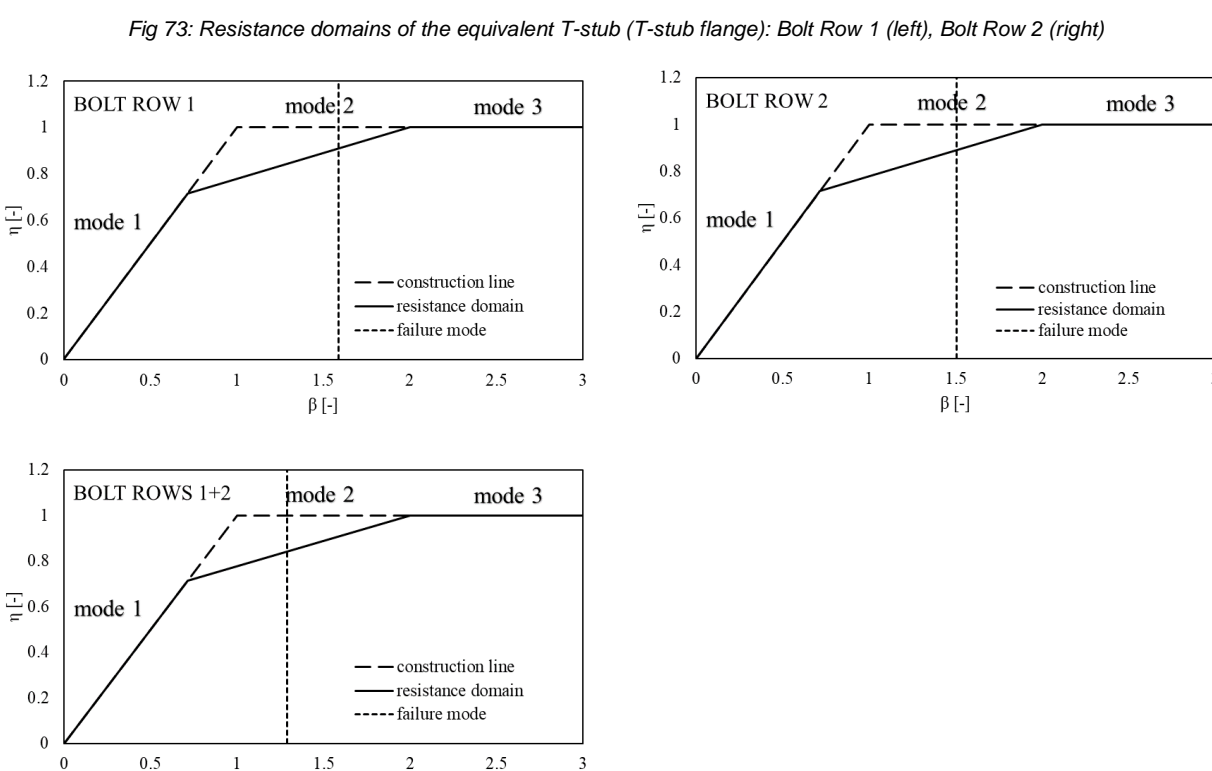


Fig 74: Resistance domains of the equivalent T-stub (column flange): Bolt Row 1 (up left), Bolt Row 2 (up right), Bolt Rows 1+2 (bottom)

β[-]

B.8. Conclusive remarks about the activities of sub-task 2.3.a

As it was expected, FREEDAM joints exhibit an excellent performance under seismic loading (both monotonic and cyclic). However, these types of connection are not enough to resist a Column Loss Scenario in large rotations, resulting in a brittle Failure Mode located at the upper T-stub (under hogging bending moment) or at the haunch and the damper bolts (under sagging bending moment).

The proposed modifications of the upper T-stub, albeit localized, can guarantee an important increase also in terms of resistance for the FREEDAM connections, providing a ductile failure mode, in case of Column Loss Scenario, with beam subjected to Hogging bending moment. In this manner the rotational capacity of the joint is enhanced up to 0,25 rad of chord rotation. The simplicity of the intervention makes it very useful and feasible. The strengthening solution consist basically in the modification of the:

- · geometrical dimensions of the plates
- number and diameter of the bolts, both on the T-stub flange and web

It has been shown that the modified T-stub doesn't interfere with the seismic behaviour of the joint, in such way all the previous studies made for the FREEDAM connections are still valid.

These considerations can be extended to the other joints of the DREAMERS building.

B.9 References

- CEN EN1993:1-8, Design of Steel Structures Part 1-8: Design of Joints; 2005.
- SCI, Publication Number: P398-Joints in steel construction: moment-resisting joints to Eurocode3, The Steel Construction Institute and The British Constructional Steelwork Association, 2013.
- Latour M., D'Aniello, M., Zimbru, M., Rizzano G., Piluso V., Landolfo, R. (2018c) Removable friction dampers for low-damage steel beam-to-column joints. Soil Dynamics and Earthquake Engineering 115, 66–81
- ANSI/AISC 341-16. Seismic Provisions for Structural Steel Buildings. American Institute of Steel Construction; 2016.
- Dassault, Abaqus 2017 Abaqus Analysis User's Manual, Dassault Systèmes Simulia Corp; 2016.

C.Pushover and time-history analyses of the DREAMERS building through OpenSees

C.1. Numerical model

The three-dimensional (3D) model of the building is developed in OpenSees [1]. The columns are force beam-column elements with five fiber sections along the height of the column in order to consider the interaction between moments and axial force in the column. The beams are also force beam column elements with aggregated sections. The flexural behavior has been obtained through a moment-curvature analysis of the section and is aggregated with the axial behavior of the section into one single section. However, it should be noted that there is no interaction between responses in different degrees of freedoms (DOFs). The behavior of the Freedam joint is obtained from a detailed model in Abaqus [2] and experimental activity. Subsequently, a model (i.e., Pinching4 Material) in OpenSees is calibrated and assigned to the zero-length positioned between the nodes of column and beams as shown in Fig. 75. It should be noted that the gravity columns and beams are simple elastic beam columns with their corresponding section properties. Moreover, stiffed elastic elements are used to model the rigid offsets from the joint. However, the gravity beams are connected to the column's web, therefore the gravity beam's length are from the center line of the columns. Considering that the bases of all columns are embedded in the concrete footing, the base of the gravity columns are also considered fixed in the numerical model. The 1st-period mode of the building in X and Z directions is 1.00 and 1.10 seconds respectively.

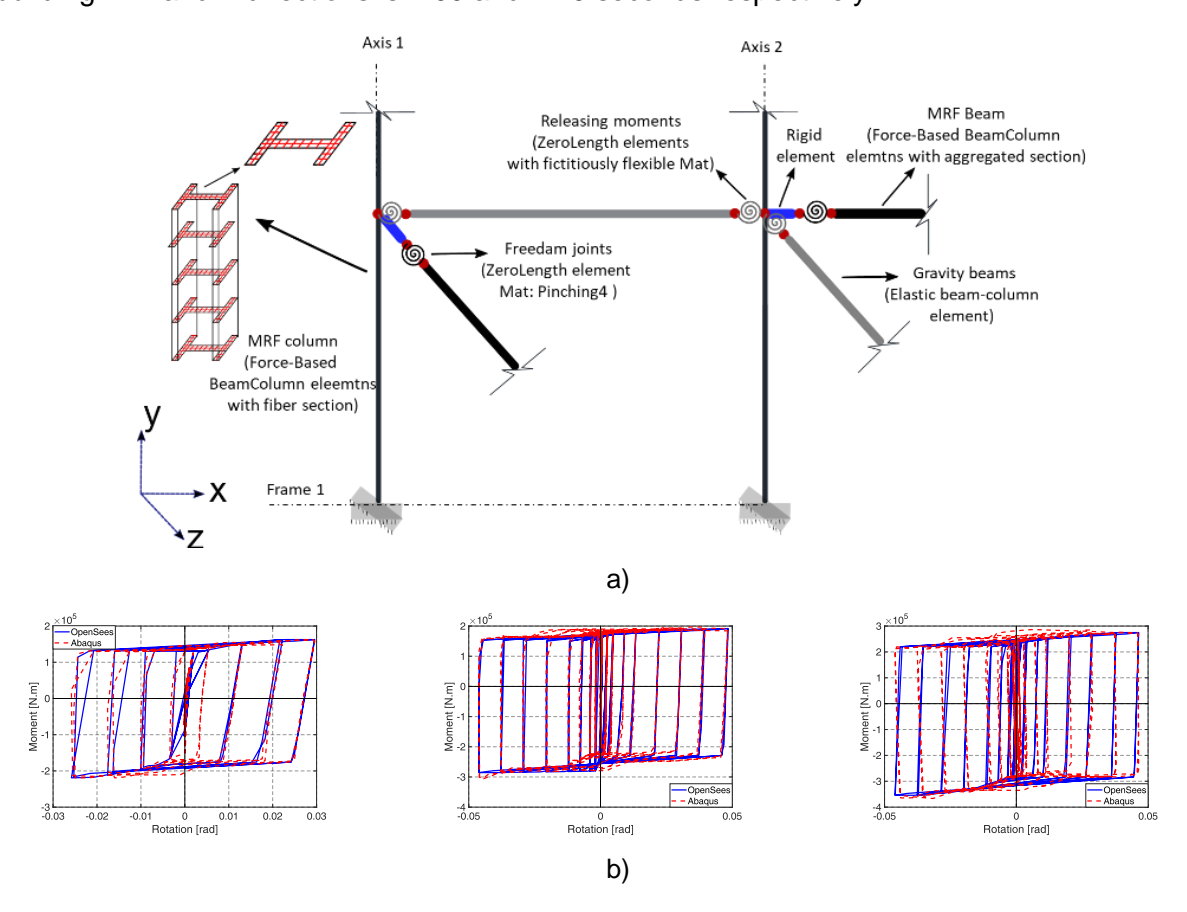


Fig. 75 a) The details of numerical modeling in OpenSees b) Calibration of the freedam joint hysteresis behavior

C.1. Nonlinear static analysis

The static pushover analysis is a simplified nonlinear analysis technique than can be used to estimate the dynamic demands imposed on a structure by earthquake ground motions. Adequate

seismic performance implies that available strength and deformation capacities exceed the demand imposed on a structure by the associated earthquake level. Ideally, performance evaluation should be based on non-linear time history analyses utilizing a suite of representative ground motions. In this section, a simpler option of the nonlinear static (i.e., pushover) analysis is employed to estimate the strength capacities and deformation demands.

The procedure involves applying a predetermined lateral load pattern that approximately represents the relative inertia forces which are generated at locations of substantial mass, and pushing the structure under this constant load pattern to the level of deformation expected in the considered earthquake level.

Pushover analyses [3] performed using the first-mode lateral load pattern. Fig. 76 shows the global pushover curve in X and Z directions normalized by the building weight of the building. The maximum strength and the occurrence of 1st nonlinear event is also superimposed on the global pushover curve. It can be seen that the structure has relatively more strength in the z direction which is a consequence of using stronger joints in that direction. It should be noted that the joint behavior has a non-degrading behavior as well as the beams. Therefor the degrading branch in the pushover curve is entirely due to p-delta effects. Moreover, the strength corresponding to 80% of the maximum strength is also highlighted on the pushover curve using a diamond marker.

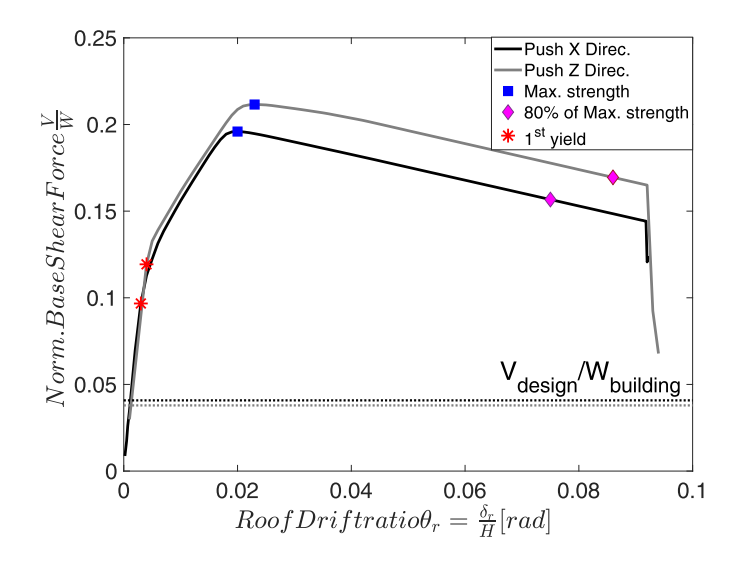


Fig. 76 Pushover curves for the x and z direction

The static system overstrength, Ω_s , factor is defined as the ratio of the maximum strength (V_{max}) to the design strength (V_{Ed}). The Ω_s factor can be subdivided into two categories such that $\Omega_s = \Omega_\epsilon \times \Omega_M$ (see Fig. 77). Ω_M accounts for the redundancy that is built into the system allowing a series of plastic hinges to form in the structure, leading to a yielding mechanism at V_{max} . Ω_ϵ represents the ratio of the formation of the first plastic hinge in a moment frame (grey square marker in Fig. 77a) over the prescribed minimum design seismic force level. Strictly speaking, Ω_s can be subdivided into three categories distinguishing between the nominal and actual material strength, however, for simplicity, we considered only two categories.

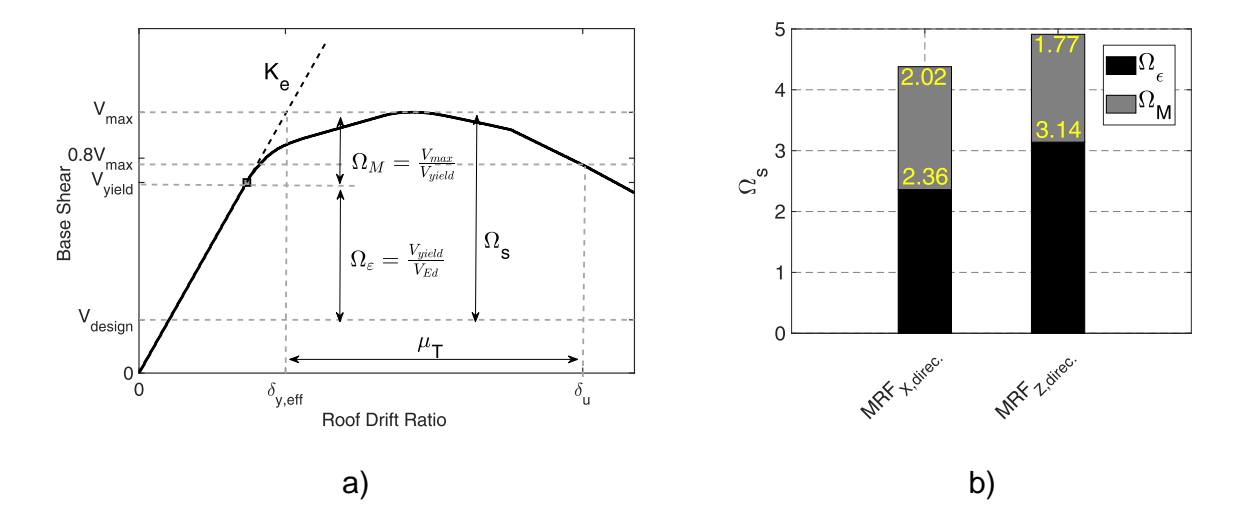


Fig. 77 a) Schematic diagram of the parameter definition in pushover analysis

C.1.1 Seismic assessment of the building based on Nonlinear static analysis

The performance of the structure is evaluated at two hazard levels corresponding to the earthquake with 475 and 2500 years return period by means of N2 method in EN1998-1. The N2 [4] method can be summarizes as follows:

- 1. Determine the base shear-top displacement relationship by a pushover analysis.
- Transforming the force-deformation relationship of the MDOF into an equivalent SDOF system.
- 3. Idealizing the force-displacement relationship of the equivalent SDOF system into an elastic-perfectly plastic form.
- 4. Determine the seismic demand for the equivalent SDOF system.
- 5. Check performance at the expected maximum displacement.

The equivalent SDoF pushover curve and its idealization is shown in Fig. 78. The idealization is conducted in a way that the area under the SDoF pushover curve up to the maximum strength is equal to the area of an idealized elastic perfectly plastic pushover curve as shown in Fig. 78b. The elastic period of the idealised bilinear system T* can be determined as:

$$T^* = 2 \times \pi \sqrt{\frac{m^* D_y^*}{F_y^*}} \tag{1}$$

Where F_y^* and D_y^* are the yield strength and displacement, respectively. The demand corresponding to the two considered earthquake levels can be computed using the computed T* and the design spectra obtained from the code as shown in Fig 78a.

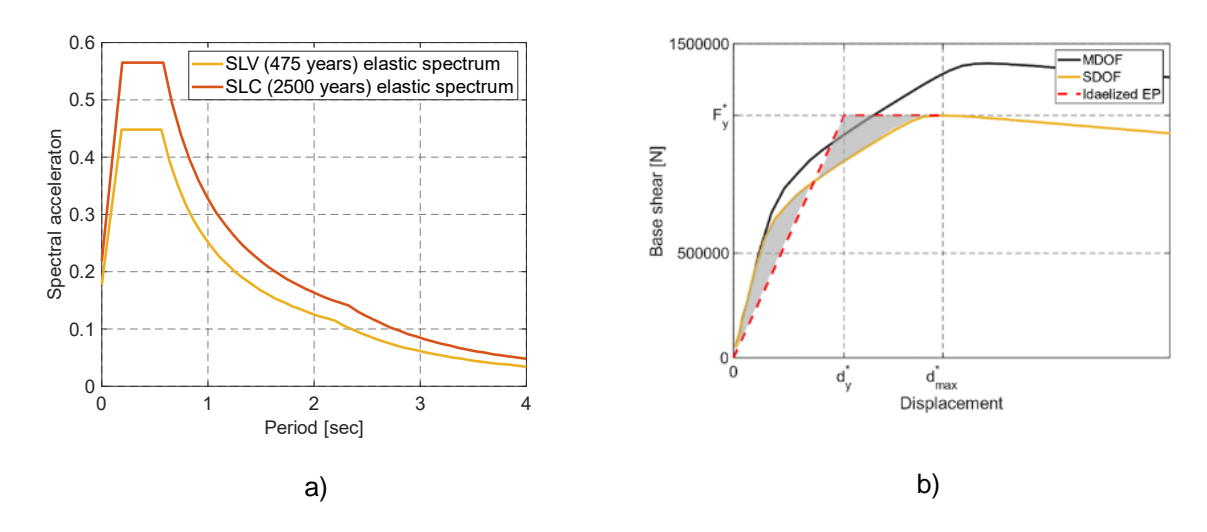


Fig. 78 a) Elastic design spectrum b) the corresponding SDoF pushover curve and its idealization

In the final step, the estimate of demand under two future earthquake levels is converted into the MDoF (i.e., the original space) and superimposed on the capacity curve of the structures as demonstrated in Fig. 79.

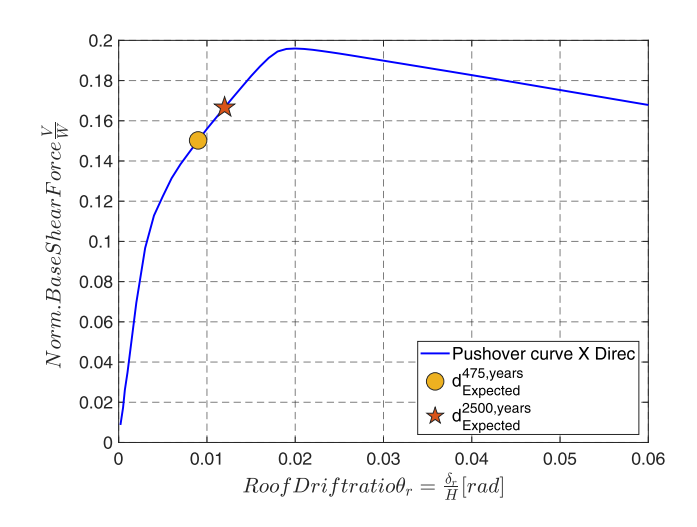


Fig. 79 Global pushover curve with the expected seismic displacement

C.2 Nonlinear dynamic analysis

In most codes and guidelines, it is assumed that adequate collapse safety (and life safety) is provided by limiting the maximum storey drift at the design earthquake level to a specific value (e.g., drift limit of 0.02 at the 10=50 hazard level or 10% of occurrence in 50 years). The drift at this hazard level is estimated from either an elastic analysis or an inelastic time history analysis. But the latter usually is executed with the use of component hysteresis models that do not account for strength and stiffness deterioration. Thus, these responses predictions provide no insight into the probability of collapse. With the advent of deterioration models that do account for important aspects of deterioration. It is becoming possible to trace the response of structures to collapse and to be specific about a collapse performance target. Such a target could be expressed as a tolerable probability of collapse (say, 10% at the 2=50 hazard level or 2% of occurrence in 50 years), or more general, as a tolerable mean annual frequency of collapse. In this section, the performance of the structure is evaluated using both approaches.

C.2.1 Mean annual frequency of collapse

A formal process for quantitative assessment of structural risk due to earthquake has been developed by the Pacific Earthquake Engineering Research (PEER) Center [5]. There are several stages to this process, consisting of quantifying the seismic ground motion hazard, structural response, damage to the building and contents, and resulting consequences (financial losses, fatalities, and business interruption). Each stage of the process is performed in formal probabilistic terms. The process is also modular, allowing the stages to be studied and executed independently, and then linked back together, as illustrated in Fig. 80.

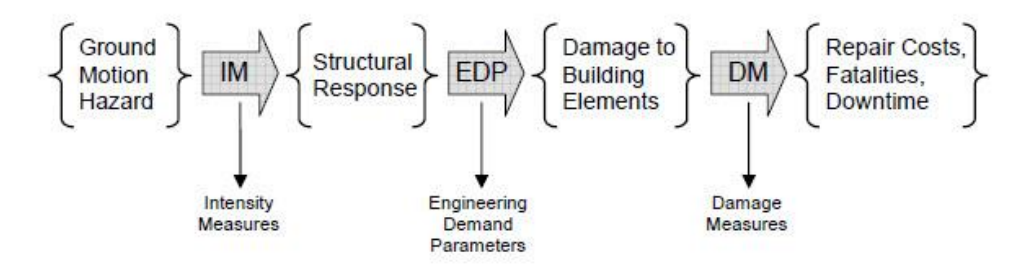


Fig. 80 Schematic illustration of performance-based earthquake engineering model and pinch points

The mathematical formulation of the problem is expressed by the following equation:

$$\lambda_{DV} = \iiint F(dv \mid dm) f(dm \mid edp) f(edp \mid im) f(im) dim dedp ddm$$
 (2)

For this method to be tractable and transparent, it is helpful to formulate the problem so that each part of the assessment is effectively independent. The independent assessment modules are then linked together using intermediate output variables, or "pinchpoint" variables [5]. In the PEER methodology the intermediate variables are termed intensity measure (IM), engineering demand parameter (EDP) and damage measure (DM). An important assumption in this methodology is that what follows in the analysis is dependent only on the values of the pinch-point variables and not on the scenario by which it was reached (e.g., the response of the structure depends only upon the intensity measure of the ground motion, with no further dependence on variables such as the magnitude or distance of the causal earthquake). Further, the relationship between each of the stages is Markovian: given knowledge of EDP, the damage to building elements is independent of IM. This model relies heavily on assumptions of conditional independence between analysis stages. If the assumptions are not valid, then modifications to the model are required before proceeding. The use of vector-valued intensity measures is one such modification.

DV is a single or a vector of decision variables, such as cost, time-to-repair or human casualties that are meant to enable decision making by the stakeholders. Defining performance without involving any decision variable DV or the closely related damage measure DM makes sense for many engineers. Engineering quantities may be much preferable, especially when working at the level of a design office, to discern which structure is outperforming the rest. This may be best achieved by moving to the familiar territory of limit-states by appropriately modifying the PEER framework. Defining DV and DM to be simple indicator variables that become one when a given limit-state (LS) is exceeded, the MAF of violating LS:

$$\lambda_{L.S} = \int_0^\infty P(F|I_M) \left| \frac{d\lambda(IM)}{d(IM)} \right| dIM \tag{3}$$

This MAF is going to be our engineering-level indicator, or metric, of performance. While deeply rooted into a performance-basis it retains a natural connection with the familiar concept of the probability of violating a certain performance level or limit-state. For example, the well-known 10% probability of exceedance in 50 years for a Life Safety limit-state will, via the Poisson assumption for seismic events, corresponds directly to λ equal to 0.21%, a threshold MAF value that can be compared to results derived via Eq. 3.

C.2.2 Incremental dynamic analysis

Incremental dynamic analysis (IDA) ([6]) is an analysis method that emerged as a promising tool for thoroughly evaluating the seismic performance of structures. Originally developed for 2D structures, it involves subjecting a structural model to a suite of ground motion records, each scaled to several intensities (i.e., IM), and recording the responses (i.e., EDPs) at each level to form IDA curves of response versus intensity. Allowing for the transparent definition of limit-states and the accurate estimation of the probabilistic distribution of the associated capacities, it forms a reliable but computer-intensive platform for performance-based earthquake engineering. Performing IDA on a structural model requires a suite of ground motion records to represent the seismic threat, an efficient intensity measure (IM) to scale the records and an appropriate choice of engineering demand parameters (EDPs) to adequately characterize the structural response. All three elements are necessary ingredients of IDA and perhaps the most important difference in selecting them when doing 3D versus 2D analysis is that we now need two components of ground motion instead of just one.

IM: In this study the primarily IM is the 5%-damped first-mode spectral acceleration of x-component. This is the scalable IM that will be used to scale the ground motions and monitor the EDP. However, a second IM is also employed to consider the information providing from the second component of the ground motion. It should be noted that since the scaling is represented by the primary IM, it would be redundant and often confusing if the secondary IM were also scalable rather than scaling-independent. That is not to say that one may not use another spectral value, but rather that it would be better if we normalized it by the primary IM to remove any redundant information. So we let our second IM be where the subscripts "x" and "y" refer to the x and y axis (and the corresponding ground motion components). Thus, we convey only the additional information that the new element brings in the vector with respect to our primary scalable IM.

Ground motion selection: The spectral shape has important effects on structural response; this is especially true when higher mode effects are important or when the building is significantly damaged, causing the effective fundamental period to elongate. Therefore, the input ground motions play an important role in the assessment of a building at collapse level. In this study, the Conditional Mean Spectrum (CMS) is used as an alternative to the classical code-based record selection. CMS method anchors the spectrum to spectral acceleration ordinate at a single vibration period T* (i.e. the fundamental period of vibration), and then other spectral accelerations can be calculated by conditioning to the single period. More details can be found in [7]. The site-specific hazard spectrum for the structure is depicted in Fig. 81a using Ambraseys et al. ground motion prediction equation [8]. In Fig. 81a the IM corresponds to an earthquake with return period of 2500 years is also superimposed on the plot. The response spectrum of the selected ground motions and scaled to match the CMS is shown in Fig. 81b.

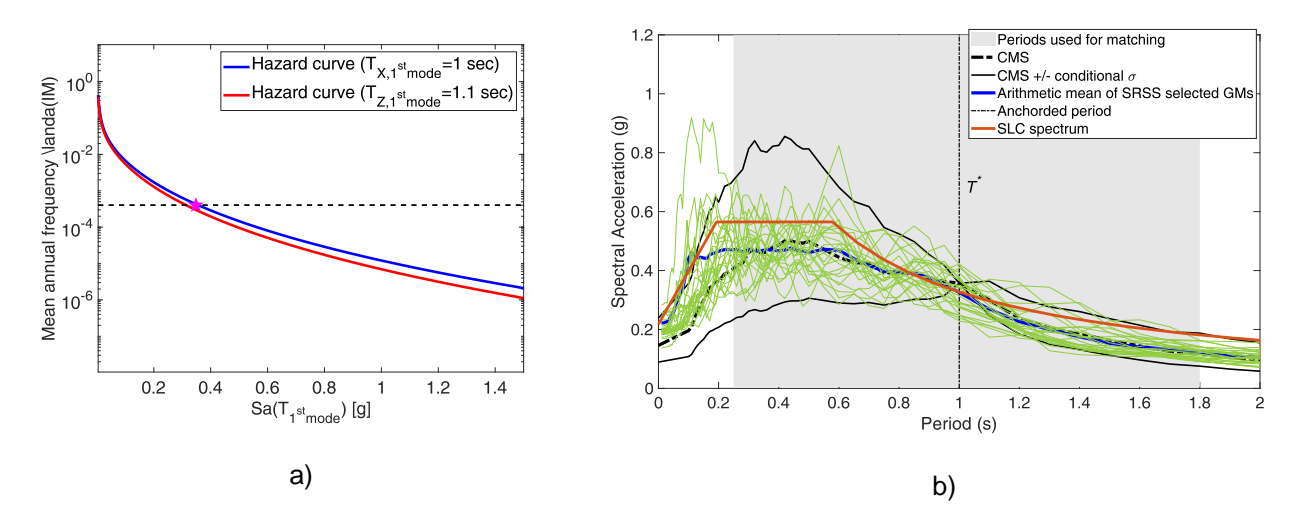


Fig. 81 a) The site-specific hazard curve b) CMS for (with T*= 1.00 s), and response spectra from ground motions selected to match CMS

EDP: Selecting the EDP is relatively straightforward for this space frame. Since maximum interstory drifts are generally considered to correlate well with story damage, we choose to monitor the maximum peak SRSS drift maxsθ, i.e., the maximum over all stories of the peak of the square-root-sum-of-squares (or vector sum) of each story's instantaneous drifts in the two principal directions. This has been illustrated schematically in Fig. 82 for the third story of the building.

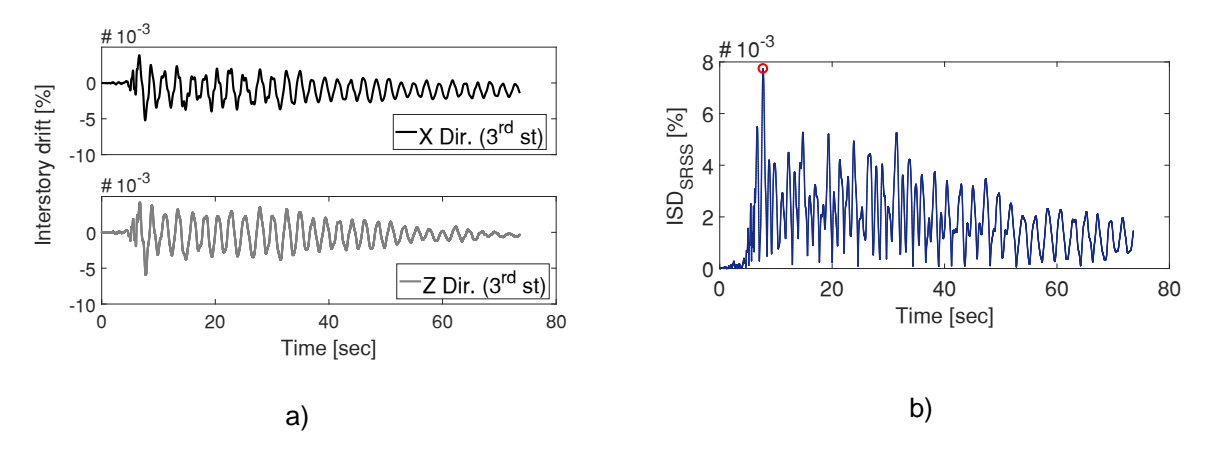


Fig. 82 a) The inter story drift in the x and z direction b) The square-root sum square of the two time series of the x and z components of ISD

It should be noted that the SRSS drift gives the peak drift of the space frame in the direction that has the largest response.

C.2.3 Performance assessment at specific hazard level

Following a procedure similar to processing a single scalable IM, we can visualize the IDA curves in the three-dimensional space by plotting the EDP and the two single IMs as demonstrated in Fig. 10a. In this case we will put the IMs in the x-y axes (representing the input) and place the EDP in the vertical axis (being the response or output). The flatlines now extend upwards, parallel to the z-axis, rather than being the customary horizontal lines. The point at which each IDA trace first reaches the EDP level of interest (max interstory drift ratio = 0.1 or the slope of the line less than the 20% of the elastic branch) defines a set of IM capacity values. These points are plotted in Fig. 83b. On the left side of Fig. 83b the information regarding the IM_2 is neglected. The expected collapse capacity of

the building and the degree of uncertainty can be computed based on this data. A common assumption is fitting a lognormal distribution to the data as shown in the right axis of the first part of Fig. 83b.

However, the data can be plotted in a scatter plot by tacking into account the information providing by the second IM. It is apparent that IM_2 can explain part of the variation in IM_1 capacity (that is, the IM_{1Cap} values tend to be larger for higher values of IM_2). Regression analysis can be used to incorporate this information. Thus, the probability of exceeding the IM capacity associated with the target EDP level can be express can be expressed in terms of a conditional distribution IM_1 given IM_2 .

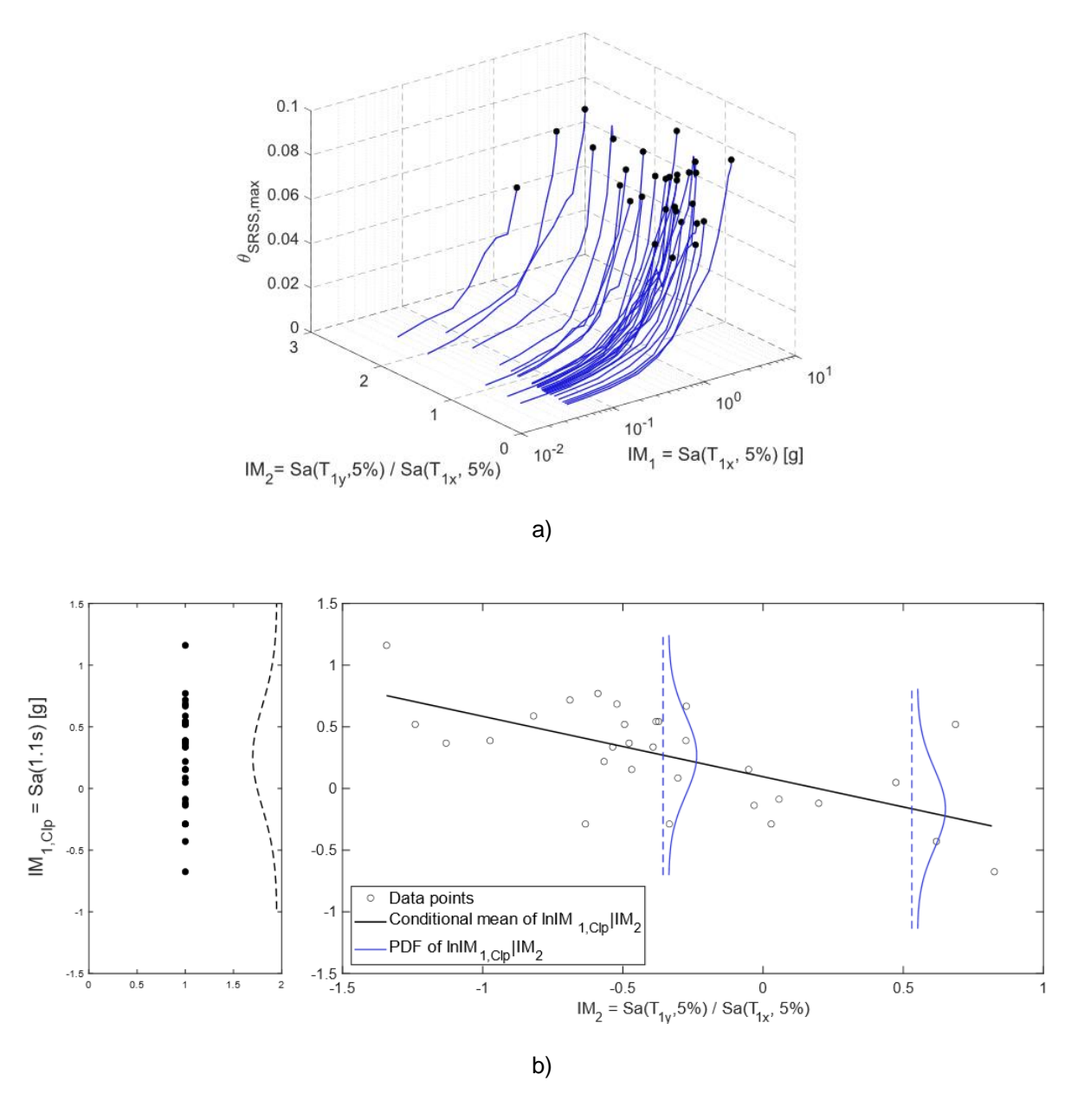


Fig. 83 a) The IDA curves b) IM₁ and IM₂ pairs correponding to the occurance of numerical collapse

Here, the conditional distribution of $\ln IM_{1Cap}$ appears to be linearly dependent upon IM₂. Therefore, linear regression can be used to find the conditional mean of $\ln IM_{1Cap}$ given IM₂

where β_0 and β_1 are coefficients to be estimated from linear regression using data points from Fig. 10b. Further, the conditional standard deviation of $InIM_{1Cap}$ given IM_2 can be estimated by computing the standard deviation of the regression residuals. This conditional standard deviation is denoted $\sigma_{lnIM_{1Cap}|IM_2=im_2}$. If the conditional distribution of $lnIM_{1Cap}$ given IM_2 is assumed to be Gaussian, then the conditional mean and standard deviation computed above completely define the conditional distribution of $lnIM_{1Cap}$ associated with reaching a numerical collapse of the model. The probability density function (PDF) of this distribution is shown in Figure 84b for two different values of IM₂. The CDF of this conditional distribution is the so-called fragility of the building corresponding to numerical collapse. Therefor by computing the CDF for a range of IM₂ one can draw the complete fragility of the building as shown in Fig. 84a. The results can also be visualized as contours of the complete fragility surface as plotted in Fig. 84b. The vertical axis indicates the collapse capacity of the building in terms of spectral acceleration (i.e., the scalable IM_1). It is obvious that as IM_2 increases (i.e., the ratio of spectral acceleration of the second component of the ground motion to the first component associated with the fundamental period of the building in each direction) the structure's capacity decreases until saturation occurs. In other words, the second component is responsible for the collapse of the structure as if the first IM provides no further information on its collapse capacity.

Adequate collapse safety of the building can be verified at intensity corresponding to maximum considerable earthquake (i.e., an earthquake that happens every 2500 years or 2% occurrence in 50years). The intensity of such earthquake is also superimposed on Fig 84.b. It can be seen that for all values of IM_2 the capacity of the structure is more than the induced demand.

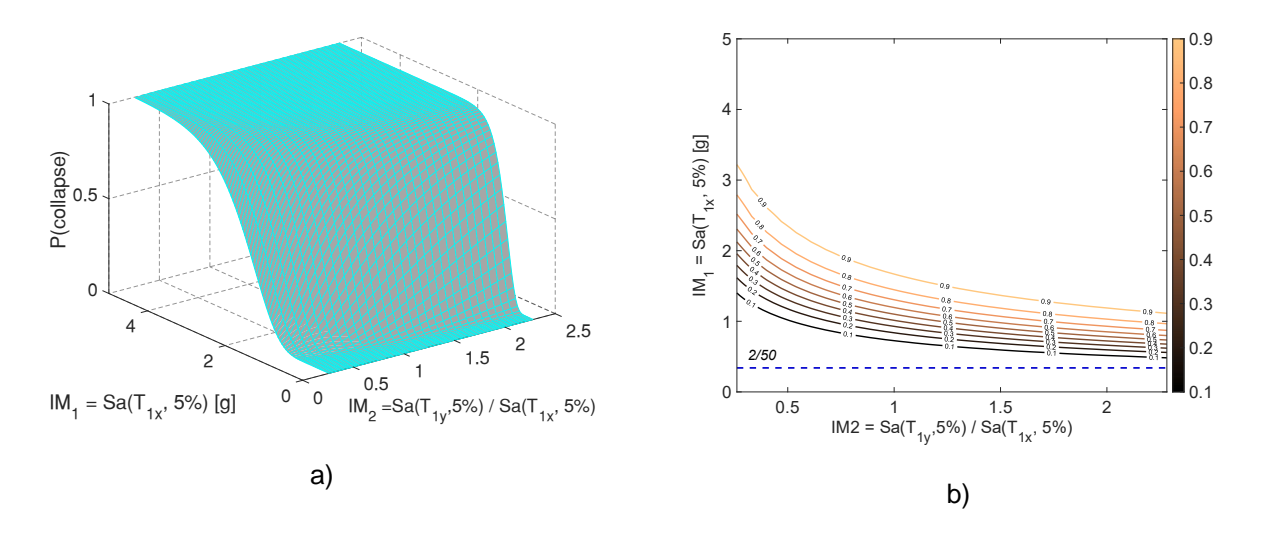


Fig. 84 a) The complete fragility of the building corresponding to numerical collapse b) Contours of the fragility surface

C.2.4 Performance assessment based on MAF

The performance of the structure can also be evaluate using MAF explained earlier. In this approach the L.S is defined as exceeding a specific story drift ratio (SDR) limit defined by code. Three different L.S is considered here and the corresponding SDR limits are shown in Table 2.

Table 2. The limit states and corresponding maximum inter story drift ratios

| Limit States | DL | SD | NC |
|--------------|----|----|----|
| MIDR (%) | 1 | 2 | 4 |

The capacity of the structure for each L.S can be computed by drawing a vertical line through the IDA curve as shown in Fig. 85 a. If we consider lognormal distribution, one can draw the fragility associated with each L.S as shown in Fig. 85b.

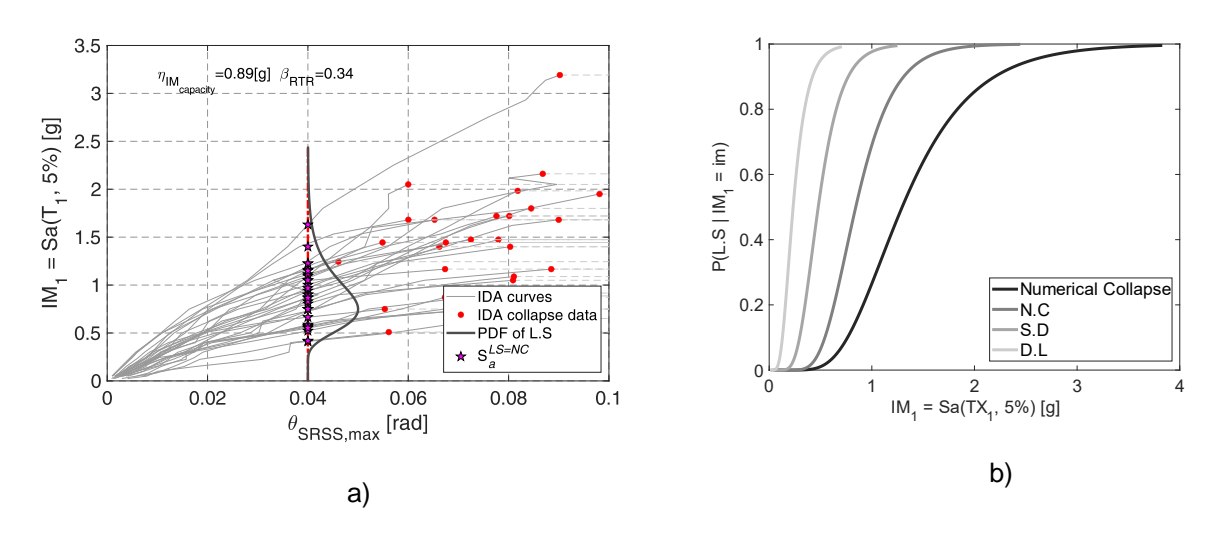


Fig. 85 a) The IDA curves and data points corresponding to NC L.S b) Fragilities for different L.S

By employing Eq. 3 and integrating the fragility over the entire hazard domain, the MAF of exceeding a limit state can be obtained. This MAF can be turned into probabilities by assuming a Poisson distribution and a lifetime of 50 years for the structure. The corresponding probability of exceeding each limit state are depicted in Fig. 86. The tolerable probability of NC and SD limit states can be assumed to the return period of the hazard, 2% and 10% in 50 years. It can be observed that both limit states are satisfied for the prototype building. It should be noted that the MAF method is a more general and comprehensive assessment compared to evaluating the performance at a specific hazard.

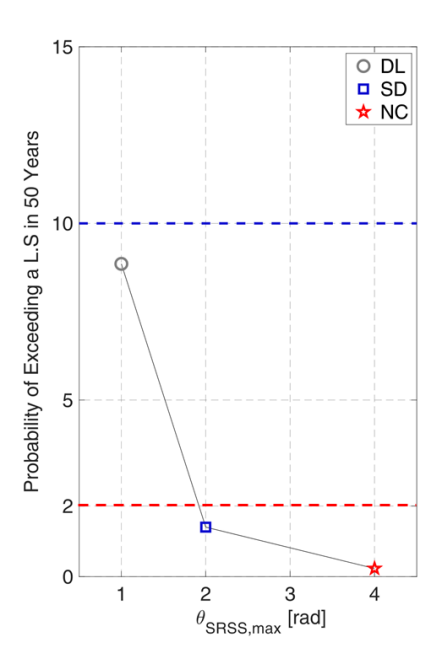


Fig. 86 Probability of exceeding a L.S in 50 years life time

C.2.5 Assessment of residual drift

It is also desirable to evaluate the residual drift of the prototype building since it has a direct impact on judging the post-earthquake safety and repairability of the building. Figure 87 (a) presents the median maximum residual drift ratio (MRDR) versus ground motion intensity. The intensity of an earthquake associated with SD, and NC limit states is also superimposed in the same figure. FEMA p58 [9] identifies four damage states (mostly judgemental) associated with residual drift ratio. It suggests that a typical value as a limit for repairability of the building can be adopted as 1%, meaning that beyond this limit the structure may not be economically or practically justified for repairing. Based on this limit, fragility can be obtained for rendering a building "irreparable". As show in Fig.87(b). It can be observed that at the maximum considered earthquake, there is a 14% probability (given the spectral acceleration) of categorizing the building as "Irreparable".

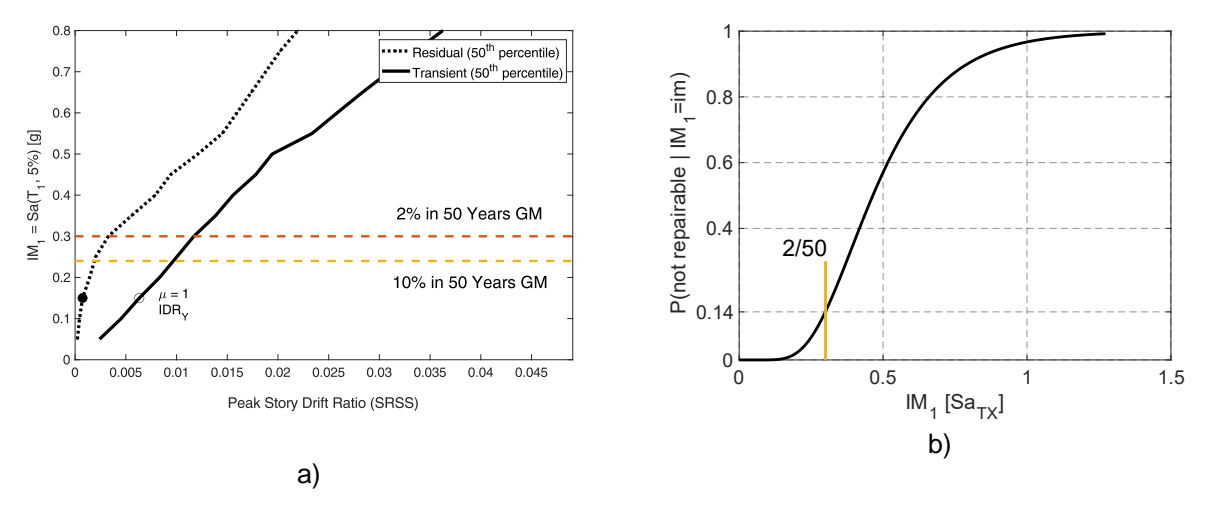


Fig. 87 a) The median of maximum transient and residual drift ratio (SRSS) b) The probability of the building beain irreparable given an occurance of an earthquake with IM_1 (2/50 means 2% probability of exceedance in 50 years)

C.2.6 Assessment of damage in the columns

The main objective of the project is to have a column free of damage for intensities corresponding to maximum considerable earthquake. This can be evaluated by the following equations:

$$P(damage\ in\ clmns|IM_1=im_i)=\frac{\sum_{GM=1}^{GM=30}I_{GM}|IM_1=im_i}{N}$$
 (4)

$$I_{GM|IM_1=im_i} = \begin{cases} I_{GM} = 1 & plastic \ deformation \ in \ any \ column > 0.0 \\ I_{GM} = 0 & plastic \ deformation \ in \ any \ column = 0.0 \end{cases}$$

Where N is the total number of the GM (i.e., 30) and $I_{GM|IM_1=im_i}$ is and indicatior function. If any plastic deformation occurs in any columns of the building regardless of the quantity, the indicator function for that particular ground motion scaled to an intensity $IM_1=im_i$ is equal to one, otherwise is zero. Therefore a stepwise function can be plotted indicating the probability of having a damage in the columns of the building as shown in Fig. 88. It can be observed that under a maximum considerable earthquake, the probability of having damage in the building is negligible.

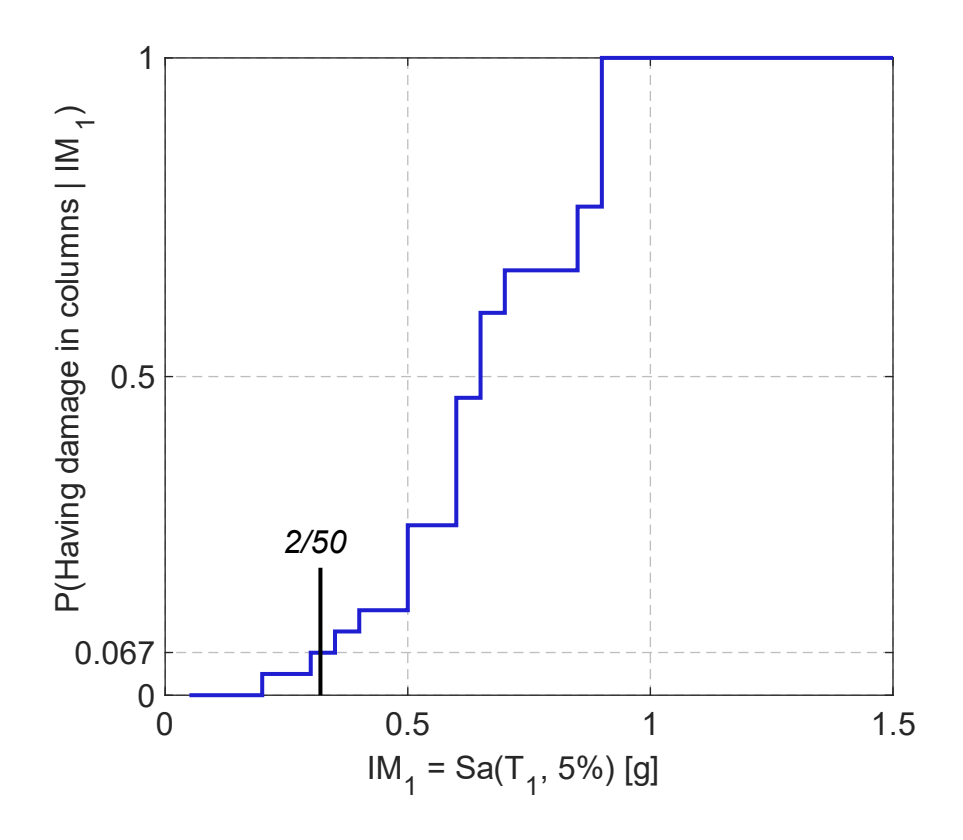


Fig. 88 the fragility of having a damage in the columns for the prototype building

C.3 Conclusive remarks on the seismic assement of DREAMERS building

On the basis of the results of both static and dynamic non-linear analyses, the following consideration can be pointed out:

- The results of the performed Pushover analyses show that the building has similar rigidity in both plan directions, but different capacity (greater in the transverse direction, i.e., «z» direction).
- The results from N2 method shows that minor damages occur in the connection at both SD and NC limit states. All other elements behave in elastic range.
- The performed incremental dynamic analyses show that the building performs well under design and maximum considerable earthquakes.
- The results shows that there is 7% probability of not having a free from damage building at earthquake level corresponding to 2% in 50 years (i.e., Near Collapse limit state), which means moderate yielding in the columns (i.e., still far from any failure mode).

C.4 References

- 1. Mckenna FT. 'Object-oriented finite element programming: frameworks for analysis, algorithms and parallel computing.' Ph.D. Thesis, Department of Civil Engineering, University of California, 1997.
- 2. ABAQUS/Standard User's Manual Version 6.9, Providence, RI: Simulia2009.
- 3. Lawson, R. S., Vance, V. and Krawinkler, H. 'Nonlinear static pushover analysis why, when and how?', Proc. 5th US Conf. Earthq. Engng, Vol. 1, Chicago, IL, 1994, pp 283-292
- 4. Fajfar, P., GASPERSIC P., 'The N2 method for the seismic damage analysis of RC buildings' Earthq. Engng Vol.25, 31-46
- 5. PEER reports 'Vector-Valued Ground Motion Intensity Measures for Probabilistic Seismic Demand Analysis' Jack W. Baker, C.Allin Cornell October 2006.
- 6. Vamvatsikos, D., and C. A. Cornell, 2004. Applied Incremental Dynamic Analysis, Earthquake Spectra 20 (2), 523–553.
- 7. Vamvatsikos, D., 2006 Incremental dynamic analysis with two components of motion for a 3D steel structure. Proceedings of the 8th US National Conference on Earthquake Engineering.
- 8. Chioccarelli E., Cito P., Iervolino I., Giorgio M.: REASSESS V2.0: software for single- and multi-site probabilistic seismic hazard analysis. Bulletin of Earthquake Engineering. 17, 1769-1793 (2019).
- 9. FEMA (2018a) FEMA P-58-1: seismic performance assessment of buildings. Methodology, vol 1. Federal Emergency Management Agency, Washington